Dissertation

THE COMBINED EFFECT OF IVABRADINE AND LPS ON THE HUMAN PACEMAKER CURRENT

submitted by
Mag.[a] rer. nat.
Susanne SCHERÜBEL

for the Academic Degree of
Doctor of Medical Science
(Dr. scient. med.)

at the
Medical University of Graz
Institute of Biophysics

under the Supervision of
Sen.-Scientist Univ.-Doz.[in] Mag.[a] Dr.[in] rer. nat. Brigitte PELZMANN

2014

Eidesstattliche Erklärung

Ich erkläre ehrenwörtlich, dass ich die vorliegende Arbeit selbständig angefertigt und abgefasst, und jene Personen und Institutionen, die am Zustandekommen der Forschungsdaten beteiligt waren, namentlich genannt habe. Andere als die angegebenen Quellen habe ich nicht verwendet und die den benutzten Quellen wörtlich oder inhaltlich entnommenen Stellen habe ich als solche kenntlich gemacht. Die Arbeit an der Dissertation und daraus entstandener Publikationen wurde gemäß den Regeln der „Good Scientific Practice“ durchgeführt.

Statutory Declaration

I hereby declare that this dissertation is my own original work and that I have fully acknowledged by name all of those individuals and organisations that have contributed to the research for this dissertation. Due acknowledgement has been made in the text to all other material used. Throughout this dissertation and in all related publications I followed the guidelines of “Good Scientific Practice”.

Acknowledgements

I would like to thank Dr.in Brigitte Pelzmann, Dr. Klaus Zorn-Pauly and Petra Lang for their professional and social guidance throughout my time at the Medical University of Graz.

Furthermore I would like to thank MSc. Chintan Koyani, Dr. Seth Hallström, Dr. Dieter Platzer and MSc. Philipp Kainz for their technical contribution to this thesis.

Table of Contents

Table of Figures

Abbreviations and Definitions

AP	action potential
cAMP	cyclic adenosine monophosphate
cGMP	cyclic guanosine monophosphate
CL	cycle length
DD	diastolic depolarization
HCN	hyperpolarization-activated cyclic nucleotide-gated
I_{CaL}	L-type calcium current
I_{CaT}	T-type calcium current
I_f	funny current
I_{inst}	instantaneous current
I_K	delayed rectifier potassium current, composed of I_{Kr} and I_{Ks}
I_{K1}	inwardly rectifying potassium current
IV-relation(ship)	current-voltage-relationship
LCR	local calcium release
LPS	lipopolysaccharide
MDP	maximum diastolic potential
MODS	multiple organ dysfunction syndrome
NCX	sodium-calcium exchanger = Na^+/Ca^{2+} exchanger
pacemaker current	I_f and I_{inst}
PKA	protein kinase A
R595	Re 595: rough mutant LPS, polysaccharide part is lacking
RyRs	ryanodine receptors
SANC	sinoatrial node cell(s)
Sepsis	SIRS caused by infection
SERCA	sarcoplasmic reticulum calcium ATPase
SIRS	Systemic inflammatory response syndrome
S-LPS	smooth LPS form, containing lipid A, core oligosaccharide and polysaccharide part
SR	sarcoplasmic reticulum

Kurzfassung

Motivation: Der durch HCN-Kanäle fließende humane Schrittmacherstrom besteht aus der spannungs- und zeitunabhängigen Komponente I_{inst} und der spannungs- und zeitabhängigen Komponente I_f, und trägt maßgeblich zur diastolischen Depolarisationsphase von Aktionspotentialen spontanaktiver Zellen des Sinusknotens bei. Durch I_f-Blockade kann die Dauer des Schrittmacherpotentials verlängert und damit die Verringerung der Herzfrequenz erreicht werden, was im pharmazeutischen Wirkstoff Ivabradin Anwendung findet. Eine derzeit laufende klinische Studie (MOD*I*$_f$Y-Trial) erforscht die Anwendung von Ivabradin an septischen Patienten, denn eine niedrigere Herzfrequenz deutet auf eine bessere Prognose hin. Sepsis wird u.a. durch Lipopolysaccharide (LPS) ausgelöst, die Bestandteile von Zellwänden gram-negativer Bakterien sind. LPS kommt natürlicherweise in zwei Grundformen vor: Die S-Form (S-LPS) enthält alle drei möglichen Bestandteile des Moleküls: Lipid A, Oligosaccharid- und Polysaccharidanteil (O-Kette). Bei der R-Form fehlt die O-Kette. Ebenso wie Ivabradin übt auch S-LPS (nicht aber R-LPS) eine hemmende Wirkung auf I_f bei akuter und chronischer Applikation in isolierten Herzmuskelzellen aus, wobei – im Gegensatz zu Ivabradin, welches an den HCN-Kanal bindet und diesen dadurch blockiert – der Mechanismus der I_f-Inhibierung durch S-LPS unbekannt ist. Da beide Substanzen I_f blockieren, ist eine Erforschung der gemeinsamen Wirkung in klinischer und therapeutischer Hinsicht von Relevanz. Die zweite Komponente des Schrittmacherstroms, I_{inst}, spielt mit großer Wahrscheinlichkeit eine Rolle in der Generierung und Stabilisierung des Schrittmacherpotentials. Daher ist eine Beschreibung der Ivabradin- und LPS-Wirkung auf diese Komponente ebenfalls von Bedeutung.

Ziele: 1) Erforschung des akuten und chronischen Effekts von S-LPS und R-LPS auf I_f und I_{inst}. 2) Analyse der Interaktion von LPS und HCN-Kanälen. 3) Untersuchung der kombinierten Wirkung von LPS und Ivabradin auf I_f und I_{inst}. 4) Ermittlung der veränderten Schlagfrequenz einer Sinusknotenzelle (Computermodell Kaninchen) bei gleichzeitiger Anwesenheit von LPS und Ivabradin.

Methodik: Elektrophysiologische Messungen wurden mittels whole-cell patch-clamp Technik an isolierten humanen Vorhofzellen durchgeführt. Intrazelluläre Ivabradinkonzentrationen in Herzmuskelzellen des Meerschweinchens wurden durch HPLC bestimmt. Mittels Dot-Blot Analyse wurde die Interaktion des LPS Moleküls mit dem HCN-Kanalprotein (isoliert aus murinen Herzmuskelzellen) getestet.

Elektrophysiologische Ergebnisse wurden in ein Computermodell einer Sinusknotenzelle (Kaninchen) implementiert (Matlab), um die Auswirkungen von Ivabradin und LPS auf die Schlagfrequenz zu bestimmen.

Ergebnisse: Nur S-LPS blockierte I_f unter akuter und chronischer Applikation (6 min bzw. 6 h Inkubationszeit, beides 10 µg/mL) und konnte an das HCN-Kanalprotein binden. Es konnte kein Akuteffekt auf I_{inst} festgestellt werden, weder durch S-LPS noch durch R-LPS. Die Blockade von I_{inst} passierte nur unter chronischer LPS-Einwirkung und war unabhängig vom Vorhandensein der O-Kette. R-LPS konnte nicht an das HCN-Protein binden.

Die I_f-inhibierende Wirkung von Ivabradine (1 µmol/L) war in LPS inkubierten Zellen (S- und R-Form) signifikant geringer als in Kontrollzellen, wobei in S-LPS inkubierten Zellen zusätzlich eine signifikant niedrigere intrazelluläre Ivabradinkonzentration gemessen wurde. Dennoch konnte Ivabradin die Schlagfrequenz der Sinusknotenzelle *in silico* in S-LPS-inkubierten Zellen weiter verringern.

Schlussfolgerungen: Experimentelle Daten wie auch Computersimulationen deuten darauf hin, dass die Verabreichung von Ivabradin eine therapeutische Maßnahme zur Herzfrequenzsenkung in Sepsis-assoziierten Krankheiten darstellen könnte. S-LPS übt eine I_f-inhibierende Wirkung durch die Bindung an das HCN-Protein aus. Der Inhibierung von I_f und I_{inst} scheinen unterschiedliche Mechanismen zugrunde zu liegen.

Abstract

Background: The human pacemaker current (carried by HCN channels), which is composed of the time- and voltage-independent component I_{inst} and the time- and voltage-dependent component I_f, plays a distinct role in the sinoatrial action potential. Through I_f-inhibition the steepness of the diastolic depolarization decreases and hence, the beating frequency is reduced. This knowledge is applied in the pharmaceutical agent ivabradine, a pure heart rate lowering agent selectively inhibiting I_f. Currently, the MOD*I*$_f$Y-trial investigates potential benefits of heart rate reduction in septic patients, since a lower heart rate is associated with better survival rates. Sepsis can be triggered through lipopolysaccharides (LPS) which are part of the outer cell wall of gram-negative bacteria and can be found naturally in two forms: The S-form (S-LPS) contains all three possible moieties of the molecule, namely lipid A, oligo- and polsaccharides (O-chain). R-form LPS (R-LPS) lacks the O-chain. S-LPS, like ivabradine, inhibits I_f, but the mechanism of S-LPS action on HCN channels is not known - contrary to ivabradine, which is known to bind to the channel pore thus blocking I_f. Since both substances, S-LPS and ivabradine, decrease I_f, investigations on the combined action are of clinical and therapeutical relevance. Furthermore, the second component of the pacemaker current, I_{inst}, is likely to play a role in the generation and stabilization of pacemaker potentials. Therefore, effects of LPS and ivabradine (also in combination) on this current component are of importance too.

Aims of the study: Investigation of 1) acute and chronic effects of S-LPS and R-LPS on I_f and I_{inst}, 2) the interaction between LPS and HCN channels, 3) the effect of ivabradine on both pacemaker current components under elevated endotoxin levels, 4) the combined effect of S-LPS and ivabradine on the beating rate in a computational model of a sinoatrial cell.

Methods: Electrophysiological recordings were carried out in the whole-cell patch-clamp technique in human atrial cardiomyocytes isolated from the right atrial appendage. A dot blot was carried out to investigate the interaction between LPS and HCN proteins (isolated from mice hearts). Intracellular ivabradine concentrations were determined by HPLC analysis using isolated guinea pig myocytes. Obtained electrophysiological data were implemented in an updated computer model of a rabbit sinoatrial cell (Matlab).

Key results: Only S-LPS significantly inhibited I_f (acute and chronic treatment, 10 µg/mL for both). Dot-blot analysis revealed that the O-chain moiety is necessary for endotoxin binding to HCN channels. In contrast to I_f, I_{inst} reduction was O-chain independent and

occurred only under chronic LPS treatment. Ivabradine (1 µmol/L) inhibited I_f in LPS incubated cells to a lesser extent than in control cells. In case of S-LPS this was associated with a significantly lowered intracellular ivabradine concentration. Computational analyses revealed that ivabradine is still able to slow down the cellular sinoatrial pacemaking process under septic conditions.

Conclusions: Experimental and modeling data indicate that ivabradine might represent a promising therapeutic approach for heart rate reduction in sepsis related diseases and that O-chain dependent binding of endotoxin to HCN channels is the primary mechanism of the S-LPS effect on I_f.

A. INTRODUCTION

Sepsis is a worldwide major health concern with an overall mortality rate of approximately 50 % [1] and can be understood as an overshooting and fulminant reaction of the non-specific immune system triggered by an infection that has moved to the bloodstream. Potential infectious agents can be viruses, bacteria, fungi or parasites (protozoa and worms). The body's immuno-inflammatory response is necessary for fighting the infection but if it gets enhanced and dysregulated it can initiate multiple organ dysfunction syndrome (MODS), septic shock and death. [1]

The cardiovascular status is crucial for survival in sepsis. Cardiovascular collapse, which occurs in almost 40 % of septic patients, doubles the risk of death as the myocardial output is insufficient to meet metabolic demands. [2] Causes of myocardial depression in sepsis are complex and yet not entirely understood. Extraordinarily high concentration of catecholamines, bacterial toxins, sepsis mediators and cardiodepressive factors may contribute to the development of this life-threatening disease. [3] LPS, which is a structural component of outer cell walls of Gram-negative bacteria is a potential elicitor of sepsis. LPS molecules comprise 3 parts: 1) Lipid A, which harbors the endotoxic activity of the molecule, 2) the core-oligosaccharide and 3) the polysaccharide part or the so called O-chain. In case of S-LPS all 3 parts of the molecule are present, in case of rough LPS-mutants the O-chain is lacking. LPS molecules of this kind are called R-form LPS. Usually, bacterial cell walls contain a mix of R-form and S-form LPS molecules. [4]

Besides initiating the inflammatory response and thus inducing sepsis, S-LPS directly affects ionic channels of immune, neuronal and cardiovascular cells. [5-7] Direct modulation of cardiac ion channel function by LPS possibly contributes to cardiovascular dysfunction under septic conditions leading to severe complications like atrial fibrillation. [8,9] Recently, it has been shown that S-LPS causes a decrease in the L-type calcium current and an increase in the delayed rectifier potassium current (most likely attributable to nitration of ion channels) in guinea pig atrial cells. Consequently, action potential duration was shortened, which in turn could be one of the possible mechanisms underlying atrial tachyarrhythmia in sepsis. [10] S-LPS also impairs the function of hyperpolarization-activated cyclic nucleotide-gated channels (HCN). [11,12] This ion channel family comprises 4 members (HCN1 - 4) which are expressed in the heart and nervous system and are activated upon hyperpolarization and regulated by intracellular

cAMP. The mixed Na^+ and K^+ current carried by HCN channels is called pacemaker current and contributes to the diastolic depolarization phase of the sinoatrial action potential. The pacemaker current is enhanced by adrenergic agonists and decreased by muscarinic agonists, both mediated via cAMP. Therefore, the pacemaker current plays a key role in the autonomic heart rate regulation. [13] The pacemaker current has been shown to comprise two current components. First, a time- and voltage-independent component referred to as instantaneous current or I_{inst} and a voltage- and time-dependent current referred to as I_f. [14] The role of I_f in cardiac pacemaking has been extensively studied, but the physiological role of I_{inst} and its ionic nature are still a matter of debate. However, I_{inst} is discussed to contribute to a stable pacing rhythm in autorhythmic cardiac cells. [15,16]

In S-LPS incubated human atrial myocytes (6 h incubation time) I_f was suppressed at membrane potentials positive to -80 mV, slowed current activation and caused a shift to more negative membrane potentials in the voltage-dependence of steady-state activation. [12] Similar results were proved for the acute application of S-LPS: a negative shift in the voltage-dependence of steady-state activation, the reduction of maximal conductance and faster channel deactivation within seconds after application. Furthermore, it has been shown that the O-chain of the LPS molecule is responsible for the acute effect of S-LPS on I_f, whereas for the inflammatory response the lipid A moiety is required. [11] Up to now no data are available about the LPS effect on I_{inst} and the mechanism of LPS action on I_f is scarcely understood.

Therefore, this study was designed to investigate the effect of S-LPS and mutant LPS lacking O-chain (R595) on both, I_f and I_{inst} under acute and chronic conditions – which constitutes the first aim of the present study.

Due to its important function of regulating pacemaker activity HCN channels have become an interesting therapeutic target for lowering heart rate as required in the treatment of chronic and acute heart failure. [17] Ivabradine, a novel heart rate lowering agent, selectively blocks I_f in a concentration- and use-dependent manner. Hence, it decreases the slope of the spontaneous diastolic depolarization phase and consequently the action potential firing rate of the sinoatrial node. [18] At higher concentrations (10 µM) ivabradine was reported to decrease the L-type calcium current and the delayed outward potassium current in rabbit sinoatrial node cells. [19] Furthermore, a significant

prolongation of the repolarization phase of action potentials in human cardiac preparations (papillary muscle) and dog Purkinje fibers was observed. [20] In isolated human cardiomyocytes ivabradine induces a concentration- and use-dependent I_f-inhibition with an IC50 of 2.9 µM at steady-state independently of the presence or absence of cAMP. [21] Reducing heart rate through ivabradine, which is lacking the negative inotropic effect, might also be beneficial to patients in septic conditions, as an elevated heart rate is correlated with an unfavorable prognosis. In 2010 the MOD*I*$_f$Y Trial [22] has been launched to investigate the application of ivabradine in patients suffering from MODS which in most cases is caused by sepsis.

Therefore, it was our second aim to investigate the combined effect of ivabradine and LPS on the human pacemaker current components I_f and I_{inst} with regard to the structure of the LPS molecule and possible molecular mechanisms for LPS-HCN interaction. Experimental data were implemented in a sinoatrial computer cell model [23] to analyze *in silico* the effect of ivabradine under elevated endotoxin levels on the sinoatrial pacemaking activity.

B. BACKGROUND

B.1 Cardiac Excitability

The heart can be considered as an electrically driven mechanical pump with rhythmic series of contractions (systole), during which blood is driven out from the heart, and relaxations (diastole) during which the chambers of the heart refill with blood.

Rhythmic beating of the heart (60 to 80 beats/min at rest) is generated in a small area (leading pacemaker site) in a specialized tissue of the heart called the sinoatrial (SA) node, which is located in the right atrium at the insertion of the vena cava superior (Figure 1). The sinoatrial electrical signal, caused by spontaneous action potentials (AP) of cardiomyocytes, spreads via the crista terminalis across the working myocardium of both atria and reaches the atrioventricular (AV) node that conducts the electrical impulse to the ventricles of the heart. From the AV node the signal is conducted to the bundle of His, which then branches into the right and the left bundle brunch (the so called Tawara-Schenkel). These fibres lead to the Purkinje fibres whose cardiomyocytes conduct the excitation impulse nearly simultaneously to the entire myocardium of both ventricles which therefore contract at the same time.

Besides the SA node, also the AV node and all other parts of the electrical conduction system of the heart have the ability to generate automaticity, serving as a back-up system in case the SA node fails, although their beating frequency is much less compared to the sinoatrial beating rate.

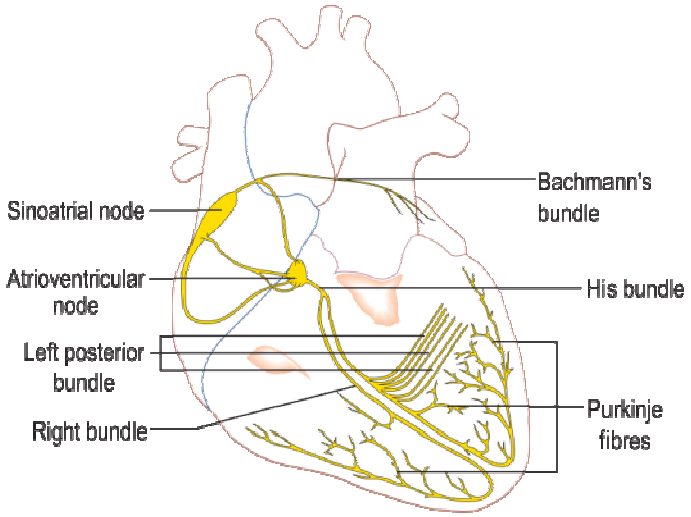

Figure 1. Electrical conduction system of the heart.
Explanations can be found in the text. Figure from Madhero 88. [24]

However, sinoatrial firing suppresses other spontaneously active tissue by a mechanism called overdrive suppression thus making the healthy heart beat in sinus rhythm.
The bases of excitation processes in excitable cells are ion channels, whose activity generates and modulates the activity of the heart.

B.1.1 Cardiac Ion Channels

Membrane ion channels are the prerequisite for the excitability of cells. In this section a short overview on ion channel families, their molecular structure, main function and biophysical properties is given. In a later chapter *The membrane clock - ion channels in the sinoatrial excitation process,* more precise descriptions of channels contributing to the sinoatrial AP will be given. As the majority of ion channels in the excitation process is gated by voltage signals, emphasis is placed on the superfamily of voltage-gated ion channels.

"Ion channels bear the same relation to electrical signaling in nerve, muscle and synapse as enzymes bear to metabolism. Although their diversity is less broad than that of enzymes, there are many types of ion channels working in concert, opening and closing, to shape the signals and responses of the nervous system. Sensitive but potent amplifiers, they detect the sound of chamber music and guide the artist's paintbrush, yet also generate the violent discharges of the electric eel or the electric ray. They tell the paramecium to swim backward after a gentle collision, and they propagate the leaf-closing response of the Mimosa plant." [25]

The beating heart is the result of the tight collaboration of cardiac ion channels, which shape the signal of constantly arising APs that keep our heart beating throughout our entire life. About 100 000 beats per day and up to three billion times throughout our whole life, the healthy heart pumps blood through the human body. Considering that the motor of all these rhythmic contractions are pacemaker cells that generate APs, which in turn are a result of ion currents that flow across the cell membrane, it is very well understandable that this field of research often gives the chance to be fascinated and amazed. Elucidation of the structure and function of ion channels explain how these ion channels open and close and also how they are regulated in health and disease. [26]

When ion channels evolved is not known, but cell membranes are thought to have first

existed more than three billion years ago. [25] Therefore, it was necessary that new transport mechanisms across this membrane evolved as well. The function of these transport devices has been a matter of research for a long time and is still of interest. In the field of physiology, bioelectric effects have been known for a long time, for instance, the activity of the electric eel. In the 18th century Luigi Galvani and Alessandro Volta carried out experiments on the connection between electricity and muscle contraction in frogs and other animals. Measuring bioelectric signals is of huge relevance in modern clinical medicine. Signals of the brain and the heart can be measured by the means of electroencephalography (EEG) and electrocardiography, just to name two examples. The origins of these electric signals are ionic currents flowing through ion channels in cell membranes.

Excitation and electrical signaling requires the flow of charge (ions) through ion channels. Sodium (Na^+), potassium (K^+), calcium (Ca^{2+}) and chloride (Cl^-) are the main charge carriers and therefore account for almost all the signaling events. Ion channels are transmembrane spanning proteins that contain ion selective pores, which favor the passage of one ion species. The current flow through ion channels does not require energy expenditure but happens down the electrochemical gradient of the specific ion species.

Gating behavior of ion channels

The channel's response according to the stimulus is a property called gating, which means opening or closing of the ion channel. Ion channels switch between open and closed states at specific rates and therefore show time-dependent properties. [26] Each channel represents an excitable element reacting to a specific stimulus that forms the basis for the classification of ion channels: Reactions on membrane potential changes, chemical stimuli and mechanical deformations, to name some examples, split ion channels in voltage-gated, ligand-gated (or receptor-operated) and mechano-sensitive ion channels. Most ion channels that contribute to the cardiac AP are voltage-gated, with Na^+, Ca^{2+} and K^+ ions serving as the primary charge carriers. Also ligand-operated potassium channels like $I_{K,ACh}$ and $I_{K,ATP}$ contribute the cardiac AP.

Furthermore, gap junction channels allow the exchange of molecules and ions between neighboring cells and are gated by voltage as well as the concentration of certain molecules in the cellular environment. [27]

The process of gating can be understood as a change of the channel protein conformation that consequently permits or prevents ion flow. Gating is a very complex phenomenon and not well understood. To keep it simple, ion channels can be in the closed, open or inactivated state. In the closed and in the inactivated state no ions can pass the channel pore. Inactivation (the term is used for voltage-gated channels, for ligand-gated it is called desensitization) means, that despite lasting gating signal, the ion channel inactivates and no ion can pass. This inactivation period is crucial for the refractory period of excitable cells. Deactivation means closing due to the removal of the gating signal. Different ion channels are thought to switch between different numbers of states as well as different transitions between these states – which causes the high degree of complexity in ion channel gating. Possible transitions are depicted below:

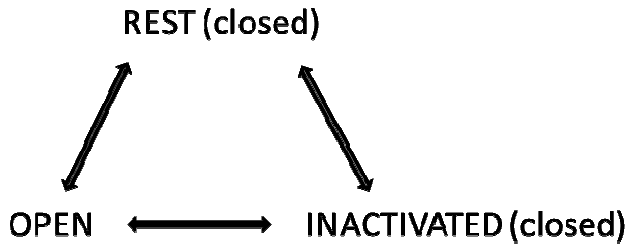

Figure 2. Possible transitions of ion channels.

In the early 1950s, Hodgkin and Huxley authored a pioneering work on the ionic basis of the AP of the giant squid axon. In their model, the activation of the fast sodium current initiates the AP and so the model is focused on the sodium current. Their theory still helps to understand the ion channel gating mechanism. In the model two kinds of gates regulate the ion flow through the sodium channel: First, the activation gate (m-gate) that consists of three m-gates which interact in a cooperative manner. The m-gate is located close to the extracellular space. Second, the h-gate (inactivation gate) that is located at the intracellular side of the channel (Figure 3). These polypeptide gates are part of the channel protein and undergo conformational changes in response to a change in membrane voltage. At the resting potential (ventricular cardiomyocyte about -90 mV) the sodium channel is closed. In this configuration the m-gate is closed and the h-gate is open. The m-gate rapidly opens in response to the voltage stimulus and allows sodium ions to pass. As the m-gate opens, the h-gate starts closing. The differences in opening and closing rates of these two gates

allow sodium to briefly enter the cell. This inactivated state persists throughout the repolarization phase, and near the resting potential the h-gate opens and the m-gate closes which brings the channel back to its closed, resting state. The m-gates close more rapidly than the h-gate opens, once the cell has repolarized. Full recovery of the h-gates can take 100 ms or longer after the resting potential has been restored. [28] This explains the crucial difference between the closed and the inactivated state: In the inactivated state the h-gate can be opened only after repolarization has returned the membrane potential to its resting level. It can be clearly seen, that ion flux through the channel pore requires the open state of all gates. These open and closed states due to activation and inactivation gates can also be found in calcium and potassium channels although they are labeled in a different manner.

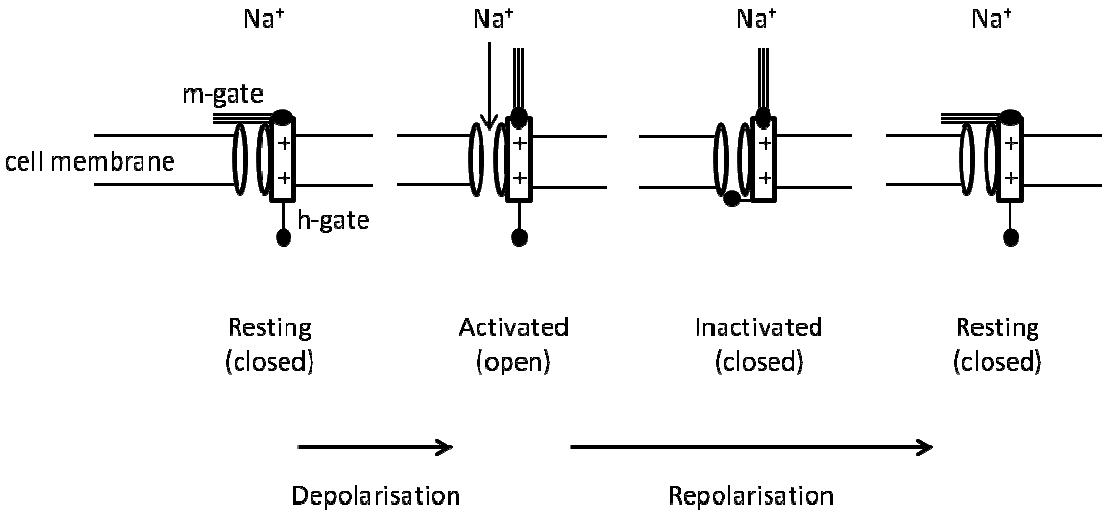

Figure 3. Open and closed states of the fast sodium channels.
Model based on the historical work of Hodgkin and Huxley. Three activating (m) gates and one inactivation (h) gate cause the three states of the channel: Open, closed and inactivated. Figure based on Jalife et al., 1999 [27] and Klabunde, 2011. [28]

Hodgkin and Huxley developed equations which predict that the sodium current is determined by the maximal channel conductance g_{Na}, which is a function of m and h and the electromotive driving force which is defined as the difference between the actual membrane potential V_m and the equilibrium potential for Na, E_{Na} (for more information see the chapter *The Origin of the Membrane Potential*). 'm' is a coefficient of channel opening

and 'h' is a coefficient of channel closing. [26] Thus, the equation that describes the voltage- and time-dependent gating mechanisms responsible for the sodium current is given as

$$I_{Na} = m^3 h g_{Na} \times (V_m - E_{Na})$$

Although subsequent work in the field of electrophysiology showed limitations of the Hodgkin and Huxley model, their work was invaluable in the understanding of ion channel gating and in the development of later models on gating behavior and cardiac excitation. [27]

Gating currents: The process of gating is controlled by the electric field that exerts a direct action on charges that are part of or associated with ion channels such as h or m particles. [25] The relevant charges are called gating charges or voltage sensor. Hodgkin and Huxley pointed out that this movement of charged gating particles must be possible to be measured in experiments as small currents that would precede the ionic currents. Gating currents were indeed measured from the 1970s on and are now an important tool for describing voltage-gated ion channels. [25] In the case of sodium channels, gating currents are now known to be elicited by movements of positively charged regions in the S4 segment (the voltage sensor of ion channels, Figure 5) of the sodium channel that correspond to the m-gate stated by Hodgkin and Huxley. [26]

Ion selectivity: Ion channels are capable of discriminating between various ion species. This is rather challenging when considering the high flow rate of ions through the channel pore that ranges somewhere around 10^6 ions per second. One mechanism might be steric hindrance since the outer mouth of a channel has a very small diameter of about 0.3 × 0.5 Å for the sodium channels and 0.3 × 0.3 Å for the potassium channels. Therefore, ions with larger diameter are rejected by steric hindrance. It is obvious that this mechanism cannot be the only one responsible for ion selectivity as very small ions would pass every channel. Another mechanism might be the binding of ions to a special site within the channel pore, thereby preconditioning the permeation of ions. Energy considerations favor the binding of one ion species over the other. [27] Ion species that bind with higher affinity cannot be displaced by ions that bind with lower affinity. Consequently, bound ions exclude other ion species by electrostatic repulsion. [26]

The structure of plasma membrane ion channels

Investigations on the molecular structure of ion channels have shown that several of these macromolecules are products of closely related genes and therefore imply closeness in ancestral origin. [27]

Ion channels consist of subunits and domains: Since mainly voltage-gated ion channels account for the cardiac excitation process, special emphasis is placed on this gene superfamily.

Voltage-dependent ion channels are membrane-spanning protein complexes with water-filled pores that allow ions to pass through the hydrophobic lipid bilayer. Ion channels can comprise several subunits which are named α, α_1, α_2, β, γ and δ.

The principal/major subunit is the α- (for the sodium and the potassium channel) or the α_1-subunit (for the calcium channel), which has a full linear sequence of 1800 to 4000 amino acids, terminated by a NH_2 group on the one end and a COOH-group on the other end. This major subunit accounts for all defining properties of the voltage-gated channels such as the characteristic toxin-binding sites, the pore, gates and also the voltage sensor. [25] The other channel subunits are referred to as auxiliary or regulatory subunits. Constantly, progress on the knowledge on ion channel subunits is made, and plenty is known about the α-subunits, but the function of the other subunits is not well understood. It is known that the varying coexpression of subunits alters the ion channel's biophysical properties. Furthermore, the specific composition of subunits varies according to the cell type and the body region in which they are expressed.

In most voltage-gated ion channels the ion-selective pore is surrounded by the large major subunit. [29] In sodium, potassium and calcium channels the α- or α_1-protein subunit consists of four domains (I, II, III, IV), as depicted in Figure 4A. Only in sodium and calcium channels these domains are covalently linked. In sodium, calcium and the majority of potassium channels, each of the four domains of the α- or α_1-subunit contains six α-helical transmembrane segments, designated S1 to S6, see Figure 4B. These six segments are organized in a specific way: S5 and S6 segments, along with intervening peptide chains edge the water-filled pore that allows ions to pass the hydrophobic cell membrane. Therefore, the region between S5 and S6 is known as the P-region (P for pore). S1, S2 and S3 mediate interactions between the ion channels and membrane lipids. [26] The S4 segment is the so-called voltage sensor that is equivalent to the previously introduced

activation- or m-gate. This α-helical ribbon contains positively charged arginine and lysine residues that pair up with the negative charges in the S1, S2 and S3 segements thereby forming the voltage sensor. The short segment linking S6 of domain III and S1 of domain IV could possibly represent the inactivation gate. Regions that surround these segments may form a hinged lid (h-gate) that could occlude the channel pore. [26]

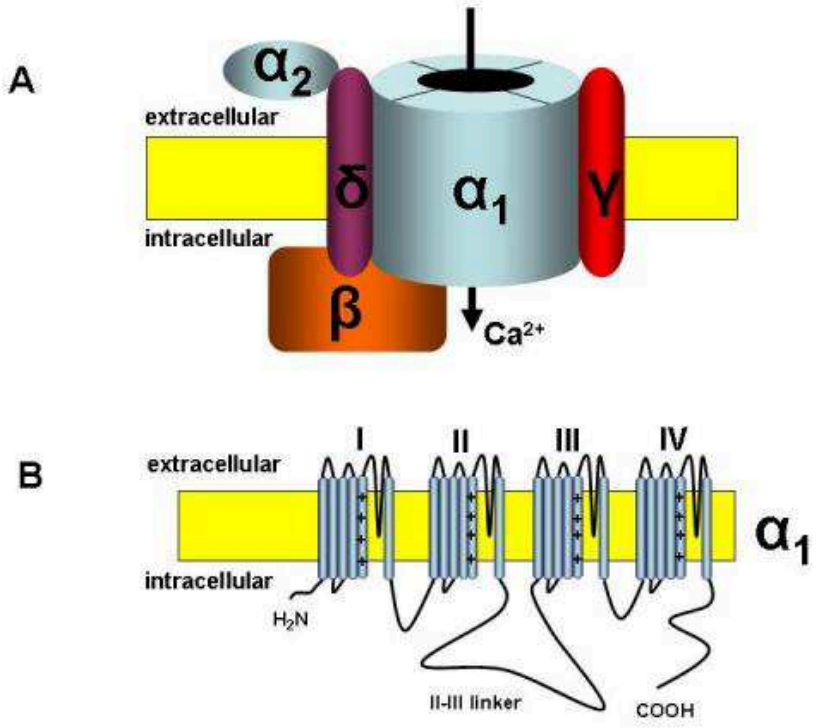

Figure 4. Structure of a voltage-gated calcium channel.
Auxiliary subunits **(A)** coassemble with the α-subunit **(B)** to form a functional pore. Figure from Iftinca et al., 2011. [30]

The α-subunit of the sodium channels contains binding sites for TTX (tetrodotoxin) and STX (Saxitoxin). TTX can be found in Tetraodontiformes, a marine order including the puffer fish and the balloon fish. STX can be found in shellfish that feed on dinoflagellates (a group of algae). Both toxins have been largely used to study the function of excitable membranes and nerves. Additionally, the α-subunit is a substrate for PKA, the Protein-kinase A, whose activity depends on intracellular cAMP levels and regulates cellular events by phosphorylation of substrate proteins, here ion channels. Mainly, activity of the PKA mediates sympathetic stimulation to electrophysiological and mechanical

responses. [26]

Ion channel subtypes

Ion channels belong to a family of proteins that most likely had a common ancestor. This ancestor was probably a monomer similar to one of the four domains composing the here described major subunit of ion channels. From this gene, encoding this primitive ancestor, two classes of voltage-gated channels evolved. One class contains the non-covalently linked potassium channels and the cyclic nucleotide-gated channels. Their opening is regulated by cAMP or cGMP and voltage. The other class is made up by calcium and sodium channels. At the beginning of the Cambrian period (540 to 480 billion years ago) when multicellular organisms rapidly evolved, calcium channels gave rise to sodium channels. These channels generate large APs that are much faster than the calcium-dependent APs. Therefore, sodium channels are found nearly exclusively in multicellular organisms whose survival depends on fast reactions towards external stimuli and fast communication between different regions of their bodies. [26]

Nomenclature of ion channels: The first naming of ion channels was based on the biophysical work on membrane permeability, pharmacology and permeating ions. Hodgkin and Huxley classified three different components of current, which they named sodium, potassium and leakage, in their principal work about ionic currents in the giant squid axon. Thirty years after their great work a new way of channel classification became possible: Molecular genetics enabled the cloning and sequencing of channel genes. A large number of channel genes are now known and many more subtypes exist than the electrophysiological approach was able to distinguish. For sodium, potassium and calcium channels there are more than 100 identified genes in a mammal like the rat or in the nematode *Caenorhabditis elegans*. [25] Therefore, it is challenging to find a nomenclature for all these ion channel genes. First, naming ion channels corresponding to the major permeating ion appears reasonable but in fact, there are ion channels that are not selective to only one ion species. Furthermore, there are channels whose permeating ion is not known. Furthermore, some kinds of channels share the same ion species which also makes it impossible to use the ion species as a tool to name them. Groups of investigators were and are challenged to develop a systematic approach based on the channel sequence that allows structural and evolutionary relationships to form the basis for the classification. [25]

The beginning of this naming system was a numbering of mammalian voltage-gated potassium channels: Kv1.1, 1.2, and so on. The IUPHAR, the International Union of Pharmacology formalizes new naming systems for receptors, channels and drugs. In this database, accepted names and such that are still awaiting approval from reviewers are listed. Ion channels are divided into the major divisions voltage-gated (VGIC) and ligand-gated ion channels (LGIC) and the following names for VGIC were stated in the database at the time of writing in August 2014 [31]:

- VGIC
  - CatSper and Two-Pore channels: CatSper1-4, TPC1, TPC2
  - Cyclic nucleotide-regulated channels: CNGA1-4, CNGB1, CNGB3, HCN1-4
  - Potassium channels
    - Calcium-activated potassium channels: $K_{Ca}1.1$, $K_{Ca}2.1$, etc.
    - Inwardly rectifying potassium channels: $K_{ir}1.1$, etc.
    - Two-P potassium channels: $K_{2P}1.1$, etc
    - Voltage-gated potassium channels: $K_v1.1$, etc., KCNQ-family, EAG-family (including herg-channels)
  - Transient Receptor Potential channels: TRPC, TRPM, TRPV, TRPA, TRPP and TRPML
  - Voltage-gated calcium channels: $Ca_v1.1$, etc.
  - Voltage-gated sodium channels: $Na_v1.1$, etc.
- LGIC
  - 5-HT_3 receptors
  - $GABA_A$ receptors
  - Glycine receptors
  - Ionotropic glutamate receptors
  - Nicotinic acetylcholine receptors
  - P2X receptors
  - ZAC

Other ion channels (non VGIC and non LGIC) include: aquaporins, chloride channels, connexins and pannexins, sodium leak channel (non-selective).

The structure and function of sodium channels: In 1984 the primary sequence and the supposed membrane topology of the voltage-gated sodium channel was described. This was the first insight into the structure of voltage-gated channels. [27] The described α-subunit counted 260-289 kD, depending on the kind of tissue. This principal subunit was associated with zero to four beta-subunits (β_1 to β_4) with between 30 and 40 kD. [27] The principal structure is similar to that of a voltage-gated calcium channel with a major

exception: The sodium channel comprises only α- and β-subunits (Figure 5).

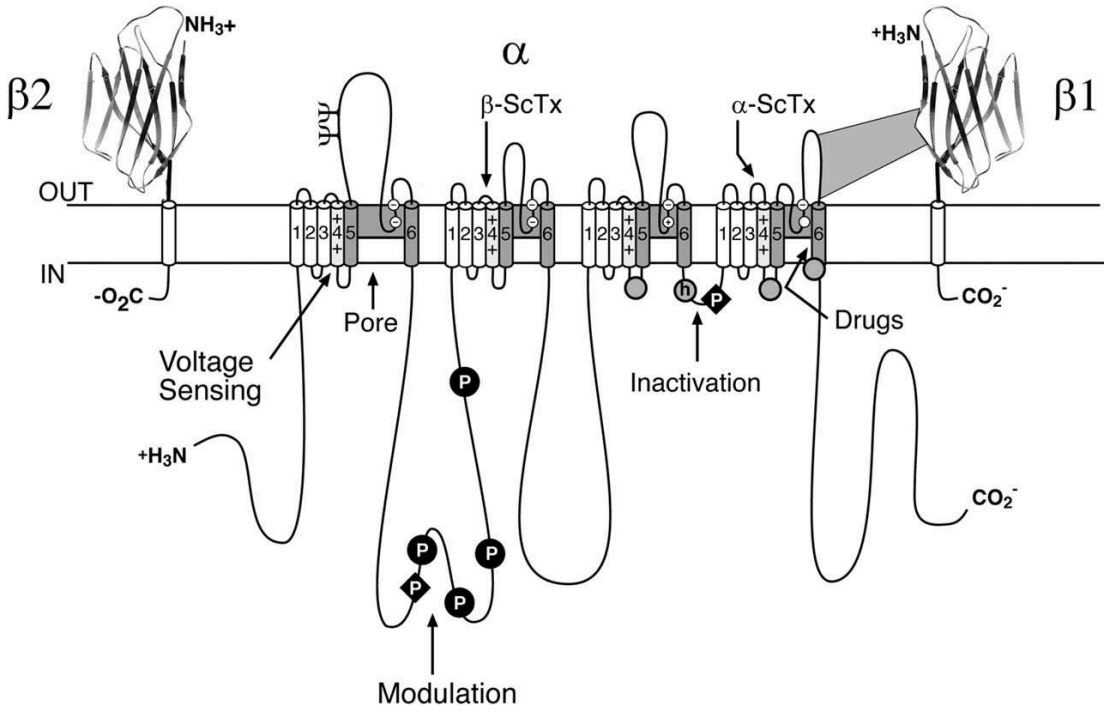

Figure 5. Subunit composition of a voltage-gated sodium channel.
P demonstrates protein phosphorylation sites by protein kinase A (circles) and protein kinase C (diamonds). Figure from the IUPHAR database. [31]

Sodium channels take part in the initiation and propagation of APs in excitable cells. This channel type is also found in non-excitable tissue, but its function is not clear.

The structure and function of calcium channels: Native calcium channels are formed by five subunits, α_1, α_2, β, γ and δ. The α_1-subunit is made up by four homologous domains each consisting of six transmembrane segments including one P-loop each, as can be seen in Figure 4. Similar to the sodium channel the α_1 subunit forms the ion channel pore and contains the phosphorylation site for PKA. The α_1 subunit has an apparent mass of 212 kD, α_2 of 140 kD. The hydrophobic transmembrane δ subunit has a mass of 27 kD and is linked to the extracellular α_2 subunit by a disulfide bond. The intracellular β subunit has a mass of 54 kD and is a substrate for multiple protein kinases. The γ subunit with 30 kD has several N-linked glycosylation sites. Still, the function of these subunits is not well understood. [26]

There are many calcium channel subtypes and the structure of all members of this family is not known, but these membrane proteins are homologous to each other and to the extended family of tetrameric voltage-gated plasma membrane ion channels. [26]
Calcium channels play pivotal roles in the skeletal and smooth muscle and heart excitation-contraction coupling, in the cardiac pacemaker activity and transmitter release from neuronal cells.

The structure and function of potassium channels: Cardiac potassium channels were probably present together with tetrameric calcium channels in the common ancestor of protozoa, green algae and green plants and are considered to be the most primitive form of voltage-gated ion channels. [26] They can be found in simple organisms like protozoa, coelenterates and ctenophores. Although these channels can be found in primitive animals, they are still very complex structures and are encoded by a variety of genes. Potassium channels are tetramers of non-covalently linked domains and that's why they can assemble in homo- or heterotetramers. Each subunit of the potassium tetramer is equivalent to one domain of the Na^+ or the Ca^{2+} channel α-subunit. Therefore, this large family of genetically variable subunits allows the formation of many various kinds of channel subtypes. [26] Despite their diverse architectural structures they have common characteristics: Potassium channels share a pore-lining P-loop of consistent amino acid sequence, which is called the signature sequence of the potassium channel. In any case, four P-loops are necessary to form a functional pore. [32] There are three groups of potassium channels, classified according to their membrane topology and physiological characteristics (Figure 6)*:* 1) Voltage-gated (K_v) and calcium-gated (K_{Ca}) channels, which consist of 4 subunits that again comprise six or seven transmembrane segments. S4 forms the voltage sensor of these potassium channels. 2) Inward rectifying potassium channels (K_{ir}). Members of this family are the ACh-, ATP- and the G-protein coupled receptors which form channels by assembling to tetramers but each subunit consists of only two transmembrane segments. 3) The third family comprises members with two P-loops and four transmembrane segments in each subunit. Thus, these channels have two pores and are called K_{2P} potassium channels. They produce leak/background currents which contribute to the maintenance of negative resting potentials. [32] Auxiliary subunits (β-subunits) mostly supplement the channels. [25]

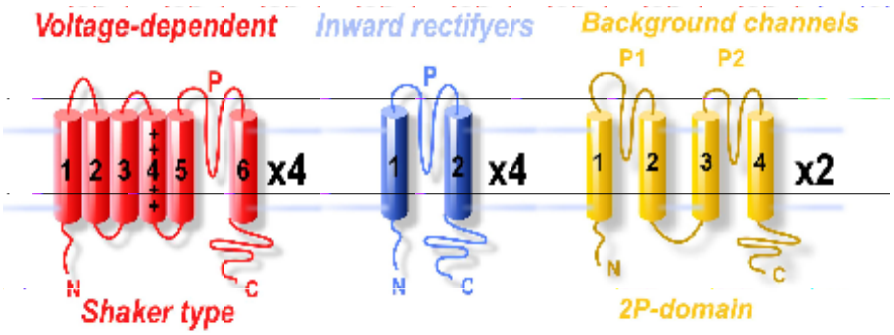

Figure 6. Structure of potassium channels.
From Sandoz et al., 2013. [32]

Figure 7 shows again the three types of potassium channels with their encoding genes and prominent representatives. The first group, the voltage-dependent potassium channels, includes hERG channels, Shaker-related potassium channels, calcium-activated potassium channels and KCNQ channels. These channels are activated upon depolarization. Native currents include I_{Kr}, I_{Ks}, I_{KTO}, I_{KUR}, BK_{Ca} and IK_{Ca}. [33] (I_{KTO} in Figure 7 is equivalent to I_{to} in the following sections.)

The second group, two transmembrane one-pore channels, is commonly known as inward rectifier potassium channels and is important in setting the membrane potential. This rectification is attributed to gating mechanism involving internal magnesium and polyamines which prevent the access of potassium ions to the inner vestibule of the channels. Native currents of this type include I_{K1}, $I_{K,ACh}$ and $I_{K,ATP}$. [33]

The third group is made up by four transmembrane two-pore channels that are also weak inward rectifier channels. Among all potassium channels this group might be the most abundant one, which was proven for at least the nematode *C. elegans*. [33]

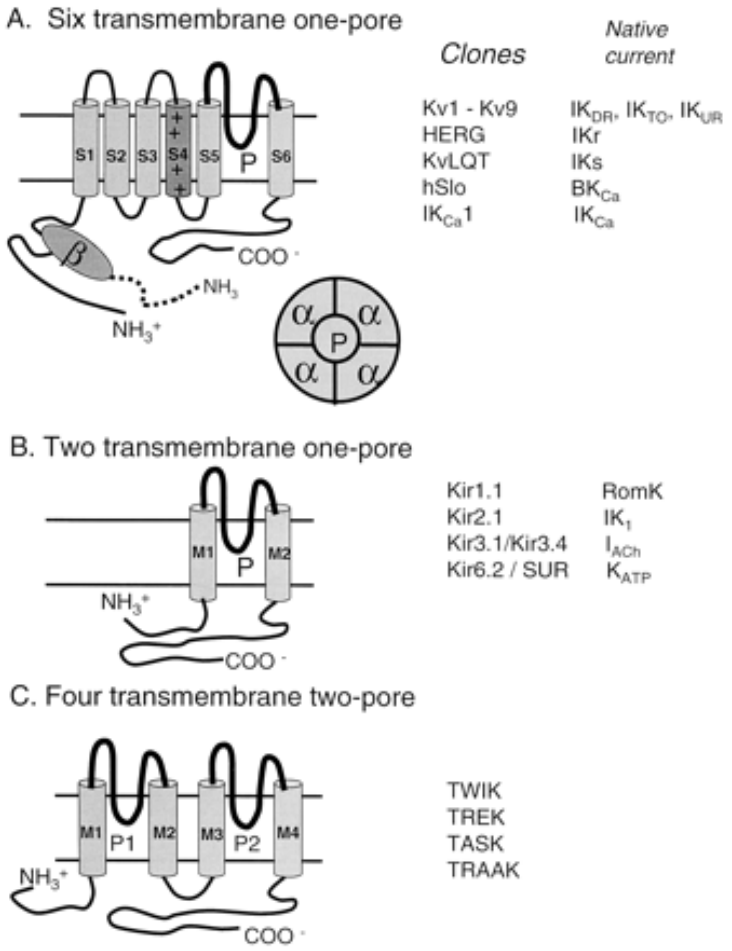

Figure 7. The categories of potassium channels and their representatives.
Figure from Shieh et al., 2000. [33]

Potassium channels are a ubiquitous family of membrane proteins, and they are present in excitable and non-excitable cells. Members of this diverse family play roles in cellular signaling processes thereby regulating neurotransmitter release, heart rate, insulin secretion, neuronal excitability, epithelial electrolyte transport, smooth muscle contraction and cell volume regulation. [33]

Potassium channels play an essential role in the "stabilization" (which is an old terminology) of the membrane potential. In excitable cells, potassium channels are responsible for the resting potential, for the repolarization after fast APs in order to keep it short, they time the interspike intervals during repetitive AP firing and generally lower the effectiveness of excitatory inputs on a cell. [25]

All channels together form the basis for the excitability of cells and are responsible for the generation of the resting potential and the AP, which are described in the following sections.

B.1.2 The Origin of the Membrane Potential

The cell membrane (Figure 8), a lipid bilayer, forms a barrier to separate and protect the interior of the cell from the outside environment. Membrane proteins account for signal transmission and transport of ions and molecules through the membrane. The precondition for the excitability of cells are the electrical properties of its membrane deriving from its lipids and proteins, among them ion channels and transporters.

For understanding the functioning of excitable cells, it is essential to deal with fundamental rules of electricity because cell membranes can be pictured as capacitors, and membrane spanning ion channels as resistors. Therefore, they build a parallel RC circuit together and Ohm's law can be applied to describe the electrical activity of cell membranes.

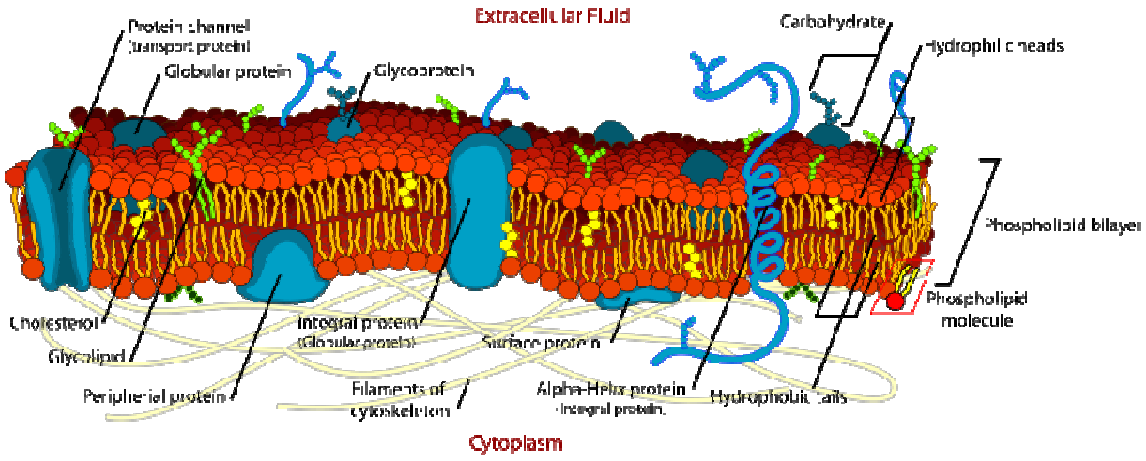

Figure 8. Cell membrane of a eukaryotic cell.
Water, gases and small nonpolar molecules can diffuse freely across the lipid bilayer, but charged ions and large molecules like proteins require various transport systems. Figure from Mariana Ruiz. [34]

Ohm's Law – a relation between current, voltage and conductance

Before introducing Ohm's law a few basic terms are explained:

Charge: "All matter is made up of charged particles". [25] Electricity is the result of charged particles of opposite sign that attract each other. Most bodies are electrical neutral because negatively and positively charged particles equalize each other. A mole of any ion contains Avogadro's number ($N = 6.02 \times 10^{23}$) of particles. The quantity of charge is measured in coulombs (C). The elementary charge, which is determined by the charge of a

proton, amounts to $q_e = 1.6 \times 10^{-19}$ coulomb. The Faraday constant F is the amount of electric charge per mole of charged particles and therefore calculated by $F = N \times q_e = 6 \times 10^{23} \times 1.6 \times 10^{-19} \approx 10^5$ C/mol. This is the charge of one mole of a monovalent cation, for divalent cations the charge of one mole of the respective ion is $2F$. The charge of a mole of a monovalent anion is $-F$, of a divalent anion $-2F$. [25]

Current: If charges of opposite sign are separated or move independently, electrical phenomena arise. If a positively and a negatively charged electrode (anode and cathode, respectively) are placed within a conductive medium, charge flows from one to the other along the gradient. Any net flow of charge is called current, which is defined as the magnitude of the charge moving through a cross section per unit of time, [27] and is measured in amperes (A), with one ampere corresponding to a steady flow of one coulomb per second. [25] Ions constantly travel across membranes via ion channels thus creating an ionic current. Ion channels can be understood as electric resistors that connect intra- and extracellular spaces and determine the magnitude of the current by their conductance. By convention, inwardly directed ionic currents show a negative sign, outwardly directed currents a positive one. Currents measured by electrophysiological equipment range from picoamperes to microamperes. There are two regulating factors to determine the size of the current: The potential difference between the two electrodes and the conductance of the solution between them.

Potential difference: Charged particles cause an electric field in which other particles are subjected to an attracting or repelling force. The work necessary to move a unit test charge from point "A" to point "B" in this electric field is called potential difference or voltage. One joule of work is needed to move one coulomb of charge across a one volt potential difference. Transmembrane potentials are generated when charges accumulate unequally across the cell membrane. [27] The cell membrane is a good insulator, therefore the voltage difference persists if charges are not conducted through the membrane via open pores or channels. In animal cells membrane potentials between -30 and -90 mV can be measured (minus because negatively charged ions accumulate at the cytoplasmic side of the cell membrane compared to the outside). In plant cells much higher membrane potentials can be found, amounting up to -200 mV.

Conductance and resistance: Electrical conductance is a measurement for the ease of

flow of current between two points with the SI unit of siemens (S). Ohm's law expresses the relation between current (*I*), conductance (*G*) and potential difference (*V).*

$$I = GV$$

The inverse of conductance is called resistance (*R*) and is measured in ohm (Ω) with 1 Ω = 1 V/A. Correspondingly, Ohm's Law can be written as

$$I = \left(\frac{1}{R}\right)V$$

or

$$R = \frac{1}{G} = \frac{V}{I}$$

In electrophysiology it is convenient and common to talk about conductance instead of resistance in order to determine the total flow of current, because side-by-side conductance sums up and the total conductance is the collective conductance of all open channels. The conductance of biological membranes results from embedded ion channels, selectively allowing charges (ions) to pass.

Ohmic resistors show a linear relationship if current is plotted as a function of voltage (*I-V* relation(ship) = current-voltage-relationship). Their behavior is independent of voltage and time and follows Ohm's law. The time course of the change in current is similar to the time-dependence of the change in voltage.

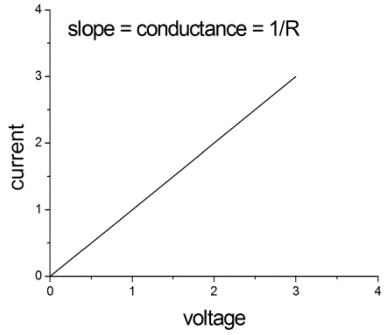

Figure 9. *I-V* relation of an ohmic resistor.

Non-ohmic resistors do not follow Ohm's law. Voltage and current are not proportional to each other. The resistance is not constant but depends on the current flowing through the resistor. Therefore, the slope of the *I-V* relation changes with voltage. Rectification is one example of the behavior of a non-ohmic resistor: Some cardiac ion channels are rectifier channels. That means that current can e.g. pass more easily in the inward than in the outward direction (inward rectifier) thus showing inconstant resistance of the channel. There are two possibilities to calculate the conductance of such channels. The first approach is to determine the slope resistance, which happens by calculating the slope line which is tangential to the *I-V* relation at a certain point. [27] Figure 10 shows a red dashed tangential line at a voltage of -50 mV, which represents the slope conductance. The inverse is the slope resistance of this channel at this voltage. It is clearly visible that the conductance of this channel varies in dependence of the voltage.

The other possibility to determine the conductance of a non-ohmic resistor is to calculate the chord resistance, which is shown as a green line in Figure 10. A line is drawn between two points (A and B) and the resistance is measured from the slope of this line (= chord). In ohmic resistors slope and chord conductance are the same. [27]

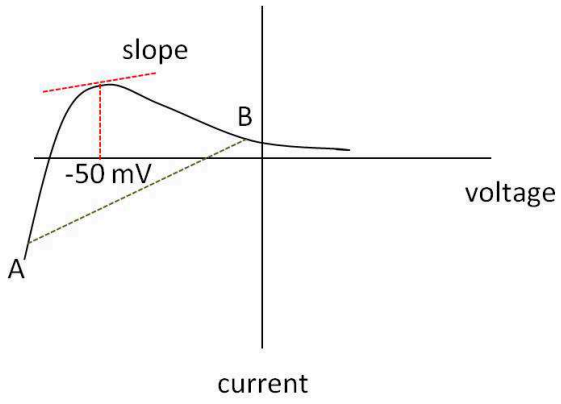

Figure 10. *I-V* relation of a non-ohmic resistor, here an inward rectifier channel.
Figure based on Jalife et al., 1999. [27]

Time Dependence: In the resistors mentioned above, the amplitude of a current varies instantaneously in response to a change in voltage. Additionally, the current evoked by a certain voltage change can also vary as a function of time. For instance a sudden voltage

change causes an increase in current that still continues even if the voltage is held constant, as can be seen in

Figure 11. This is due to intrinsic properties of the resistor, that allows the passage of varying amounts of current as a function of time. [27]

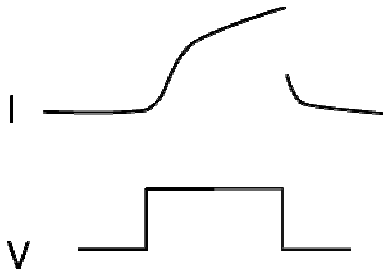

Figure 11. Example of a time-dependent current.
The ability of the conductor to pass current changes with time. While the voltage is held constant after a sudden voltage change, the current amplitude still increases. Figure based on Jalife et al., 1999. [27]

Resistivity: Homogenous conducting materials possess a material property called resistivity (rho, ρ), which is the resistance measured by two 1 cm^2 electrodes applied to opposite sides of a 1 cm cube of material. [25] The dimension of resistivity is ohm × cm and tells how strongly current passing through a given material is opposed.

$$R = \frac{\rho l}{A}$$

In saline solutions pure phospholipid bilayers show a resistivity of 10^{15} Ωcm. The electrical conductivity derives from embedded ion channels. Indeed, ions could move in the lipid, but they prefer the aqueous environment surrounding the lipid bilayer. Therefore, conductivity comes with ion channels. [25]

To sum up the mentioned principles of electrophysiology: If 1 volt is applied across a 1 Ω resistor or a 1 S conductor, a current of 1 ampere (=1 C/s) is flowing; with every second 1/F moles of charge flow (10.4 μM) and 1 joule (0.24 calories) of heat is produced. [25] Ohm's law is of fundamental significance and helpful in order to understand ion channels

as membrane spanning conductors and the cell membrane itself as a capacitor, as described in the following section.

The membrane as a capacitor

The cell membrane, a thin lipid bilayer, separates intracellular and extracellular conducting solutions. Therefore, the cell membrane is equivalent to a parallel plate capacitor, which is formed when two conducting materials are separated by a thin layer of non-conducting material (insulator or dielectric). Capacitors offer the possibility to store electric charge.
For generating a potential difference across this insulator a separation of charges must be established: On one side an excess of positive charge versus an excess of negative charge on the other side is setting up the potential difference. Capacitance (C) tells how much charge (Q) has to be transported from one conductor to the other to set up a given potential difference and is expressed by

$$C = \frac{Q}{V}$$

Capacitance is a measure for the amount of charge that can be stored in a capacitor at a given voltage. The amount of charge that a parallel plate capacitor can store, is directly proportional to the potential difference, and depends on the size of the plates and the distance between the two plates.

Capacitance is measured in farad (F). If the plates of a 1-F capacitor are charged to +/-1 C, respectively, a potential difference of 1 V is generated.
If a potential difference is imposed to the capacitor in an electrical circuit charge travels towards the cathode till it reaches the capacitor. Since there is the dielectric between the two plates, positive charge collects at the plate closer to the anode till a steady –state condition is reached and no current is flowing. When the voltage difference is switched back to zero charges flow in the opposite direction and the capacitor is discharged. Correspondingly, a negative capacitive current is observed. Hence, in an ideal capacitor the passage of current removes charge from one conductor and shifts it to the other – a fully reversible process. [25]
The rate of change of voltage under a current I_C can be calculated by taking the time derivate of the equation expressing capacitance ($C = Q/V$):

$$\frac{\mathrm{d}V}{\mathrm{d}t} = \frac{I_C}{C}$$

The capacitive current (I_C) is expressed as

$$I_C = C\frac{\mathrm{d}V}{\mathrm{d}t}$$

As the capacitance of the cell membrane, equivalent with a parallel-plate capacitor, depends on the distance between the two plates and the area (A) of the plates, the capacitance can be calculated by

$$C = \frac{\varepsilon\varepsilon_0 A}{d}$$

d thickness of the insulator (cell membrane)

ε dielectric constant of the insulator

ε_0 natural constant = dielectric constant of the vacuum = 8.85×10^{-12} $CV^{-1}m^{-1}$

1 cm^2 of a cell membrane shows a capacitance of around 1 µF, which is nearly equal to the capacitance of a pure lipid bilayer with 0.8 µF/cm^2. [25]

The parallel RC circuit

The cell membrane and the ion channels build an electrical circuit with a resistor and a capacitor in parallel (RC circuit), as depicted in Figure 12.

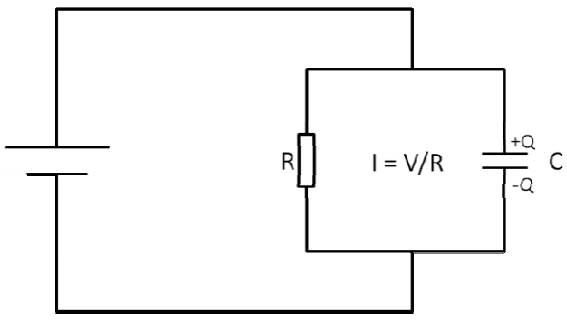

Figure 12. Cell membrane and ion channels as parallel RC circuit.

In this RC circuit the total current is equal to the sum of the current moving through the capacitor and that moving through the resistor, which is expressed in

$$I_t = I_C + I_R$$

The capacitance of the cell membrane determines how many ions must move ($C = Q/V$) and how rapidly they must move ($\mathrm{d}V/\mathrm{d}t = I_C/C$) to make a given signal. [25] The needed time to charge a capacitor in a RC circuit is proportional to the magnitude of the resistor and to the capacitance of the capacitor. The product of resistance and capacitance is called time constant tau τ and is calculated by

$$\tau = RC$$

Therefore, capacitance slows down the voltage response to any current by this characteristic time constant τ. Supposing a capacitor is charged to 1 V and then discharges through a resistor, this discharge is not instantaneous and the current in the resistor follows Ohm's law:

$$\frac{\mathrm{d}V}{\mathrm{d}t} = \frac{I_C}{C} = -\frac{V}{RC}$$

The solution of this first-order differential equation shows that voltage decays exponentially in time [25]:

$$V(t) = V_0 \exp\left(-\frac{t}{RC}\right) = V_0 \exp\left(-\frac{t}{\tau}\right)$$

V_0 starting voltage

t time in seconds

exp exponential function (power of e, base of the natural logarithm)

The time constant measures (usually in seconds) the duration $t = T_{1/e,}$ which an

exponentially decaying process needs to reach 1/e (≈36.8 %) of its starting value. An exponentially rising process grows by 63.2 % within this duration.

For biological membranes the product of capacitance and resistance is called membrane time constant = τ_M. Using the equation above the membrane time constant can be determined by measurements of the time course of membrane potential changes when small current steps are applied. Keeping in mind that the cell membrane capacitance amounts to ≈1 $\mu F/cm^2$ a measurement of τ_M allows an estimation of the specific membrane resistance. In various biological membranes τ_M ranges from 10 µs to 1 s, which corresponds to resting R_M values of 10 to 10^6 Ωcm^2. [25]

The generation of the membrane potential

All living cells are characterized through an unequal distribution of electric charge across their membranes. The inside of the cell is negatively charged compared to the outside, thus creating a voltage gradient. This voltage difference is called membrane potential and ranges between -50 to -100 mV in animal cells (plant cells from -50 to -200 mV).

The membrane potential is generated due to two conditions: First, differences in the ion composition between the intra- and the extracellular space and second, the selective permeability (conductance) of the plasma membrane acting as a barrier for ions. The (electrochemical) membrane potential is defined by the Nernst equation. For understanding this equation a vessel with two compartments can be imagined. The vessel is divided by a semipermeable membrane that allows only cations to pass. A solution of potassium chloride is placed in compartment 1 and both ions, potassium and chloride tend to move down their concentration gradient to compartment 2. But the membrane is only permeable for potassium, and so negative charge is left behind in compartment 1. Thus, two forces are created that counteract each other: The diffusional (=osmotic) force that pushes the potassium ions along their concentration gradient and an electric force that opposes the osmotic force since the positive side begins to repel potassium ions. The membrane potential builds up until finally an equilibrium value E_K (K for potassium) is reached at which the electric force opposing the potassium flow balances the osmotic force and the systems stops changing. [25] Calculating the **equilibrium potential** for a specific sort of ions can be done using the **Nernst equation**. But before having a closer look at this formula it is helpful to understand its derivation from a basic physical equation called the Boltzmann equation of statistical mechanics, that describes relative probabilities (p_1, p_2) at

equilibrium of finding a particle in state 1 or state 2 provided the energy difference between these states is $u_2 - u_1$. [25]

$$\frac{p_2}{p_1} = \exp\left(-\frac{u_2 - u_1}{k_B T}\right)$$

k_B is the Boltzmann's constant and T the temperature on the Kelvin scale. This equation tells that at equilibrium particles spend more time in states of lower energy than in states of higher energy. If substituting probabilities by concentrations (c) and single-particle energies to molar energies U, the equation can be written as follows:

$$\frac{c_2}{c_1} = \exp\left(-\frac{U_2 - U_1}{RT}\right)$$

With R being the gas constant that is defined with $R = k_B N$.

Taking natural logarithms of both sides transforms the equation into

$$U_1 - U_2 = RT \ln\frac{c_2}{c_1}$$

Now the equilibrium relation between energy differences and concentration ratios can be rearranged into membrane potential differences and one mol of an ion with the charge z_S. $U_1 - U_2$ then becomes $z_S F(V_1 - V_2)$.
The equation for the equilibrium potential (E_X) dependent on concentration and potential differences now is

$$E_{x.} = V_1 - V_2 = \frac{RT}{z_S F} \ln\frac{[S]_2}{[S]_1}$$

This important equation is called **Nernst equation**, and it relates numerical values of a concentration gradient that is balanced by an electrical gradient.
Correspondingly to physiological conventions side 1 is the intracellular side and side 2 is the extracellular side. Membrane potentials are always measured inside minus outside. The

Nernst equation can be written for all relevant ions that contribute to the membrane potential, examples for potassium and sodium are given (*o* stands for outside, *i* for inside):

$$E_{\mathrm{K}} = \frac{RT}{F} \ln \frac{[\mathrm{K}]_{\mathrm{o}}}{[\mathrm{K}]_{\mathrm{i}}}$$

$$E_{\mathrm{Na}} = \frac{RT}{F} \ln \frac{[\mathrm{Na}]_{\mathrm{o}}}{[\mathrm{Na}]_{\mathrm{i}}}$$

The equilibrium potential is also called zero-current potential since at this specific value no net flux of ions takes place. Another term for the equilibrium potential is reversal potential E_{rev} since at this specific membrane potential the current reverses direction regarding the flow of ions through the cell membrane (from inward to outward or the other way round). With measured reversal potentials and known ion concentrations the permeability ratios can be calculated.

In living cells the intracellular potassium concentration amounts to approximately 150 mmol/L in contrast to the outside potassium concentration that amounts to about 5 mmol/L. For sodium it is opposite, as can be seen in Table 1. Over time, on account of the constant sodium inward current and the resulting potassium outward current the concentration gradients for these ions would diminish. But an active transport mechanism establishes and maintains the concentration gradients for these two sorts of ions, namely the Na^+/K^+-ATPase. This membrane protein pumps three Na^+ ions out of the cell in exchange for two K^+ ions that are pumped into the cell under the usage of ATP. For more information see the chapter *Ion pumps and exchangers*.

If the cell membrane was only permeable to potassium, the Nernst equation would predict a resting membrane potential of -90 mV. The actual value is slightly more positive (in ventricular cardiomyocytes around -85 mV), based on other membrane conductivities for ions with more positive equilibrium potentials, mainly sodium, as mentioned above. Therefore, the actual value of the membrane potential is established by the balance of the equilibrium potentials of ions to which the cell membrane is permeable and the conductivity the membrane has for this sort of ions. Naturally, beside potassium, also sodium, chloride and organic anions A^- (negatively charged amino acids and proteins)

determine the membrane potential. The table below shows concentrations and equilibrium potentials characteristic for mammal cells. Obviously, E_K sets the negative limit and E_{Ca} the positive limit for the membrane potential.

Ion	Intracellular concentration (mmol/L)	Extracellular concentration (mmol/L)	Equilibrium potential at 37 °C (mV)
Na^+	12	145	+67
K^+	155	4	-98
Ca^{2+}	100 nM	1.5	+129
Cl^-	4.2	123	-90
A^-	155	-	

Table 1. Free ion concentrations and equilibrium potentials for mammalian skeletal muscle cells. [25]

The **Goldman-Hodgkin-Katz voltage equation** predicts the resting membrane potential for cells membranes permeable to potassium, sodium and chloride and takes into account equilibrium potentials and conductivities.

$$V_m = \frac{RT}{F}\, ln\, \frac{P_K[K^+]_o + P_{Na}[Na^+]_o + P_{Cl}[Cl^-]_i}{P_K[K^+]_i + P_{Na}[Na^+]_i + P_{Cl}[Cl^-]_o}$$

V_m membrane potential

P permeability

Calcium plays a central role in the bioelectrical activity of cells, in particular in the excitation process of generic cells and in the excitation-contraction coupling of muscle cells. In the resting state of cells, the extra- and the intracellular calcium concentration is

comparatively low and so is the calcium permeability of the membrane. Apparently, calcium does not play a significant role in the generation of the resting membrane potential and is therefore omitted in the Goldman-Hodgkin-Katz voltage equation.

Current-voltage relations of ion channels

As described in the previous chapter, most membrane conductances are non-ohmic. Specific biophysical properties of ion channels are described in a later chapter, but for now it is necessary to state that the conductivity of ion channels changes during the cardiac excitation process. Thus, the AP is generated by variations in the magnitude of individual ion channel conductances, thus creating ionic currents that flow as a result of the difference between the actual membrane potential and the equilibrium potentials for the ions involved in the excitation-recovery-process. [27] If positive charges enter the cell, the membrane potential gets less negative and the cell is depolarized. Oppositely, the cell is hyperpolarized if the negative charge is increased. By convention, inward currents are characterized by a negative sign, outward currents by a positive sign. Depicting currents, downward deflections represent inward currents, upward deflections outward currents.
Back to ion channels that can electrically be thought of as resistors. According to Ohm's law, the current resulting at a certain membrane potential can be calculated as follows:

$$I = V/R$$

I current
V voltage
R resistance to current flow

According to this fundamental rule of electricity, at zero voltage the resulting current would necessarily be 0. But measuring ionic currents over cell membranes shows that the current drops to zero at the equilibrium potential, not at zero voltage. This is due to the above described concentration gradients, which act like a battery with an electromotive force (emf) in series with the resistor, [25] just to remember the description of the membrane as a RC circuit.
Therefore, after substituting resistance with conductance, Ohm's law can be modified into

$$I_X = g_X (V_m - E_X)$$

This modified equation (by Hodgkin and Huxley) for the resulting current of ion X shows that the current is a product of the (changing) conductance of the membrane for X and the driving force, that is defined by the difference between the membrane potential and the equilibrium potential for the ion X. Thus, if the membrane potential and the equilibrium potential are equal no current will flow despite potentially conductive ion channels. Hence, current will be elicited provided the membrane potential is different from the equilibrium potential and channels are conductive. Furthermore, if the equilibrium potential is positive to the membrane potential the elicited current is of negative sign. If the equilibrium potential is more negative than the membrane potential the evoked current has a positive sign. In the case of time- and/or voltage-dependent ion channels the value of the conductance *g* of a certain kind of ion channel can change constantly. For instance, the sodium conductance is almost zero at rest but if the threshold for eliciting an AP is reached, g_{NA} increases transiently (up to 1000 fold compared to the resting state) which consequently depolarizes the cell as a huge influx of sodium ions occurs.

Most ion channels show non-linear *I-V* relations. Most measured *I-V* relations can be interpreted in terms of electrical equivalent circuits and the modified form of Ohm's law ($I_X = g_X (V_m - E_X)$) that also considers the electromotive force in channel pores. [25]

Examples of linear and non-linear *I-V* relations are depicted in the same section in an earlier passage about Ohm's law.

Through measuring *I-V* relations, useful knowledge on ion channels can be obtained. Linear *I-V* relations that pass through the origin indicate that there is either no effective ion gradient and no electromotive force or that the channels are non-selective since at zero voltage no current flows through the channels. Slopes of successive measured *I-V* relations of one particular current allow conclusions on the number of open channels. Ion selectivity can be deduced from zero-current potentials in *I-V* relations.

Rectification, as mentioned earlier in this section, also represents a non-linear behavior of the resistor or ion channel. In this case, membrane conductance changes with voltage, which means for biological membranes that at some voltages the channel conducts current and at others it does not. Very often current is passed more easily in one direction than the other, which accounts for the terms inward and outward rectifier channels. A detailed description of *I-V* relations including figures of the described examples can be looked up in *Ion Channels of Excitable Membranes* by Bertil Hille. [25]

Single channel conductance varies – according to the equivalent driving force- between 0.1 pS and 400 pS. Most biological channels show an electrical conductance between 1 and 150 pS. [25]

Additionally to the *I-V* relation that is characteristic for a certain ion channel type, the voltage-dependence of activation can be calculated on the basis of the measured current and the modified form of Ohm's law. Thereby, the specific ionic conductance is determined according to the equation $g_X = I/(V_m - V_{rev})$, where g_X is the conductance calculated at the membrane potential V_m, I is the current amplitude, and V_{rev} the reversal potential which can also be experimentally obtained. Plotting membrane voltage against conductance gives the voltage-dependence of steady-state activation. The obtained curve can be fitted by a Boltzmann equation and then gives characteristic values of the specific current. In the *MATERIAL AND METHODS* section this procedure is described in detail.

B.1.3 The Cardiac Action Potential

The sinoatrial electrical impulse is propagated to the whole heart. Atria and ventricles are functional syncytia. This means, that cells are connected through gap junctions and therefore are electrically coupled. A stimulus which arrives anywhere in the atria or the ventricles causes a complete contraction of the respective chambers. The tissue of the heart comprises cells which generate and propagate electrical impulses (excitable cells) and such that respond to these stimuli with contractions (working myocardium).

The sinus node serves as an autonomic pacemaker – each AP generated in the sinus node causes a contraction of the heart. Nevertheless, heart activity must be adjusted to metabolic demands, which happens through several possibilities. AP frequency, conduction velocity and the contractility of the heart can be modified, which is achieved through various regulating mechanisms: Two groups of nerve fibres, that counterbalance each other, adjust the heart frequency to the physiological demand: the sympathetic part and the parasympathetic part that build together the autonomic nervous system. Sympathetic stimulation increases heart rate, conduction velocity of electric signals, blood pressure and contractility of the heart. Many ion channels respond to the transmitter norepinephrine, which is released by sympathetic nerve fibres. Parasympathetic activity (transmitter acetylcholine ACh) slows down heart activity.

Also hormones contribute to the regulation of the heart activity, for instance norepinephrine, which is synthesized in the adrenal glands. Norepinephrine as well as

epinephrine bind to β-receptors of heart cells, which increases intracellular cAMP, which in turn regulates ion channel activity. β-adrenergic stimulation accelerates the beating rate whereas stimulation of muscarinic receptors through ACh decelerates heart rate. Furthermore, body temperature as well as physical work are regulating factors for the heart frequency.

The ionic basis of the action potential: Each cardiac cycle is initiated by an AP. "The AP is a sudden regenerative depolarization of the transmembrane potential and subsequent repolarization back to the resting potential", [35] due to ionic currents flowing through ion channels. APs are characteristic for excitable cells and serve the signal generation and transduction between excitable cells (i.e. neurons, muscle cells, sensory receptors), the excitation-contraction coupling in muscle cells and the control of secretory action in endocrine tissue. [35] The AP duration varies according to the cell type and can range between less than one ms (in nerves) up to a few hundred ms (in cardiomyocytes).

Controlled ion channels (in the heart through voltage or ligands) in the plasma membranes of excitable cells enable the cell to change its resting potential in response to a stimulus. Dependent on the stimulus, corresponding ion channels open and according to the driving force (see chapter *The Origin of the Membrane Potential*) ionic currents flow through these channels. If, for instance, potassium channels open, positive charge leaves the cell and the membrane potential becomes more negative which is termed hyperpolarization. On the contrary, if, for instance, sodium channels open and sodium enters the cell, the membrane potential becomes more positive which refers to the term depolarization. Through stimuli caused changes of the membrane potential are graduated potentials whose amplitudes are determined by the magnitude of the stimulus. A stronger stimulus opens more potassium, sodium or calcium channels than a weaker stimulus and thereby increases the conductance of the membrane for this specific ion species. Correspondingly, the depolarization or hyperpolarization is stronger compared to a weak stimulus.
In excitable cells, the response to depolarizing stimuli is only up to a certain potential – the threshold potential - correlated with the intensity of the stimulus. Once this threshold potential is reached, an AP is triggered that follows the all-or-non-law. This principle says, that the magnitude of the AP is not determined by the magnitude of the eliciting stimulus. If the stimulus exceeds the threshold potential a complete response is the consequence. If the threshold potential is not reached there is no response. Stronger stimuli cause a higher

frequency of APs, which means that the stimulus intensity is encoded by the frequency and not the amplitude of APs.

Once the AP is triggered the membrane potential passes through several stereotyped phases (described below and depicted in Figure 14). In the depolarizing phase the membrane potential changes sign, it becomes positive, which means the interior of the cell is positive compared to the outside (reaching up to about +30 mV). This change of polarity is referred to as overshoot.

Then, the repolarizing phase follows, in which the membrane potential returns back to the niveau of the resting potential. In nerve cells, all these phases occur within only a few milliseconds.

In heart cells the AP is markedly longer. Cells of the working myocardium exhibit a plateau phase which is caused by calcium influx and the counterbalancing potassium efflux. This is crucial since the previous excited parts of the myocardium are still refractory when the excitation impulse reaches the last parts of the myocardium. Thus, re-entries can be prevented. Reentry means that an electrical impulse travels within a tight circle of the heart instead of moving from one end to the other.

The shape and the duration of APs differ between different cell species and regions of the heart. There are several major differences between APs of the working myocardium and those of the electrical conduction system. In the working myocardium the AP shows a characteristic plateau phase and a resting potential, whereas in sinoatrial cells there is neither a plateau phase nor a resting potential but the so called pacemaker potential. Another major difference between APs of different cell types of the heart is the ion species that accounts for the AP upstroke. In the working myocardium voltage-gated sodium channels cause the fast upstroke, in the sinus node and the AV-node calcium is responsible for the upstroke, which is also slower compared to the working myocardium.

The AP of a cardiac ventricular myocyte (working myocardium) comprises five phases (Figure 13). The sinoatrial AP is described in detail further down. (For a precise description of involved ion channels see chapter *The membrane clock - ion channels in the sinoatrial excitation process*).

Structure and information are according to Jalife et al., 1999. [27]

Phase 0: Rapid depolarization for action potential upstroke: At rest, mainly the potassium conductance determines the membrane potential at around -85 mV. If V_m

reaches the threshold at approximately -65 mV, sodium channels open and the membrane is conductive for sodium. According to the driving force (pushing towards E_{Na}) a huge influx of sodium ions occurs that charges the interior of the cell positively, and results in the upstroke of the AP. Then, sodium channels enter a nonconductive state after a few milliseconds. At a membrane potential of around +20 mV depolarization stops and the membrane begins to repolarize.

Phase 1: Rapid repolarization: For the most part, the AP upstroke is ended by inactivation of sodium channels. In this phase of APs, potassium channels account for the dominating membrane conductance. With regard to the heart region, active ionic currents vary in this phase of the AP. In most parts of the heart and in most animals, I_{to}, the transient outward potassium current provides most of the repolarizing charge. Therefore, on account of non-conductive sodium channels and conductive potassium channels the membrane potential moves towards E_K. I_{to} inactivates rapidly and its contribution to the repolarization during the next phases of the AP is much less than in this phase.

Phase 2: Action potential plateau: The membrane depolarization also activates the inward calcium current (I_{CaL}) and the delayed rectifier potassium current I_K, which comprises two separate components: I_{Kr}, a rapid component and I_{Ks}, a slow one. Therefore, the shape of the plateau phase is determined by the counterbalance of the calcium influx and the potassium efflux.

Phase 3: Final repolarization: The end of the plateau phase is determined by the inactivation of calcium channels and that the membrane potential heads towards E_K as the potassium channels are still open. I_{Kr} and I_{Ks} close and I_{K1}, the inward rectifier potassium current, is the dominating current in the final repolarization phase.

Phase 4: Diastolic potential: In the atrial and ventricular working myocardium, the resting potential is kept stable at around -85 mV. In these cell types I_{K1} is the dominant conductance at rest and therefore responsible for setting the membrane potential. Background conductance keeps the membrane potential slightly more positive than E_K. Cells of the working myocardium remain at the resting potential until the next stimulus brings the membrane potential to the threshold and elicits the next AP.

Phase 4 in pacemaker cells is characterized by the diastolic depolarization, see the chapter *The Sinoatrial Excitation Process.* In the diastolic depolarization phase the membrane potential is – succeeding the previous AP and the repolarizing phase - continuously brought towards the threshold potential without having a stabile resting phase in between.

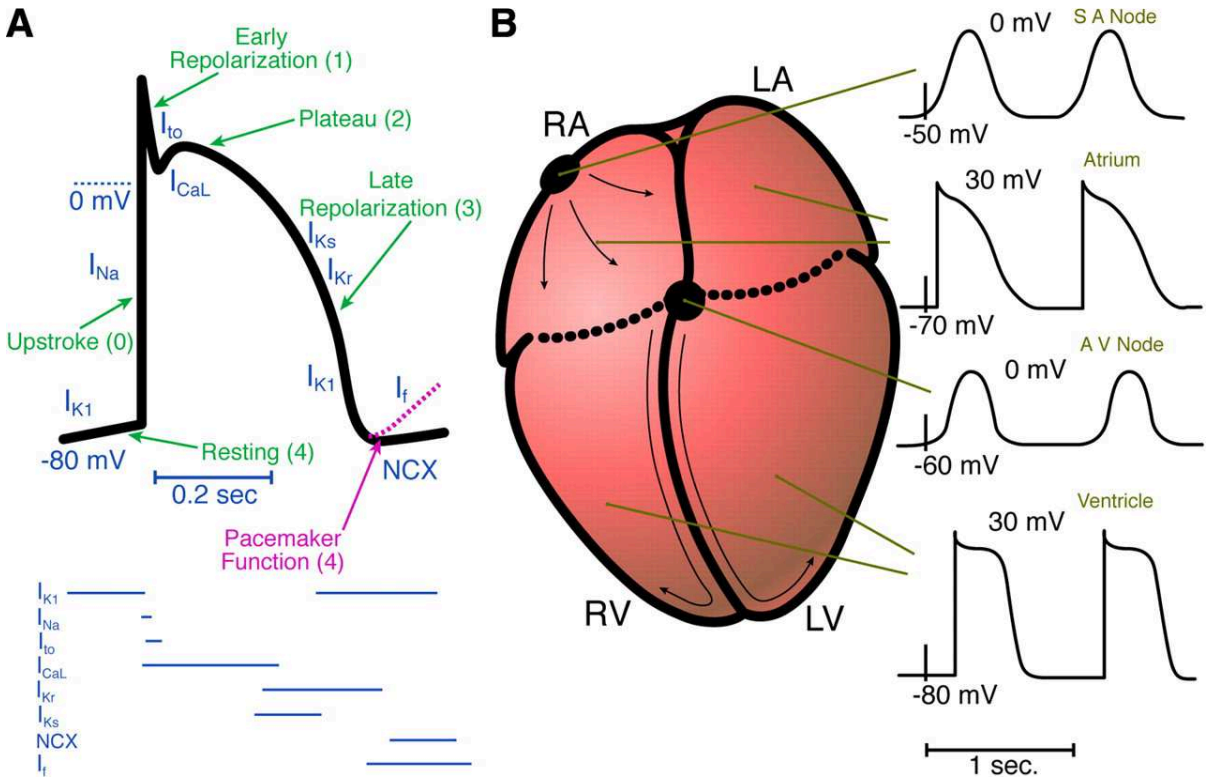

Figure 13. Cardiac electrical activity.
A schematic cardiac AP **(A)** with the typical phases of upstroke, early repolarization, plateau, late repolarization and diastolic potential. Contributing currents and the portions of the AP during which the current flows are also depicted. **(B)** shows the different shapes of APs according to the region of their origin. The short vertical lines in the APs indicate the time of onset of activity in the SA node for one beat. I_{Na} = inward sodium current; I_{CaL} = inward L-type calcium current; Potassium currents: I_{K1} = inward rectifying potassium current, I_{to} = transient outward potassium current, I_{Ks} and I_{Kr} = the delayed outward rectifier potassium currents; I_f = funny current; NCX = Na^+/Ca^{2+} exchanger. Characteristics of ionic currents are explained in the chapter *The membrane clock - ion channels in the sinoatrial excitation process*. Figure from Nattel, 2007. [36]

The action potential of atrial cells

The shape of the atrial AP is similar to the ventricular AP, but in ventricular cells AP

duration is longer and the plateau phase is clearly pronounced. Differences in repolarizing currents generate varying AP shapes. I_{Kur}, a delayed rectifier potassium current, which is highly expressed in atrial myocytes, forms the basis for the much shorter AP duration. [37]

Action potential parameters

Several parameters are used to describe the properties of APs (see Figure 14), among them the AP amplitude (APA), the overshoot (amplitude of the AP in the positive membrane potential range), the maximum upstroke velocity ($V = dV/dt$), APD_{50} (AP duration measured at 50% repolarization), APD_{90} (90% repolarization), the resting membrane potential in the working myocardium and the maximum diastolic potential (MDP) in spontaneously active cells.

The refractory period

The refractory period refers to a period of time in which a second AP cannot be elicited, in order to avoid tetanic contraction which would be disastrous in the heart tissue. During the absolute refractory period (ARP) the cell cannot at all be excited. During the relative refractory period (RRP) the current for eliciting an AP (I_{th}, threshold current) is much larger than the current needed for evoking an APs from a cell at rest. The long refractory period of myocardial cells is a result of a) the long plateau phase in which the membrane potential cannot return towards the resting potential at which sodium channels would be excitable again and b) the slow rate of recovery of the sodium channels after the repolarization of the membrane. [26] APs elicited in the RRP have a slower upstroke velocity and a lower amplitude and therefore conduct slowly.

The full-recovery time indicates the time between the onset of depolarization and the return to the resting potential and the full excitability which is achieved a few milliseconds after complete repolarization.

B.1.4 The Sinoatrial Excitation Process

The SA node contains spontaneously active cells (SANC = sinoatrial node cells) with a specific feature: these specialized cells do not show a resting membrane potential between two APs, but the so-called diastolic depolarization that continuously brings the membrane potential to the excitation threshold.

The upstroke of an AP in SANC is mainly carried by the L-type Ca^{2+} current (I_{CaL}) directed inwards. The depolarization activates outwardly directed delayed rectifier

potassium currents ($I_{Kr\ and}\ I_{Ks}$) which repolarize the membrane potential to the maximum diastolic potential (MDP, ~-65 mV) from which the phase of diastolic depolarization restarts. The involved ionic currents are shown in Figure 14 and described further down.
Basically, as already mentioned in the introduction, each cell of the conduction system is capable of beating autorhythmically (compare Figure 1), but the sinoatrial node plays the leading role (sinus rhythm around 60 to 100 beats per minute). The reason for the dominating sinoatrial signal is the slower AP frequency of the other parts of the conduction system due to a flatter slope of the diastolic depolarization and the repolarization phase. Thus, the excitation wave generated in the sinoatrial node arrives at all parts of the heart before the diastolic depolarization in other parts of the electrical conduction system reaches the threshold for eliciting an AP. [38] If the conduction of sinoatrial signal is interrupted, distal parts of the conduction system take over. The heart then beats in the AV-rhythm (40 to 55 beats per minute) or possibly even more slowly in the frequency of the Bundle of His (25 to 40 per minute).
The AP frequency of the SA-node decreases if a) the slope of the diastolic depolarization is decreased b) the threshold potential becomes more positive or c) the MDP reaches more negative values. All of this mentioned possibilities share the fact that the threshold for an AP is exceeded later. The fourth possibility is a prolonged repolarization phase after the AP.

The diastolic depolarization

The diastolic or pacemaker depolarization (DD) is a complex interplay between many time- and voltage-dependent currents (I_K, I_f, I_{CaT}, $I_{CaL,}$ possibly I_{st}) in the presence of background currents, [39] the Na^+/K^+ pump current ($I_{Na/K}$) and I_{NCX} (= the Na^+/Ca^{2+} exchange current.
Additionally to this cyclic activation and deactivation of membrane ion channels (= voltage clock, membrane oscillator), rhythmic spontaneous Ca^{2+} release from the cardiac sarcoplasmic reticulum (= SR) and reuptake into the SR takes part in regulating the sinoatrial node automaticity. This mechanism is referred to as calcium clock. [40] Voltage- and calcium clock work tightly together, one cannot keep up proper activity without the other. [41] The relative extent of contribution of the two clocks to pacemaker activity is still a matter of debate. Both clocks are described further down, and their interplay is illustrated in Figure 15.

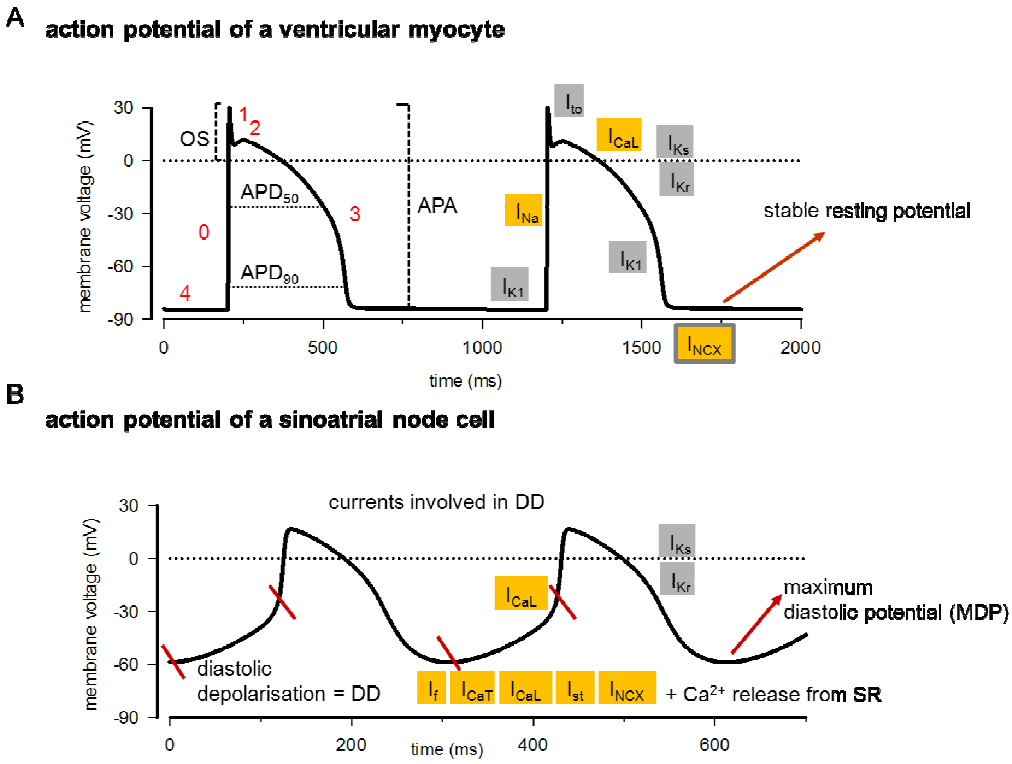

Figure 14. Action potential of a ventricular and a sinoatrial node cell.
(A) AP of a ventricular myocyte. Red numbers indicate the 5 characteristic phases: 0 = upstroke, 1 = rapid repolarization, 2 = plateau phase, 3 = final repolarization, 4 = diastolic potential. OS = overshoot, APA = AP amplitude, APD_{50} = AP duration at 50 % repolarization, APD_{90} at 90 % repolarization. Outward currents are indicated by grey boxes, inward currents by yellow boxes. NCX is shown in yellow with grey frame: Because of its electrogenic property it generates an inward or an outward current. [37] At rest it pumps calcium out of the cell. **(B)** AP of a sinoatrial cell. Pacemaker depolarization involves deactivation of I_K (= I_{Kr} and I_{Ks}) and activation of the shown inward currents. [42] Additionally the calcium clock plays an important role in pacemaking – the relative importance of voltage and calcium clock is still a matter of debate (see next chapter).
I_{Na} = sodium current; I_{st} = sustained current which is a inwardly directed sodium current; I_{CaL} = L-type calcium current; I_{CaT} = T-type calcium current; I_{K1} = inward rectifying potassium current; I_{to} = transient outward potassium current; I_{Ks} and I_{Kr} = the delayed outward rectifier potassium currents; I_f = funny current; NCX = Na^+/Ca^{2+} exchanger.

The diastolic depolarization comprises two parts: 1) The early DD, which is the linear part of the DD and is mainly determined by the decay of the I_K conductance after having reached the MDP. [41] This increasing negative membrane voltage activates the mixed cation (Na^+ and K^+) inward current I_f, that brings the membrane potential towards the AP threshold, supported by the background current I_b. [39] 2) The late diastolic depolarization,

representing the non-linear part of the DD, in which I_{CaT} and I_{CaL} as well as the calcium clock (including NCX) and possibly I_{st} come into play, thus providing an exponentially rising phase in the DD. [41]

ß-adrenergic stimulation is the key factor in regulating steepness and therefore duration of the diastolic depolarization. Ionic currents of the voltage clock as well as contributors of the calcium clock respond to ß-adrenergic stimuli. By blocking SR Ca^{2+} release and I_f, ß-adrenergic mediated heart rate acceleration was completely abolished. [43] Data gained by Bucchi et al., 2007 in rabbit SANC demonstrate that rate changes caused by autonomic agonists influence the steepness of the early DD and involve I_f to a great extent, but both clocks contribute to the regulation of heart rate. [44]

The calcium clock

Pacemaker cells, like other excitable cells, have an apparatus for cycling calcium into and out of the SR. This includes a calcium pump (SERCA, = the SR Ca^{2+}-ATPase for the re-uptake) and calcium release channels RyRs [45] (Ryanodine receptors, RyRs, are calcium channels that mediate calcium induced calcium release in excitable tissue). Local spontaneous calcium (LCR) release from the SR enhances the intracellular calcium concentration [Ca_i], which in turn activates I_{NCX}. NCX is the electrogenic $Na^+/Ca2^+$-exchanger, that – by using the electrochemical gradient (established by the Na^+/K^+-ATPase) – removes one Ca^{2+} ion from the cell for the exchange of three Na^+ ions. This positive net-influx of ions happens shortly before the following AP and enhances the rate of the DD. I_{NCX} is reversible and its direction of current flow and its amplitude are controlled by intra- and extracellular sodium and calcium concentrations as well as the membrane potential. If E_m is negative to E_{NCX}, Ca^{2+} is transported out of the cell although the low calcium concentration at rest limits the rate of calcium extrusion and the extent of diastolic inward directed I_{NCX}. [46] If during the AP upstroke the membrane potential passes the equilibrium potential of NCX, the current changes its direction, so that calcium is transported into and sodium out of the cell. But soon the current reverses sign again: The inward calcium current I_{CaL} activated by membrane depolarization, and additionally the triggered SR calcium release via RyRs activation cause a high increase of the intracellular calcium concentration, which drives E_{NCX} above E_m and I_{NCX} is again inwardly directed. [46] NCX is described again and in more detail in the later chapter *The membrane clock* -

ion channels in the sinoatrial excitation process. Release of calcium from the SR happens spontaneously, as mentioned above, or can be triggered via I_{CaT} or early I_{CaL} that transport calcium into the cell and by that activate the ryanodine receptors of the SR which consequently leads to calcium release. [46]

Calcium is transported back into the SR by the activity of SERCA under the consumption of ATP. (For review see ref [40,47]). Most of the calcium that enters the cell via I_{Ca} (L-type and T-type) is extruded from the cell via NCX.
LCR can occur roughly periodically without preceding or concomitant changes in the membrane potential (shown in rabbit SANC), even when the SR is disconnected from the cell membrane. [41] Furthermore, LCR periodicity is tightly linked to the cycle length of spontaneous APs. [45] ß-adrenergic stimulation accelerates the calcium clock by activating more RyRs, thus causing a further increase in $[Ca]_i$ that again activates I_{NCX}.
Studies in rabbit SANC have shown that distorting or preventing the calcium waveform as well as blocking of I_{NCX} reduce the spontaneous beating rate in rabbit SANC. [48,49]

The role of calcium in cardiac myocytes is not limited to pacemaking.
Indeed, calcium is a very important ubiquitous second messenger that takes part in regulating various cellular processes. Calcium contributes to electrophysiological events like APs and the development of arrhythmias. The latter is caused on account of very high SR calcium levels that through spontaneous release cause an aftercontraction and activate an transient inward current (which is very likely identical with I_{NCX}) that depolarizes the membrane potential towards the threshold for an AP. [46] Furthermore, calcium plays a crucial role in the excitation-contraction coupling, the modulation of contractile function, the energy supply-demand balance, cell death, and the transcriptional regulation. [46]

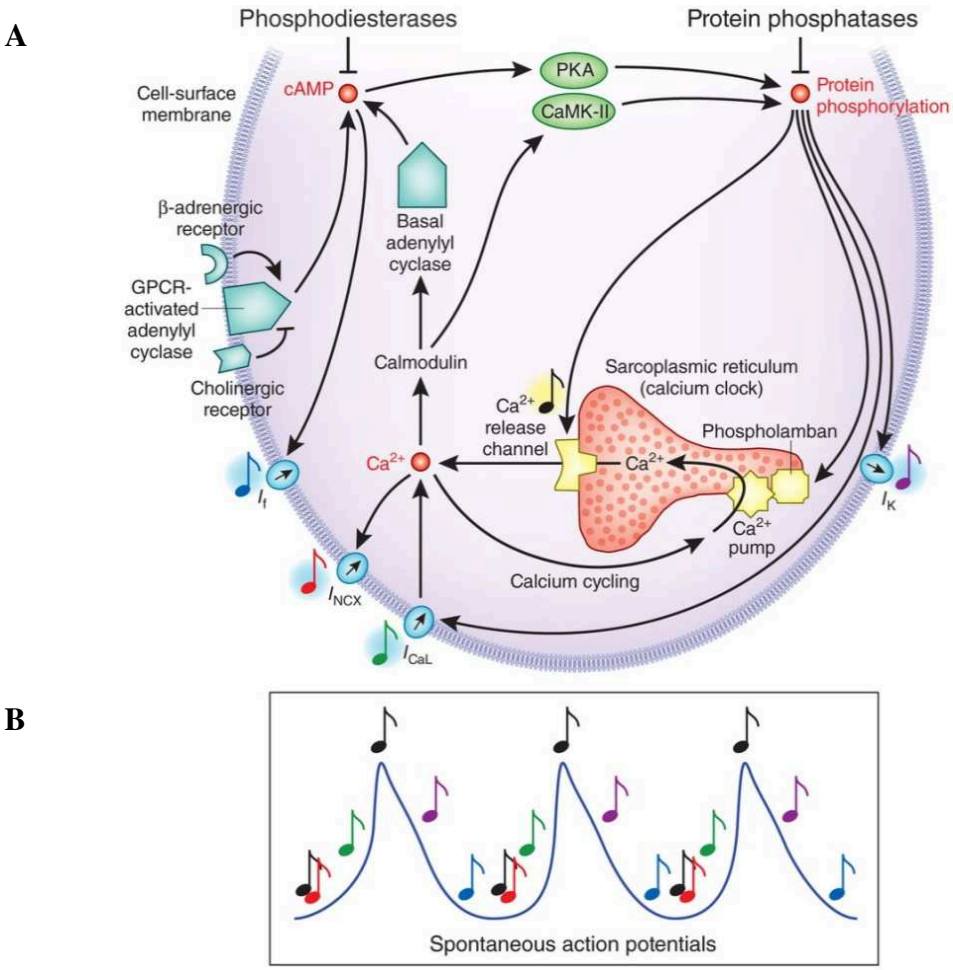

Figure 15. Interplay of voltage clock and calcium clock.
(A) The membrane clock (voltage- and time-dependent membrane ion channels) and the calcium clock (which consists of oscillatory local Ca^{2+}-release from the SR via the RyRs and the reuptake by SERCA) are interlinked by NCX, that causes an inward Na^{+} current in response to local Ca^{2+}-release and prompts the membrane clock to generate rhythmic APs. Binding of cAMP activates PKA, which phosphorylates phospholamban and Ca^{2+}-channels, which in turn increases the Ca^{2+} inward current and Ca^{2+}-uptake, thus accelerating the calcium clock. [50] beta-adrenergic and cholinergic receptor activation enhances or slows down the AP firing rate, respectively. **(B)** Ionic current activation with regard to the AP is shown. This pacemaker symphony requires signals from the membrane clock (coloured notes) and from the calcium clock (black notes). GPCR, G protein coupled receptor; PKA, protein kinase-A; CaMK-II, calmodulin-dependent protein kinase II; I_K, delayed rectifier potassium current; I_{CaL}, L-type Ca^{2+} current; I_{NCX}: Na^{+}/Ca^{2+} exchange current; I_f, funny current. Figure from Lakatta & Maltsev, 2013. [51]

The membrane clock - ion channels in the sinoatrial excitation process

Ion channels on the surface membrane of SANC are the proximal cause of an AP. [52] Cardiac ion channels are mostly gated by voltage or ligand-binding, only little is known about stretch-activated channels. Ionic currents shown in Figure 16 below contribute to the sinoatrial excitation process; Figure 14 and Figure 15 show their precise function.

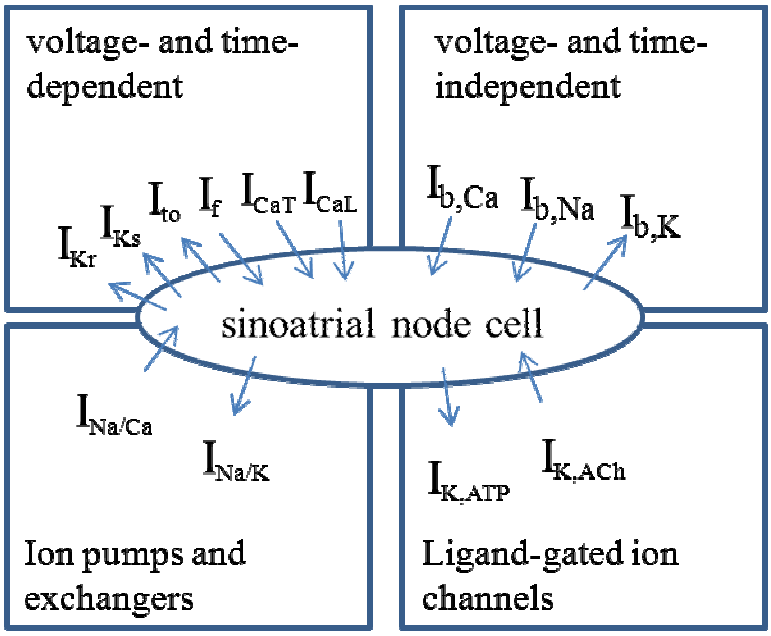

Figure 16. Ionic currents in the pacemaking process.
I_{st} and I_{Na} (see further below) are not shown as their presence in SANC is still controversial. Voltage- and time-independent currents are referred to as background currents I_b. $I_{Na/Ca}$ = I_{NCX}. Figure modified from Pelzmann, 1996, with permission. [53]

In this chapter all contributing currents are listed in Figure 16 and are described in detail below. As the electrophysiological work of this thesis is performed on the pacemaker or funny current I_f, this ion channel is described most extensively.

The pacemaker current

The pacemaker current is carried by hyperpolarization-activated cyclic nucleotide-gated channels (HCN). This ion channel family comprises of 4 members (HCN1 - 4) that are expressed in the heart and nervous system and are activated upon hyperpolarization and intracellular cAMP. This mixed cation current (Na^+ and K^+) is called pacemaker current

and contributes to the diastolic depolarization in the AP of SANC (Figure 14). The pacemaker current is enhanced by beta-adrenergic agonists and decreased by muscarinic agonists, both mediated via adenylate cylcase and cAMP. Therefore, the pacemaker current plays a key role in autonomic heart rate regulation [13] and in the control of neuronal excitability. [17] HCN channels are regulated by auxiliary subunits, low-molecular-weight factors, protein kinases and phosphatases. [17]

The pacemaker current has been shown to comprise two current components. First, a time- and voltage-independent component referred to as instantaneous current or I_{inst} which is fully activated within a few milliseconds. The second current component is voltage- and time-dependent, referred to as I_f (or I_h or I_q) [14] and reaches its steady state level within one to several seconds when fully activated.

Nature and physiological role of I_{inst} are still a matter of research. Up to now it is not known whether I_{inst} is produced by a distinct population of HCN channels [14] or is flowing through a "leaky" closed state of these channels. [54] However, I_{inst} is discussed to contribute to a stable pacing rhythm in autorhythmic cardiac cells. [15,16,55,56]

Both current components show similar reversal potentials between -20 and -40 mV at physiological ion concentrations.

Molecular structure of HCN channels

HCN channels belong to the pore loop cation superfamily and comprise four homologous members, namely HCN1- HCN4. In cell membranes HCN channels assemble to tetramers consisting of either homomeric or heteromeric channel subunits. Each subunit consists of six transmembrane alpha helices (S1 – S6). The fourth helix S4 forms the putative voltage sensor, the ion selectivity filter is built by S5 and S6.

A binding region for cAMP, the CNBD (cyclic nucleotide binding domain) is linked to the channel pore via the C-linker. [17] Figure 17 shows the structure of a HCN channel.

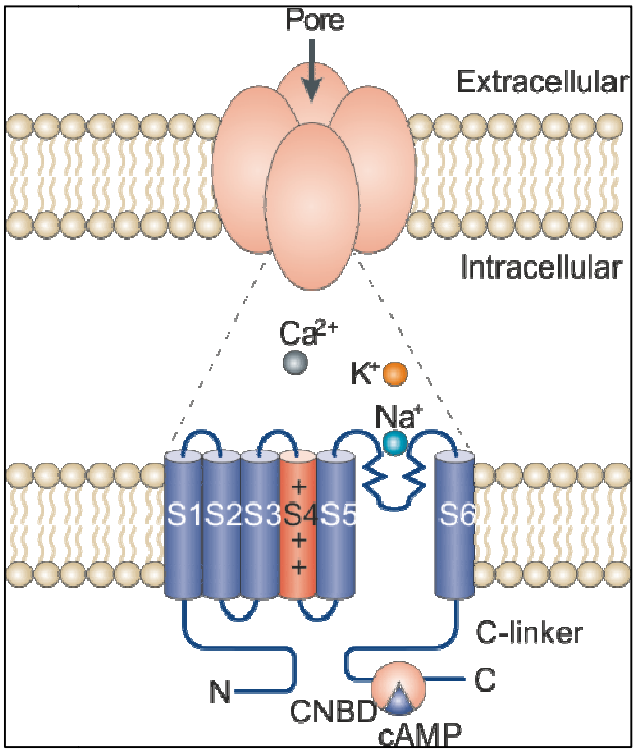

Figure 17. Schematic diagram of a HCN channel.
6 transmembrane segments assemble to form one channel with S4 being the voltage sensor and S5 and S6 forming the channel pore. Besides Na^+ and K^+ HCN channels also allow the passage of calcium ions. [57] Figure from Biel et al., 2009. [58]

Tissue expression of HCN channels

All isoforms of HCN channels are found in the nervous system and the heart. [58] HCN3 and HCN4 have also been reported for other tissues: HCN3 for mouse liver, lung and kidney; HCN4 for lung, skeletal muscles and human testis, but at very low levels. [17] In the mammal sinoatrial node HCN4 is the predominant isoform and experiments demonstrate that SANC of HCN4-deficient mice show 70 – 80% I_f reduction. [59] Mutations involving HCN4 are associated with bradycardia. [17] HCN channels are also abundantly expressed in non-pacemaking tissue of the heart. In human atria, HCN2 seems to be the most prevalent isoform, but also HCN4 is expressed to a high extent. [21]

I_f – The funny current

I_f, the voltage- and time-dependent current component of the pacemaker current, was termed “funny” because of its unusual voltage-dependence of activation. I_f is activated upon hyperpolarization, the threshold for activation varies between -40 and -60 mV. At

voltage levels of the diastolic depolarization, I_f is mainly carried by Na^+ ions. [42] I_f does not show a voltage-dependent inactivation and can be blocked by extracellular caesium.
The activation curve shows a sigmoidal shape (typical steady-state activation curves are depicted in the *RESULTS* section) and additionally deactivation follows a sigmoidal time course. [25] Single channel conductance amounts to around 1 pS, [58] but so far contradictive values have been reported that amount up to 30 times higher values for native HCN channels. [60] The steady-state activation curve can be shifted to more positive membrane potentials in the presence of cAMP (which activates the channels due to ß-adrenergic stimuli).

HCN channel kinetics vary between the four isoforms, with HCN1 being the channel with the fastest kinetics and the most positive half-maximal voltage ($V_{1/2}$ = -73 mV) of the steady-state activation curve. (At $V_{1/2}$ 50 % of the maximal conductance level is reached; for calculation see the material and methods section). HCN2 activation kinetics are slower than HCN1 kinetics, but still faster than those of HCN3 and especially HCN4, which is the slowest of all and shows a $V_{1/2}$ of about -81 mV. [13] Values differ between different studies, but the ranking is consistent. Also the sensitivity to cAMP varies between subtypes, changes in $V_{1/2}$ according to increased cAMP levels are as follows: HCN1: 2-6.7 mV, HCN2: 12-15 mV, HCN4: 15.2-23 mV. [13] In native tissue properties of I_f can vary due to diverse compositions of subunits (HCN 1-4) forming one channel pore and on account to varying subunit expression.

HCN channels as therapeutical target

HCN channels can constitute a promising target for anticonvulsant, anaesthetic and analgesic drugs due to their abundant expression in the heart and nervous system. [17] Addressing HCN channels in the treatment of neuronal diseases like epilepsy, neuropathic pain and peripheral pain disorders seems to be auspicious. [17] In cardiac disease HCN channels offer a starting point for heart rate lowering therapy. Reducing heart rate is beneficial for patients suffering from heart diseases like angina pectoris, hypertension and coronary heart disease. Since I_f contributes to the diastolic depolarization in sinoatrial cells, a blockage of I_f reduces the slope of the DD and consequently AP firing rate, which decreases myocardial oxygen demand and improves diastolic coronary perfusion. Several specific I_f blockers have been developed such as zatebradine, cilobradine and ivabradine (see the chapter *The Heart Rate Lowering Agent Ivabradine*), though these substances

most likely have different binding sites at the HCN channel protein.

Potassium currents

In excitable cells, potassium channels are responsible for the establishment of the resting potential, for the duration of fast APs, they time the interspike intervals during repetitive AP firing and generally lower the effectiveness of excitatory inputs on a cell. [25]
In cardiomyocytes three types of K^+ channels are of importance: voltage-gated outward rectifying potassium channels (I_{to}, I_{Kur}, I_{Kr}, I_{Ks}), inward rectifying channels ($I_{K1,}$ [voltage-gated], $I_{K,Ach}$, $I_{K,ATP}$ [ligand-gated]) and background K^+ currents, [37] see Figure 14. This section will deal only with I_{Kr} and I_{Ks}, as they largely contribute to the sinoatrial AP.
The other potassium currents play a role in the control of AP duration in other regions of the heart: I_{K1} substantially contributes to a stable resting potential in non-pacemaking cells. I_{to} is responsible for a very fast first repolarization phase of a typical ventricular AP and is also prominently expressed in Purkinje fibres and atria of humans and rabbits. I_{to} has been reported for rabbit SANC, that are located close to the crista terminalis. [39] However, the role of I_{to} in SANC is still not well understood. I_{Kur} is responsible for the short AP of atrial cells. The subscript "ur" stands for ultrarapid. [26]

Voltage-gated potassium currents: The outward (delayed) rectifying potassium currents

The delayed rectifier potassium current I_K is an outward current responsible for the repolarization phase of an AP [37] and therefore contributes to the control of AP duration. The name delayed rectifier is derived from its property of late opening at the end of the AP plateau. [26] When the heart rate rises the AP duration has to decrease, which can be attributed to increasing net-efflux of positively charged ions during repolarization: The Na^+/K^+ pump current (outward directed positive current) (see the chapter *The Na+/K+-ATPase)* increases, and the prolonged activation of I_K contributes to the fast repolarization. Between APs, I_K does not completely deactivate, so g_K onwardly cumulates resulting in progressive shortening of AP duration. Class III antiarrhythmic drugs address I_K, resulting in a prolonging effect on AP duration. [61]
Probably all cells possess K^+ channels (voltage- or ligand gated), but in pacemaker tissue of the heart two delayed rectifier currents are of relevance: I_{Ks} and I_{Kr} (*s* stands for slow, *r* for rapid activation), which show different electrophysiological properties and sensitivities

to pharmacological substances. [62] In 1990 it was first described, that I_K comprises I_{Kr} and I_{Ks} [63] and that expression levels vary across species. Therefore, their relevance relative to each other in the pacemaking process is also species-dependent. Typically, delayed rectifier open upon depolarization.

I_{Kr}: The major subunit of the I_{Kr} channel belongs to the eag channel family called HERG. Activation of this channel follows an unusual time course. The HERG channel opens rapidly but only partially at the beginning of the AP plateau but at its end these channels open fully so as to end the AP. [26] I_{Kr} current activates at around -50 mV, $V_{1/2}$ is reached at around -15 mV in rabbit SANC. [23] The *I-V* relationship is linear at more negative membrane potentials but I_{Kr} shows inward rectification when fully activated. The reversal potential of I_{Kr} amounts to -95.9 mV. Single channel conductance at an outward potassium concentration of 150 mmol/L amounts to 10 pS and activation time constant at 0 mV amounts to 50 ms.

I_{Ks}: This current activates at -40 mV with a slower time course than I_{Kr} in rabbit sinoatrial cells and reaches $V_{1/2}$ at 14 mV. [64] Time constants of I_{Ks} activation are approximately by 10 times higher than that of I_{Kr}. [53] The equilibrium potential for I_{Ks} is more positive than E_K because I_{Ks} carries Na^+ ions besides K^+ ions (E_{Ks} = -83.3 mV). [65] Single channel conductance at an outward potassium concentration of 150 mmol/L amounts to 1-3 pS, activation time constants at 0 mV: 400 - 2500 ms. [27]

Ligand-gated potassium channels - $I_{K,ATP}$ and $I_{K,ACh}$

Ligand-gated ion channels (LGIC) are the second major group of cardiac ion channels. [37] These ion channels respond mainly to chemical ligands which are mostly transmitters binding to receptors at the extracellular side of the membrane. Besides, there are intracellular receptors located at the ion channel protein or at a separate receptor protein. In this case channel and receptor communicate via GTP-binding proteins. [53]

$I_{K,Ach}$: The most studied channel among LGIC is the acetylcholine-activated K^+-channel $I_{K,ACh}$. Acetylcholine binds to the muscarinic receptor which activates a G-protein-signaling pathway. The results is an activation of the inward rectifying potassium current $I_{K,Ach}$, which in turn hyperpolarizes the membrane potential. In the heart, these channels are abundantly expressed in atrial cells as well as in the sinoatrial and the atrioventricular node

and take part in the vagal control of the heart. [37] $I_{K,ACh}$ belongs to the family of GIRK channels (G-protein gated inwardly rectifying potassium channels).

$I_{K,ATP}$: The ATP-sensitive potassium channel $I_{K,ATP}$ is abundantly distributed all over the heart. This channel couples the duration of the AP to the metabolic state of the cell, as its open probability is proportional to the [ADP]/[ATP] ratio in the cell. At physiological ATP-concentrations $I_{K,ATP}$ is blocked. Therefore, in healthy tissue this current is not of relevance regarding the control of AP duration. [53] During ischemia the [ADP]/[ATP] ratio increases, $I_{K,ATP}$ is activated and the AP duration shortened, which is of cardioprotective effect. [37]

Calcium currents

Calcium ions are essential and principal intracellular signaling ions, which regulate the excitation-contraction coupling, secretions, the activity of enzymes and ion channels. [37] Calcium channels play an extensive role in the regulation of the intracellular calcium concentration – i) as principal entry for calcium into the cell (L- and T-type calcium channels), ii) triggering local calcium releases from the SR (see chapter *The Sinoatrial Excitation Process.*) and iii) transporting calcium out of the cell via NCX. Calcium channels play a major role in the sympathetic stimulation of the heart through beta-adrenergic stimulation, which induces positive inotropic and chronotropic effects, mediated via L-type channels. Acetylcholine and adenosine inhibit channel opening. [26]

In cardiac cells two types of voltage-gated calcium channels are of high relevance, namely L-type and T-type calcium channels. The classification of T-type and L-type is based on earlier electrophysiological and pharmacological studies, revealing the different activation behavior of these two channel subtypes.

T-type calcium current

T-type calcium channels are found in various tissues including the heart and vascular smooth muscle cells. “T” stands for tiny and transient, referring to a small single channel conductance of 8.5 pS at extracellular [Ca^{2+}] = 5 mM and fast current inactivation. [27] T-type channels activate positive to -70 mV in rabbit sinoatrial cells and at around -60 mV in human tissue. [23] Therefore, this channel type is called low-threshold type. Current inactivation depends on voltage and shows a monoexponential course with τ_{inact} = 7.3 – 11.8 ms. Recovery from inactivation is biexponential with τ_{fast} = 83 ms and τ_{slow} = 444 ms. [53] $V_{1/2}$ is reached at around -40 mV and the reversal potential amounts to around +50 mV. T-type calcium channels are mainly expressed in pacemaker (they contribute to the DD), atrial and Purkinje cells [37] and are not sensitive to isoproterenol, contrary to L-type channels. Both channel types conduct also monovalent ions in absence of calcium. [53]

L-type calcium current

“L” stands for large and long-lasting, meaning the slow kinetics of current decay. [66] L-type channels are found in all cardiac cell types. They activate at membrane potentials between -30 and -40 mV (thus they are considered as high-threshold type). $V_{1/2}$ is reached at around -20 mV. Single channel conductance at extracellular [Ca^{2+}] = 5 mM amounts to 16 pS. [27] Voltage ranges of steady-state activation and inactivation overlap, thus resulting in a steady-state window current, which is a permanent Ca^{2+} inward current between -30 and 0 mV (T-type channels: -60 and -40 mV). [53] The inactivation of L-type channels depends on voltage and $[Ca^{2+}]_i$ and shows a biexponential time course with τ_{fast} = 2 – 11.8 ms and τ_{slow} = 30 – 107 ms. Recovery from inactivation is monoexponential with τ_{rec} of 30.6 – 64 ms. [53]

I_{CaL} plays three important roles in cardiac cells: 1) Providing an inward current causing a long-lasting depolarization, which is mainly responsible for the plateau phase of the ventricular AP. 2) I_{CaL} plays a major role in the excitation-contraction coupling, and 3) takes part in the AP upstroke in pacemaker cells. [27] L-type calcium blockers act as antiarrhythmic or antihypertensive drugs. Characteristically, L-type channels are inhibited by dihydropyridine, a molecule on which a class of drugs is based on. Examples are nifedipine, nisoldipine and isradipine. [66] Another two classes of Ca^{2+} antagonists act on L-type calcium channels: 1) Phenylalkylamine like verapamil or devapamil and 2) Benzothiazepine like diltiazem.

Sodium currents

Sodium current I_{Na}: The presence and significance of the sodium current in sinoatrial cells are still discussed. It was suggested that I_{Na} is responsible for the AP upstroke in peripheral SANC, whereas I_{CaL} is responsible for the upstroke in central regions of the sinoatrial node. [67] Baruscotti et al., 2000, showed that at least in newborn rabbit SANC I_{Na} substantially contributes to pacemaking, but the exact molecular basis of this channel shown in the mentioned study is not clear. [68] In most muscle and nerve cells the fast sodium current is responsible for their excitability and the conduction of excitation. In the heart the AP upstroke in non-pacemaker tissue is carried by I_{Na}, (Figure 14).

Sustained inward current I_{st}: This sodium current, sensitive to Ca^{2+} antagonists and enhanced by ß-adrenergic stimulation, has been recognized in SANC of rabbit, guinea pig and rat as well as in the rabbit AV node [69] and is absent in quiescent cells. I_{st} activates in the diastolic range (-60 to -40 mV [42]) and is called sustained inward current because it does not show marked inactivation during a depolarizing pulse. [70] Single channel experiments showed a smaller current amplitude and slower gating kinetics [70] than can be observed with conventional sodium and L-type calcium channels, the reversal potential is +13 mV. [42]

However, only a few groups have described I_{st}, so its physiological significance and presence has to be further elucidated. The molecular basis remains to be determined. In mathematical models I_{st} leads to slightly increased pacemaker rate, depending on I_{st} amplitude relative to other inward currents. [42]

Background currents

The background current I_b shows a linear *I-V* relation. In SANC Na^+, Ca^{2+} and K^+ are charge carriers of this time-independent net inward current at the diastolic potential range. Its elimination stops pacemaker activity. [27] The Na^+-dependent background current is generated by a low number of sodium channels that are in the open state between -70 and -45 mV, which is caused by the overlap of the steady-state activation and inactivation curve (“window current”). [71] Another theory indicates a certain kind of sodium channels which are not completely inactivated and therefore contribute to I_b in the range of the DD. [72]

The background calcium conductance is based on the window current of T-type calcium

channels. [53]

The K^+ background current could be identical with I_{K1} [73] which is reported for Purkinje cells but not yet for SANC.

Ion pumps and exchangers

The Na^+/K^+-ATPase

The active transport of the sodium potassium pump (Na^+/K^+-ATPase) keeps the internal potassium concentration relatively high and the sodium concentration relatively low compared to the outside of the cell. Under use of one molecule ATP, which gets hydrolyzed to ADP + P_i, three Na^+ ions are pumped out of the cell and two K^+ ions are transported into the cell. The resulting net outward current of $I_{Na/K}$ is repolarizing and shows voltage-dependence. [53] The activity of the pump is regulated by the internal sodium concentration and half maximal activation is reached at 10 mmol/L. The *I-V* relation shows a sigmoidal shape. [74]

The Na^+/Ca^{2+} exchanger

NCX is the electrogenic Na^+/Ca^{2+} exchanger, that – by using the electrochemical gradient established by the Na^+/K^+-ATPase – exchanges one Ca^{2+} ion for three Na^+ ions. NCX carries the ionic current I_{NCX} which can either be a net inward current (transporting calcium out of the cell) and thereby keeps up a low intracellular calcium concentration or a net outward current (transporting calcium into the cell), whereby the direction of I_{NCX} depends on the membrane potential and the electrochemical gradients for Na^+ and Ca^{2+}. I_{NCX} amplitude is determined by the concentration of both ions. [75] At membrane potentials negative to E_{NCX} I_{NCX} is directed inwards (forward mode), thus providing a positive net-influx of ions contributing to the diastolic depolarization. At membrane potentials positive to E_{NCX} the exchanger works in the reverse mode and I_{NCX} is directed outwards, thus transporting calcium into the cell and contributing to the plateau phase in non-pacemaking tissue.

For the specific role of NCX in pacemaking see the chapter *The diastolic depolarization.*

B.2 The Pathophysiology of Sepsis and the Potential Elicitor LPS

B.2.1 The Pathophysiology of Sepsis

Innate and adaptive immunity

The body's immune system is divided in two major subdivisions, the non-specific = innate immune system and the adaptive/acquired = specific immune system. The latter reacts towards molecular, cellular and particulate antigens by generating specific antibodies against surface structures of these pathogens. Cells of the adaptive immune system are able to remember and recognize specific pathogens, so that each time the pathogen is encountered in the body the immune response is much faster and more efficient. The specific immune response is tightly linked to and activated by the innate immune system, but its response takes rather days than hours to develop.

The non-specific immune system acts as the first-line defense of the body and its response is much faster than that of the adaptive immune system. Its reaction towards infectious agents is uniform.

The Systemic Inflammatory Response Syndrome (SIRS)

The body's initial defense strategies against infectious agents are physical and chemical: Anatomical barriers include e.g. mechanical factors like ciliary action on epithelial surfaces with partly mucous secretion. Chemical protective tools comprise enzymes (like lysozyme and acids) as well as gastric acid or sweat which both inhibit bacterial growth. If pathogens cross these barriers they are first encountered by the innate immune system that comprises humoral and cellular components. The humoral part of the innate immune system consists of lysozyme and cytokines and the complement system. The latter is made up by a large number of distinct plasma proteins and represents an enzyme cascade which marks pathogens for destruction by phagocytic cells (these are cellular components of the innate immune system such as neutrophil granulocytes, monocytes and macrophages).

According to Galley and Webster 1996, activation of the complement system initiates the production of primary pro-inflammatory mediators, tumor necrosis factors (TNF) and interleukin 1 (interleukin = IL). [76] As a consequence secondary mediators such as cytokines, prostaglandins and platelet activating factors (PAF) are then released from immunocompetent cells such as phagocytes, mast cells and platelets. Furthermore, additional complement and acute phase proteins (e.g. C-reactive protein, whose

measurement is a screen for inflammatory and infectious diseases) are activated. The expression of adhesion molecules, T-cell selection, antibody production and release of oxygen-derived radicals is initiated. The described processes are part of the inflammation response, which is the body's first common reaction towards tissue injury (of whatever cause). The response includes coagulation and fibrinolytic cascades, vasodilation, cellular activation, increased microvascular permeability and reduced vascular resistance. [77]

In SIRS, this inflammatory response becomes systemic due to extensive and locally unrestricted exposure to inflammatory mediators. SIRS can be evoked by infectious or non-infectious causes e.g. autoimmune reactions, burns, pancreatitis, acute respiratory distress syndrome (ARDS), surgeries, and trauma. [78] SIRS shows at least two of the following symptoms: Body temperature above 38°C or below 36°C, heart rate above 90 beats per minute, respiratory rate above 20 breaths per minute, white blood cells per mm^3 below 4000 or above 12000, partial pressure of CO_2 less than 4.3 kPa. [77] Uncontrolled systemic vasodilation leads to hypotension with impaired microcirculatory flow. Taken together these negative conditions, sufficient supply of organs cannot be maintained bearing the potential risk of MODS (= multiple organ dysfunction syndrome) finally leading to death.

Sepsis

Sepsis is referred to as SIRS caused by an infection, Figure 18. This reaction can progress to severe sepsis with hypoperfusion of organs and dysfunction of at least one of them. In septic shock patients additionally suffer from hypotension despite fluid replacement going along with irregularities in blood perfusion. Additionally, disseminated intravascular coagulation occurs. Finally, severe sepsis can lead to MODS with two or more organs failing, bearing the high risk of death. The overall mortality rate in sepsis yields to ~ 50 % [1] despite maximal therapy.

In about 60 % of septic patients an infection with Gram-negative bacteria is responsible for the development of severe sepsis. In other cases it's mainly Gram-positive bacteria. [1] Furthermore, viruses, fungi or parasites are infectious agents with the potential to cause sepsis.

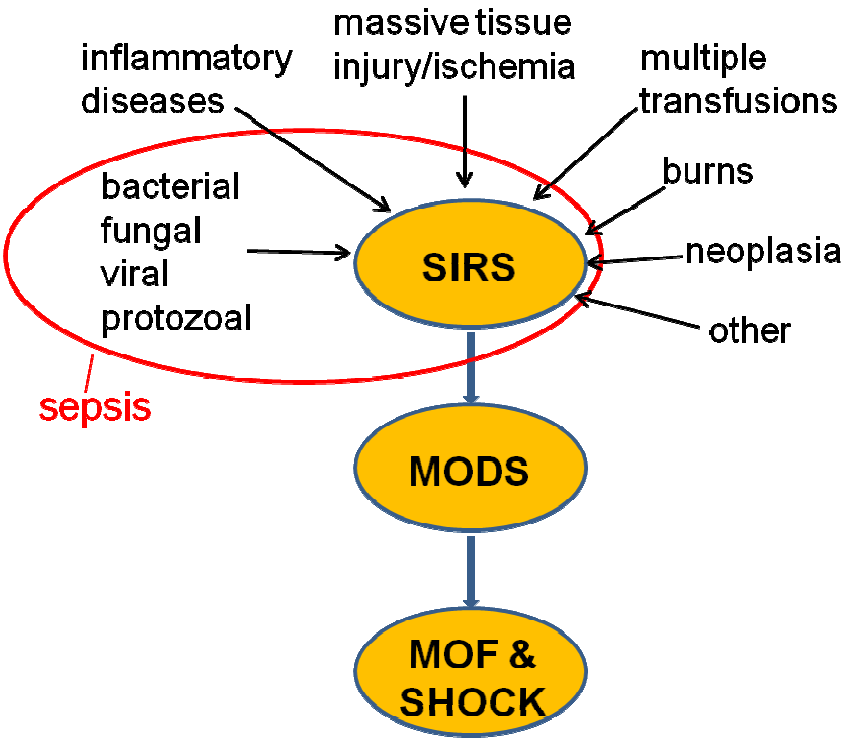

Figure 18. Definition of sepsis.
Sepsis is defined as SIRS caused by an infection. SIRS: systemic inflammatory response syndrome; MODS: multiple organ dysfunction syndrome. MOF: multiple organ failure.

B.2.2 A Potential Elicitor of Sepsis: Lipopolysaccharide (LPS)

The structure of LPS

One of the most powerful elicitors of sepsis is lipopolysaccharide (LPS), also known as endotoxin, which is set free from dying or multiplying Gram-negative bacteria and is able to trigger the immuno-inflammatory cascade. [77] During infection bacteria infiltrate various tissues, can enter the bloodstream and release LPS from their membranes which is additionally amplified by antibiotics that kill bacteria and cause further release of LPS. [79]

Lipopolysaccharides form a part of the outer cell membrane of Gram-negative bacteria (pathogens and commensals). These molecules contribute to physiological membrane functions of the bacterial organism and are necessary for growth and survival. [80] LPS molecules of wild type bacterial strains are negatively charged amphiphilic molecules and consist of three parts (Figure 19). 1) Lipid A, a hydrophobic lipid portion which anchors

the molecule in the cell membrane and is covalently linked to a hydrophilic polysaccharide. The latter part is divided in the 2) core oligosaccharide (containing up to 15 monosaccharides) and the so called 3) O-polysaccharide chain, [81] that consists of repetitive (up to 40) polysaccharide units. The O-chain forms the serological specificity and is present to different extent of completion in different bacterial strains and species. The lipid A portion is the highest conserved region of the molecule, but still varies between species. More structural diversity between bacterial strains can be found in the polysaccharide parts with the highest variability in the O-chain. [82] Provided, the O-chain, core oligosaccharide and lipid A moiety are present the LPS molecule is referred to as smooth LPS (S-form, S-LPS). If the O-chain is lacking the resulting LPS type is called rough or R-type LPS. [81] Both kinds, R- and S-form LPS are wild type LPS forms. Membranes of wild type bacteria comprise a mix of R-form and S-form LPS molecules, e.g. *Chlamydia* and *Neisseria* membranes contain a lot of R-form LPS. [4]

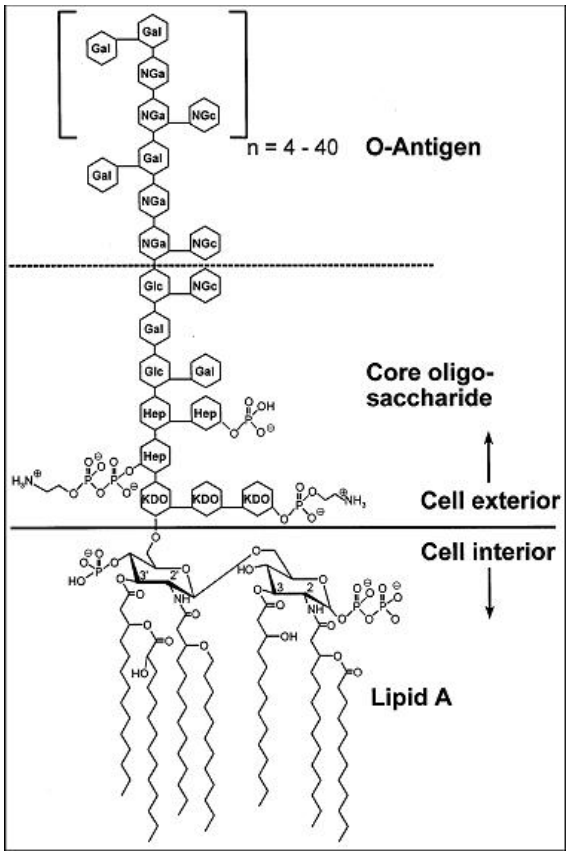

Figure 19. The structure of LPS.
Figure from Tipmj. [83]

Bioactivity of LPS

Immuno-inflammatory response

Various cells respond to LPS, the most responsive among them are those of the immune and vascular system. Triggered reactions are mostly production of inflammatory mediators, phagocytosis, proliferation and differentiation of immunocompetent cells. [81]

Essential for triggering the inflammatory response is the recognition of infectious agents via plasmalemmal or intracellular receptors. Well known receptor families comprise Toll-like receptors, R-protein families (in plants) and the CATERPILLAR family (prominent members are NOD1 and NOD2 proteins. [84]) Mostly, binding to receptors induces intracellular signal cascades leading to immune responses as previously mentioned, see the chapter *The Systemic Inflammatory Response Syndrome (SIRS)*.

The lipid A moiety contains the endotoxic activity of the molecule and is essential for triggering the response of the immune system. [85] Differences in the core region and structure of the O-chain are not crucial for the endotoxic activity. [86]

S-form and R-form LPS (which both contain lipid A) can induce a variety of adverse effects like apoptosis in B- and T-lymphocytes, [87,88] which is also an important mechanism during the pathogenesis of sepsis. Not endotoxin directly but elevated levels of cytokines, TNF, etc. (induced by endotoxin) trigger cell death. The loss of cell populations (immune/non immune cells, cells of different organs like hepatocytes, endothelial cells in lung and gut, etc.) initiated by the anti-inflammatory response most likely contributes to immunosuppression, organ failure and death. [88] These findings were shown in non-survivors of sepsis [89] as well as in experimental sepsis. [90]

S-form and R-form show different pathways of activating cells. S-form LPS binds to the lipopolysaccharide binding protein (LBP) and is then transported to CD14 (Cluster of Differentiation). Next, this complex is transported to a LPS receptor consisting of Toll-like receptor 4 (TLR-4), and the associated myeloid differentiation protein 2 (MD-2). [79] Activation of this receptor complex results in the production of cytokines (inflammatory response). TLR4-ligands derive from pathogenic agents but are never found in hosts themselves. [91] This enables the immune system to react only against cells that are foreign to the body.

R-form LPS can also activate cells of innate immunity expressing TLR4/MD2 but does not require CD14 and LBP, which enables R-form LPS to activate a larger spectrum of cells compared to S-form LPS. [4]

Myocardial dysfunction in sepsis

The cardiovascular status in sepsis is crucial for survival. [2] Ischemia, impaired cardiac pressure-volume relations and myocardial depression can double the risk of death and occur in nearly 40 % of the patients. [2] Maintaining a sufficient stroke volume as well as peripheral circulation is essential for myocardial function. Myocardial depression is a complex but reversible process underlied by several contributing factors. When the inflammatory response decreases, the myocardial function improves too. [2]

Cardiovascular dysfunction in sepsis has been a matter of research for more than five decades now but is still not well understood. Several factors like endotoxin, TLR-4, myocardial depressant factors (inflammatory mediators like TNF-α, interleukin 1-β, C5), nitric oxide (NO, affects vascular tone by causing vasodilation), endothelin (has vasoconstricting effects; affects also contractile properties of the heart and is of big relevance in the endothelium), oxidative stress (among other causes also induced by endotoxin), autonomic dysregulation and impaired calcium metabolism contribute to the myocardial depression. [2]

The effect of LPS on cardiac ion channels

Besides triggering the inflammatory response, S-LPS directly affects ionic channels of immune, neuronal and cardiovascular cells. [5-7] Modulation of cardiac ion channel function in sepsis contributes to cardiovascular dysfunction and can lead to severe complications like e.g. atrial fibrillation, [8,9] as the following reported results indicate:

Recently it has been shown in guinea pig atrial myocytes that S-LPS most likely mediates a nitration of ion channels. Thereby, a decrease in the L-type calcium current and an increase in the delayed rectifier potassium current (I_K) is caused, which can lead to shortening of the AP duration and therefore to supraventricular tachyarrhythmias. [10]

In HEK293 cells expressing cardiac sodium channels it was shown that acute application of S-LPS shifts both, current activation and inactivation to more negative membrane voltages and slows recovery from inactivation. This finding indicates that *in vivo* the sodium current is decreased, conduction velocity is reduced and re-entrant arrhythmias could occur. [92]

The effect of LPS on the pacemaker current

S-LPS administration substantially impairs human atrial I_f. This may in turn (partly) underlie the clinically observed reduction of heart rate variability under septic conditions, since I_f mediates autonomic inputs to the regulation of heart rate. Zorn-Pauly et al., 2007, reported that in S-LPS incubated human atrial myocytes (6 h, 10 µg/mL) the voltage-dependence of steady-state activation was shifted to more negative membrane potentials expressed in a shift of $V_{1/2}$ of – 14 mV (from – 78.4 to -92.7 mV). Furthermore, I_f could not be detected at membrane potentials more positive than -70 mV. Current densities in S-LPS treated cells were significantly smaller at -70 and -80 mV compared to control cells. Furthermore, time constants of I_f activation were slowed down by S-LPS and the responsiveness of S-LPS incubated cells to ß-adrenergic stimuli (1 µmol/L) was much higher than in control cells. [12]

S-LPS does not only impair I_f in incubated cardiomyocytes but additionally exerts an acute effect on I_f within several seconds after application. [11,93] Klöckner et al., 2011, reported that, similar to chronic conditions mentioned above, the voltage-dependence of current steady-state activation was shifted to more negative membrane potentials (shift: -20 mV). Furthermore, the whole-cell conductance of I_f was significantly reduced. I_f current amplitude was reduced by about 30% within 8 sec. Data gained by this group clearly indicate that 1) S-LPS causes a decreased open probability of HCN channels and a reduction of maximal conductance, thus causing a substantial impairment of I_f and 2) the O-chain of the LPS molecule is required for the LPS effect on I_f. [11] Meanwhile it was shown that the LPS molecule intercalates into the cell membrane and that most likely the polysaccharide part exerts a reducing effect on I_f by interacting with the channel protein. [94]

Wondergem et al., 2010, showed in HL-1 cells that S-LPS (1 µg/mL) inhibited activation of I_f and enhanced its deactivation. The same authors showed that S-LPS reduced Ca^{2+} oscillations and basal Ca^{2+} concentration, which negatively influences the contractility of the myocardium. [93] Furthermore, S-LPS treatment reduced beating rate in spontaneously active HL-1 cells by prolonging AP duration due to impairment of I_f, I_{Na} and I_{Kr}. [95]

Taken together these findings, it is likely that I_f impairment contributes to myocardial dysfunction in sepsis: As I_f mediates sympathetic and parasympathetic autonomic inputs to the pacemaking process, alterations in I_f characteristics are likely to have an impact on the

generation of sinoatrial APs and therefore heart rate. Usually septic patients show a very high heart rate which does not correlate well with S-LPS induced I_f impairment. A possible explanation is that *in vivo* the bradycardic action of endotoxin (via I_f blockade) is overruled by a combination of autonomic dysfunction (attenuated vagal tone, increased endogenous catecholamine release) and increased sensitivity of HCN channels to beta-adrenergic stimulation. [12,96]

Anyhow, further elucidation of the LPS-effect on the pacemaker current is required in order to understand the mechanism of LPS action on I_f, which is not known up to date. It is either possible that LPS directly affects the pacemaker channel or that membrane properties are altered due to LPS impairment and therefore ion channel characteristics are changed.
Up to date, research has only focused on I_f impairment by LPS, not taking into account the second current component I_{inst}, which also contributes to the pacemaking activity. Because of its (not well understood) role in pacemaking, also I_{inst} needs to be investigated regarding its possible modulation by LPS, which constitutes a target of the present study.

B.3 The Heart Rate Lowering Agent Ivabradine

Due to its important function of regulating pacemaker activity HCN channels have become an interesting therapeutical target for bradycardic compounds as required in the treatment of chronic and acute heart failure (for review see Ref. [17]). Decreasing heart rate allows a better supply of the myocardium with oxygen and therefore improves cardiac function. Ivabradine, a novel heart rate lowering agent, selectively blocks I_f in a use- and concentration-dependent way, thereby slowing down the spontaneous diastolic depolarization and consequently the AP firing rate of the sinoatrial node [18] without having other cardiovascular side effects. The I_f-reducing property of ivabradine is well documented for native cardiomyocytes (including human atrial cells [21]) as well as for HCN expressing cell lines. [18,97] For information about clinical trials on ivabradine please see references [98,99]. In 2005 ivabradine was approved by the European Medicines Agency and is the first clinical approved compound selectively inhibiting HCN channels. [17] Ivabradine, provided by *Servier,* is traded under the name *Procoralan*.

The establishment of the ivabradine block: The positively charged ivabradine molecules pass through the cell membrane and then reach into the channel pore when channels are

open and the current is directed inwards. The block is manifested when channels deactivate at depolarized voltages. [97]. For this reason ivabradine acts as an open channel blocker with an exception for HCN1, which can also be blocked in the closed state. [97]
Ivabradine is more effective at faster heart rates while its action declines during bradycardia [100,101] due to its use-dependent behavior. The more often channels open, the more effective is the ivabradine block. At high concentrations (10 µmol/L) ivabradine also decreases the L-type calcium current and the delayed rectifier outward potassium current I_K in rabbit SANC. [19] Ivabradine causes a significant prolongation of the AP in human cardiac preparations (papillary muscle) and dog Purkinje fibers. [20] In isolated human cardiomyocytes ivabradine induces a concentration- and use-dependent I_f inhibition with an IC_{50} at steady state of 2.9 µM independent of the presence or absence of cAMP. [21]
In pulmonary vein cardiomyocytes, which are considered to be a source of atrial fibrillation, ivabradine has been shown to have an inhibitory effect on pulmonary vein activity by decreasing I_f and calcium transients. [102]

Long-term treatment with ivabradine shows indirect beneficial effects through heart rate reduction. For example, electrophysiological cardiac remodeling is reversed, i.e. the functional overexpression of HCN channels in post-myocardial infarcted rats is counteracted. [103] Additionally, heart rate reduction by ivabradine improves endothelial function, reduces atherosclerotic plaque formation, attenuates markers of vascular oxidative stress and expression of inflammatory cytokines, as shown in apolipoprotein E-deficient mice. [104,105]
Reducing heart rate through ivabradine might also be beneficial to patients in septic condition, as an elevated heart rate is correlated with an unfavorable outcome. Administration of beta-blockers is contraindicated due to the huge amount of catecholamines needed in order to stabilize blood pressure. In 2010 the MODI_fY Trial has been launched to investigate the application of ivabradine in patients suffering from MODS (multiple organ dysfunction syndrome), which in most cases is caused by sepsis and cardiogenic or hemorrhagic shock (Results are outstanding). [22]

Since S-LPS as well as ivabradine substantially impair I_f and ivabradine is administered in patients with elevated LPS levels (MODI_fY trial), the interference of LPS and ivabradine action on the pacemaker current (I_f and I_{inst}) needs to be investigated at the single cell level.

B.4 The Patch-Clamp Technique

As the majority of results in this study is obtained by electrophysiological experiments, a short overview of the patch-clamp technique is given.

Erwin Neher and Bert Sakmann developed the patch-clamp technique in the late 1970s as a refinement of the voltage-clamp method, which was invented by Kenneth Cole and H.J. Curtis in the late 1930s.

The patch-clamp method made it possible to record currents through single ion channels and the collectivity of currents flowing through all ion channels of a single cell. By means of this technique the function of excitable cells was and is investigated. In 1991 Neher and Sakman were awarded the Nobel Prize in Physiology for their fundamental work.

The experimental setup

Within the patch-clamp technique four setups can be distinguished: Cell-attached-configuration (on-cell), whole-cell-configuration, inside-out-configuration and outside-out-configuration. The initial step for all configurations is the same, as can be seen in Figure 20: Using an inverse microscope, cells are placed in a test chamber, superfused with the bath solution. A glass patch pipette is approached to the cell surface employing a micromanipulator. This glass micropipette (borosilicate, diameter around 1 µM), filled with a conductive pipette solution, functions as an electrode, in which a chlorided silver wire is placed for conducting current to the amplifier.

Between the cell surface and the glass pipette a seal with high resistance must be established in order to avoid recording of noise. Therefore, after closely approaching to the cell surface a little membrane patch is sucked (mostly per mouth via a tube) towards the pipette opening till the membrane and the pipette stick to each other, thus isolating the membrane patch electrically from its surrounding and the background noise. The resistance of such a seal amounts to several gigaohm, hence the seal is called gigaseal. Several patch-clamp configurations can be established (Figure 20), and each of them offers different advantages:

Cell-attached: The cell membrane is intact and at the intracellular side all molecules are in their native environment; membrane resting potential, second

messengers and ion concentrations remain unchanged; single channel recording possible (Figure 21).

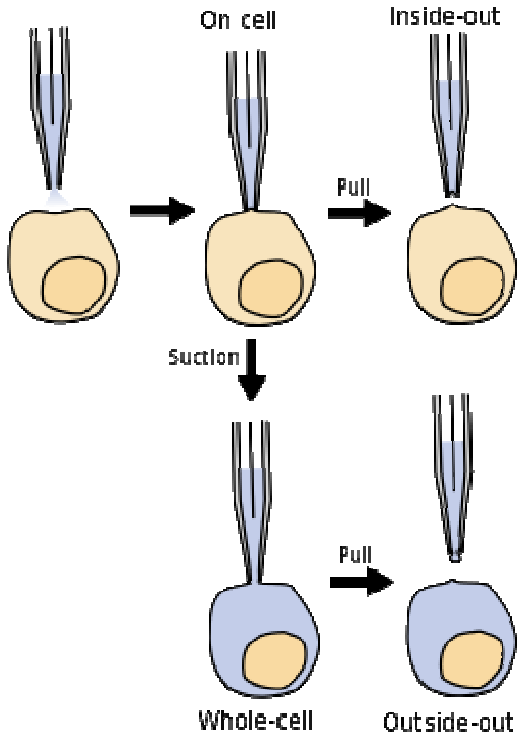

Figure 20. Patch-clamp configurations.
By sucking the cell membrane to the pipette tip, a gigaseal and hence the cell-attached configuration (on cell) is established. By pulling the pipette from the cell membrane, the inside-out configuration is formed with the cytoplasmic surface exposed to the bath solution. By sucking in the cell attached state the membrane patch is ruptured and sticks to the inside of the glass pipette: The whole-cell configuration is established with an open connection to the cytoplasm. When pulling back the pipette from the whole-cell state the outside-out configuration is achieved with the extracellular side of the cell membrane exposed to the bath solution. Figure from Bilz0r. [106]

Inside-out: The membrane proteins and structures attached to the inside of the membrane (like parts of the cytoskeleton, proteins and organelles) stay with the patch; single channel recording possible.

Whole-cell: The most common technique, currents across entire membrane can be recorded; cytoplasm is exchanged for pipette solution of defined composition (Figure 21).

Outside-out: The membrane potential is equivalent to the pipette potential, ion gradients and reverse potentials can be measured; the bath solution is

equivalent to the extracellular space: this configuration is suitable for measuring properties of ligand-gated ion channels as substances and solution can easily reach the outside of the membrane, single channel recording possible.

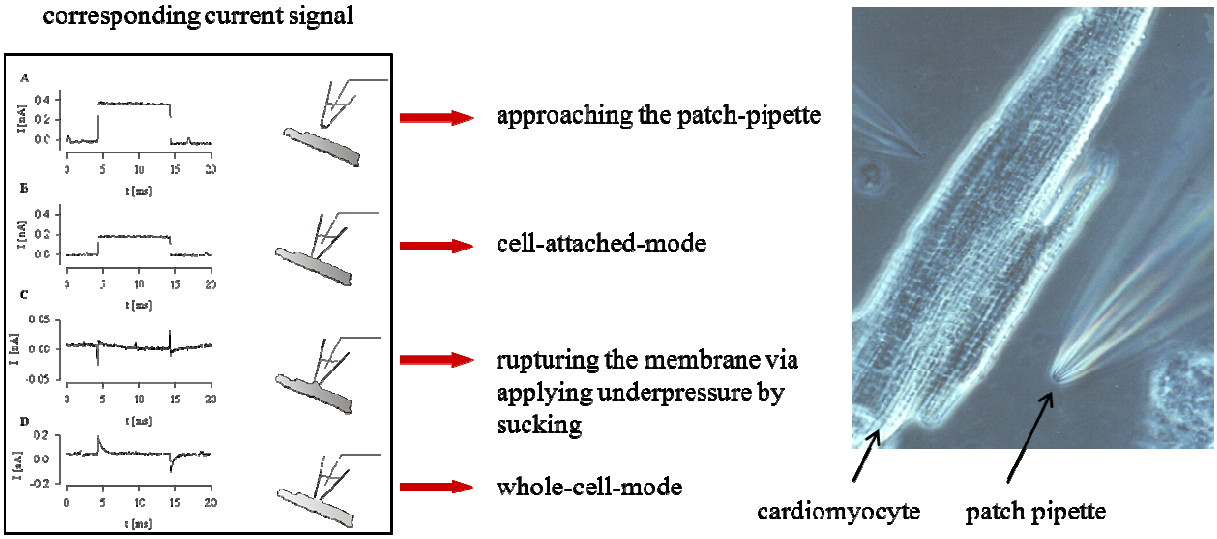

Figure 21. Establishment of the whole-cell configuration and corresponding electrical signals.

Operating principle of a patch-clamp amplifier

Employing the patch-clamp technique in the voltage-clamp mode means that the membrane voltage is kept constant at a desired value. The current required for compensation is equivalent to the current flowing across the cell membrane at the respective membrane potential and can be measured. A more precise explanation can be found in Figure 22.

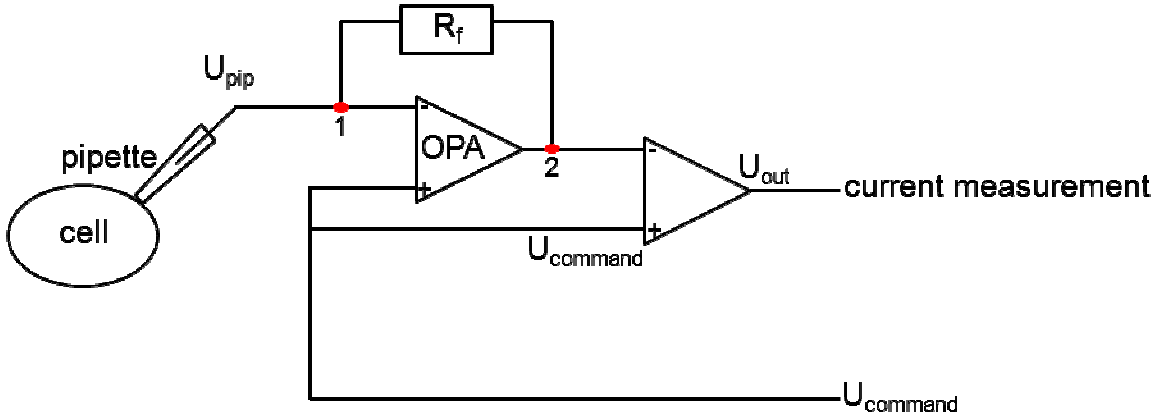

Figure 22. Function principle of a patch-clamp amplifier.
An Operational Amplifier (OPA) compares the command voltage with the measured potential (U_{pip}). The output voltage of the OPA is proportional to the measured potential difference between U_{pip} and $U_{command}$. The potential difference between point 1 and point 2 results in a current flow via the resistor in the feedback path (R_f) into the electrode and consequently the cell, until U_{pip} and $U_{command}$ are equal. This equilibration happens so fast, that U_{pip} and $U_{command}$ are equal at any timepoint. U_{out} is measured and the current injected into the cell is calculated in dependence of R_f. This compensating current is equivalent to the current flowing across the cell membrane at a specific voltage.

C. MATERIAL AND METHODS

C.1 Isolation of Human and Guinea Pig Myocytes

Human right atrial appendages were obtained from 44 patients (28 men, 16 women) aged between 27 and 82 years (mean 65.83 ± 1.68). All patients were in sinus rhythm before surgical intervention, such as aortic valve replacement, coronary bypass graft or aorta aneurysm repair. All patients were under treatment with various combinations of drugs like β1-adrenergic blockers, statins, diuretics, angiotensin-converting enzyme inhibitors and calcium channel blockers (Table 2). All experiments were carried out in accordance with the Declaration of Helsinki. [107] The ethics committee of the Medical University of Graz approved the use of human tissue and all patients gave informed consent.

Atrial samples were transported to the laboratory within 10 to 15 min in cold saline containing (in mmol/L): 90 NaCl, 30 KCl, 2 $NaHCO_3$, 2 HEPES/Na^+, 5.5 D(+)-glucose, 42 sucrose (pH 7.4, adjusted with NaOH). The tissue pieces were cut into fragments of about 1 mm^3 and washed with saline to remove Ca^{2+}. Fragments were transferred to a dissociation vessel and gently stirred at 37° C in saline containing 0.25 % (w/v) trypsin (Sigma-Aldrich, St. Louis, MO, USA) for 2 min followed by saline containing 300 IU/mL collagenase (CLS-2, Cell Systems, Germany). The supernatant was replaced by collagenase solution every 15 min. After the third change, collagenase concentration was reduced to 150 IU/mL. Isolated myocytes were washed with saline followed by stepwise increase in Ca^{2+} to a final concentration of 500 µmol/L. Myocytes were then transferred to M199 cell culture medium (Sigma-Aldrich) containing penicillin 50 IU/mL, streptomycin 50 µg/mL (both Sigma-Aldrich) and kept at 37° C under 5% CO_2. Experiments were performed 6 h (recovery time) after isolation of myocytes within a 24 h time period.

Guinea pig (Dunkin Hartley, Charles River Laboratories, Germany) ventricular myocytes were isolated by Langendorff perfusion [108] and stored in M199 medium at 37° C. Experiments were performed 24 h after cell isolation.

Patients	ACE inhibitor	Angiotensin receptor antagonist	Antiarrhythmics	Anticoagulants	β-blocker	Calcium channel blocker	Digitalis	Diuretics	Nitrates	Statins
1		+								
2		+		+	+	+				
3	+			+	+			+	+	
4	+					+		+		
5		+								
6				+	+				+	+
7										
8					+					+
9									+	
10	+				+					
11				+	+					
12					+			+		+
13						+		+		
14	+			+	+					+
15	+				+					+
16	+			+	+			+		
17					+	+		+		
18					+					
19	+				+					
20	+									+
21					+		+	+		
22				+	+	+				+
23					+					+
24					+			+		+
25				+		+			+	+
26				+					+	
27	+			+	+					+
28	+			+				+		+
29	+			+		+				+
30	+				+	+		+		
31	+			+		+				+
32	+				+					+
33		+		+	+			+		
34	+			+	+					+
35	+			+	+			+		
36		+		+				+		
37					+					
38			+		+					
39					+			+		+
40	+				+	+				+
41	+			+	+			+		
42					+					+

Table 2. Medication of patients.

C.2 Cell Culture of the Murine Atrial Cardiomyocyte Cell Line

HL-1 cells [109] were cultured in fibronectin (0.5 %, w/v)/gelatin (0.02 %, w/v) (Sigma-Aldrich) coated flasks and supplied with Claycomb medium (Sigma-Aldrich) containing 10 % (v/v) fetal bovine serum (Sigma-Aldrich), 0.1 mmol/L norepinephrine (Sigma-Aldrich), 2 mmol/L L-glutamine (Sigma-Aldrich), 100 IU/mL penicillin and 100 µg/mL streptomycin at 37° C under 5% CO_2. For experiments cells (104/well) were plated in 6-well plates.

C.3 Incubation Protocols

In order to investigate acute effects of endotoxins on the pacemaker current, human myocytes were superfused with I_f-Tyrode containing 10 µg/mL S-form LPS (wild-type *Escherichia coli* serotype 0111:B4 or *Salmonella enterica* serotype *Minnesota*, Sigma-Aldrich) or 10 µg/mL O-chain lacking R-form LPS (LPS Re of the deep rough mutant from *Salmonella enterica* serotype *Minnesota* strain R595 for 6 min. Chronic effects of endotoxins were evaluated after 6 to 10 h incubation of myocytes under conditions described above. In the present manuscript S-form LPS is referred as S-LPS, while R595-mutant LPS is referred as R595.

The effect of ivabradine (kindly provided by Servier Laboratories, France, 1 µmol/L in I_f-Tyrode) on the pacemaker current was investigated by patch-clamp after superfusion of myocytes for 7 min.

HL-1 cells were incubated with endotoxins for 6 h followed by cell lysis for RNA and protein isolation (see below).

C.4 Patch-Clamp Solutions

(i) Superfusion (extracellular) solution: I_f-Tyrode solution contained (in mmol/L): 137 NaCl, 25 KCl, 1.8 $CaCl_2$, 1.2 $MgCl_2$, 1 $BaCl_2$, 2 $MnCl_2$, 0.2 $CdCl_2$, 3 4-aminopyridine, 5 glucose, 5 HEPES (pH 7.35, adjusted with NaOH). Mn^{2+}, Ba^{2+}, Cd^{2+} and 4-aminopyridine were added to avoid interference with potassium and calcium currents.
(ii) Pipette (intracellular) solution: Patch pipettes (2.5 to 4 MΩ) were filled with a solution containing (in mmol/L): 100 K^+-aspartate, 30 KCl, 5 Na^+-ATP, 4 $CaCl_2$, 11 EGTA, 10 HEPES (pH 7.2, adjusted with KOH).

C.5 Electrophysiological Recordings and Analysis

Electrophysiological recordings were performed in the whole-cell patch-clamp technique at 36-37° C using the amplifiers List L/M-EPC 7 (List, Darmstadt, Germany) and Axopatch 200B (Molecular Devices, CA, USA) and the A/D - D/A converters Digidata 1322A and Digidata 1200 (Molecular Devices LLC). pCLAMP software (Molecular Devices LLC) was used for data acquisition and analysis.

(i) The cell membrane capacitance was determined by numerical integration of the capacitive transient elicited by a 10 mV hyperpolarizing step from -50 mV.

(ii) The pacemaker current was measured by hyperpolarizing voltage steps (3 s duration) from -40 to -130 mV (10 mV increment, holding potential -40 mV), i.e. *protocol p1*.

(iii) As ivabradine is a use-dependent inhibitor its effect was measured employing the following protocol: Trains (total duration 9 min) of activating/deactivating voltage steps (-100 mV for 3 s; 0 mV for 0.4 s) from a holding potential of -40 mV at 1/6 Hz (i.e. *protocol p2*) *p1* preceded and followed *p2* (see insert Figure 35). Ivabradine superfusion started after 2 min.

In order to allow equilibration of the pipette solution with the cytosol current recordings were started 4 min after rupture of the membrane patch. I_{inst} was determined as the amplitude of the instantaneous current immediately after the decline of the capacitive transient. I_f represents the difference between I_{inst} and the current at the end of the hyperpolarizing voltage steps. I_{inst} and I_f were normalized to cell membrane capacitances and expressed as pA/pF in order to compensate for cell size variations. Mean cell capacitance of human atrial myocytes used in this study was 91.9 ± 6.0 pF (n = 87).

I_f conductance was calculated according to the following equation:

$$g_f = I_f / (V_m - V_{rev})$$

g_f is the calculated conductance at a given membrane potential V_m, I_f is the measured current amplitude, and V_{rev} represents the reversal potential of I_f in human atrial myocytes amounting to -13 mV as described for an external potassium concentration of 25 mmol/L.[110]

Next, g_{fmax} was calculated by fitting the g_f values with the Boltzmann function according to

$$g_f = g_{fmax} / (1 + exp[(V_{1/2} - V_m)/k])$$

$V_{1/2}$ is the voltage at half-maximal steady-state activation and k is the slope factor. For the calculation of steady-state activation curves conductance was normalized to maximal conductance and fitted by a Boltzmann equation. The liquid junction potential between the electrode tip and the external solution was calculated from the Henderson equation and amounted to -11.7 mV.[111] Data were not corrected for the liquid junction potential.

C.6 Immunoprecipitation of HCN2 and HCN4 Proteins

Male C57BL/6 mice (8-10 weeks, 20-30 g) were obtained from the Institute of Biomedical Research (Medical University of Vienna, Austria) and were kept on a 12 h light/dark cycle with free access to food and water. Mice were killed by cervical dislocation, hearts were removed and homogenized in RIPA buffer (150 mmol/L NaCl, 50 mmol/L Tris-HCl, 1% [w/v] NP-40, 0.1 % [w/v] SDS, 0.5 % [w/v] sodium deoxycholate, 1 mmol/L EDTA, pH 7.4) containing a protease inhibitor cocktail tablet (Sigma-Aldrich). Cell homogenates were centrifuged at 10000 rpm (4° C, 10 min) to pellet debris. Heart protein lysates were equilibrated against immunoprecipitation buffer containing (in mmol/L): 50 Tris-HCl (pH 8.0), 10 $MgCl_2$ and 150 NaCl. Protein lysates containing equal protein concentrations (1 mg) were mixed with 1 µg mouse anti-HCN2 or anti-HCN4 antibody (Abcam, Cambridge, UK) for 2 h at 4° C. The immune complexes were precipitated by mixing 20 µL of protein A/G plus agarose (Santa Cruz Biotechnology, Heidelberg, Germany) overnight at 4° C. Pellets were collected by centrifugation at 10000 rpm (4° C, 1 min). After being washed three times with RIPA buffer, pellets were resuspended in 40 µL of 4 x NuPAGE LDS sample buffer. Western blot analysis (see below) was performed to identify immunoprecipitated HCN2/HCN4 protein.

C.7 Western Blot Analysis

After treatment with LPS, 0.5-1x10^6 HL-1 cells were lysed in 100 µL lysis buffer (50 mmol/L HEPES, 150 mmol/L NaCl, 1 mmol/L EDTA, 10 mmol/L $Na_4P_2O_7$, 2 mmol/L Na_3VO_4, 10 mmol/L NaF, 1 % [v/v] Triton X-100, 10 % [v/v] glycerol, pH 7.4) containing a protease inhibitor cocktail tablet (Sigma-Aldrich) for 10 min on ice. Cells were scraped and centrifuged at 10000 rpm (4° C, 10 min) to pellet debris. After protein estimation using the Lowry method, 50 µg of total protein were added to 10 µL of 4 x NuPAGE LDS sample buffer containing 2 µL sample reducing agent (Invitrogen, Austria) and heated (70° C, 10 min). Proteins and immunoprecipitates were separated by electrophoresis on NuPAGE 4-12 % Bis-Tris gel and transferred to nitrocellulose membranes. Membranes

were blocked with 5 % (w/v) non-fat milk in TBST (Tris-buffered saline containing Tween 20) (25° C, 2 h) and incubated with anti-HCN2/HCN4 antibody (1:1000 in 5 % [w/v] BSA) (4° C, overnight). Immunoreactive bands were visualized with HRP-conjugated goat anti-mouse IgG (1:100000 in 5 % [w/v] non-fat milk in TBST) (25° C, 2 h) followed by Super Signal West Pico Chemiluminescent substrate (Thermo Scientific, IL, USA) and developed by Bio-Rad ChemiDoc MP Imaging System. Membranes were stripped (58.4 g/L NaCl, 7.5 g/L glycine, pH 2.15) and incubated with mouse monoclonal anti-β-actin antibody (Santa Cruz Biotechnology) (1:1000 in 5 % [w/v] BSA).

C.8 Immuno-Dot-Blot Technique

Polyvinylidene difluoride (PVDF) membranes (Bio-Rad Laboratories, Vienna, Austria) were prewetted in absolute methanol. S-LPS and R595 (10 µL equivalent to 10 µg) were cross-linked (dotted) to PVDF membranes under UV conditions (10 min) and dried. Dots were then incubated with 5 or 10 µL of immunoprecipitated HCN2/HCN4 protein (approx. concentration) or 10 µL (equivalent to 1 µg) solution containing high-density lipoprotein (HDL) (4° C, 2 h). HDL was isolated from human plasma as described. [112] Membranes were washed with TBST and blocked with 5 % [w/v] non-fat milk in TBST (25° C, 5 h) followed by incubation with anti-HCN2/HCN4 antibody (1:1000 in 5 % [w/v] BSA) or rabbit anti-human apolipoprotein A-I antiserum (1:3000 in 5 % [w/v] BSA) recognizing ApoA-I, the major apolipoprotein of HDL (4° C, overnight). To detect immunoreactive dots membranes were incubated with HRP-conjugated goat anti-mouse or goat anti-rabbit IgG (1:100000 in 5 % [w/v] non-fat milk in TBST) (25° C, 2 h) followed by Super Signal West Pico Chemiluminescent substrate (Thermo Scientific) and developed by Bio-Rad ChemiDoc MP Imaging System.

C.9 RNA Isolation and Real Time PCR

Total RNA was isolated from HL-1 cells after S-LPS or R595 (10 µg/mL, 6 h) treatment by using QIAshredder and RNeasy Mini Kit (Qiagen, UK). 1 µg of RNA was subjected to reverse transcription. 6 ng cDNA per template were used for gene quantification by using SYBR Green PCR Kit (Qiagen) and gene specific primers. Real time RT-PCR protocol was run by using LightCycler 480 system (Roche Diagnostics, Vienna, Austria). Following primers were used:

GAPDH (Mm_Gapdh_3_SG, Qiagen);
HCN1 (NM_010408) F: 5'-TTCTCAGTCTCTTGCGGTTATTACG-3', R: 5'-CACTGGCGAGGTCATAGGTC-3';
HCN2 (NM_008226) F: 5'-CTGCGGCTATCACGGCTCAT-3', R: 5'-CAACCGTCCCAGTGGCAGA-3';
HCN4 (NM_001081192) F: 5'-GTCCATGCGCAAGCGGCTCTA-3', R: 5'-TGCTCCTTCGGCTGGGGTCC-3'. Relative gene expression levels compared to GAPDH were calculated by using the ΔΔCT method.

C.10 Analysis of Ivabradine Concentrations in Guinea Pig Ventricular Myocytes

Ivabradine was quantified using a fluorometric HPLC technique. [113] Briefly, untreated (controls) and endotoxin-treated cells (S-LPS or R595, 10 µg/mL, 6 h) were incubated with ivabradine (1 µmol/L, 15 min) followed by four washing steps with 1.5 mL Tyrode solution (in mmol/L: 137 NaCl, 5.4 KCl, 1.8 $CaCl_2$, 1.1 $MgCl_2$ x $6H_2O$, 2.2 $NaHCO_3$, 0.4 NaH_2PO_4 x H_2O, 5.6 D-glucose, 10 HEPES, pH 7.4). Finally, cells were deproteinized with 200 µL perchloric acid (0.4 mol/L). After centrifugation (1500 rpm, 5 min) the supernatant was used for ivabradine determination and the pellet was dissolved in 1 mL NaOH (0.1 mol/L) for protein determination (BCA Protein Assay, PIERCE, Rockford, IL, USA). Additionally, the final washing solution (Tyrode – 4^{th} step) was also analyzed for ivabradine to ensure the efficacy of the washing procedure. Ivabradine was isocratically separated on a 5-µm ODS Hypersil column (250 x 4.6 mm; Thermo Scientific) guarded by a 5-µm ODS Hypersil column (10 x 4.6 mm; Uniguard holder) with a mixture of acetonitrile and 0.025 mmol/L KH_2PO_4 buffer (40:60, v/v, pH 1.7) the latter containing 0.3 % (v/v) of 1 mol/L hydrochloric acid. The flow rate was 0.8 mL/min (25° C); the injection volume was 40 µL. For calibration, ivabradine dilutions (ranging from 0.01 to 1 µmol/L) were prepared freshly in Tyrode's solution. Fluorescence was monitored at excitation/emission wavelengths of 283 and 328 nm. The HPLC apparatus consisted of an L-2200 autosampler, L-2130 HTA pump and L-2480 fluorescence detector (VWR Hitachi, Tokyo, Japan). Detector signals were recorded with a personal computer. The program EZchrom Elite (Scientific Software Inc., San Ramon, CA, USA) was used for data acquisition and analysis.

C.11 Computer Simulation

A computational model of the rabbit sinoatrial AP was used, [23] which reproduces the effect of I_f inhibition on the beating rate (e.g. ~ 20 % rate reduction by 3 µmol/L ivabradine) in good agreement to experimental findings. The dynamics of the rabbit sinus node model were computed for I_f conductance values scaled between 0.0 and 1.0 (5 % increment) and for I_f $V_{1/2}$ steady state activation values between -52.5 and -66.5 mV (1 mV step size). To achieve a stable cycle length of spontaneous APs the model was simulated 70 s for each parameter setting. Cycle length was calculated within the last 10 s. The differential equations system of the model was implemented on a personal computer in Matlab and a variable step solver (ode15s) was used for numerical integration.

C.12 Statistics

Results are presented as mean ± standard error of mean (SEM), n is representing the number of experiments or number of cells tested. Statistical significance was tested by Student´s t-test or one-way ANOVA with adequate post hoc tests (Tukey, Dunett), using IBM SPSS software. P-values ≤ 0.05 were considered statistically significant. All tests were 2-sided.

D. RESULTS

Before focusing on the combined action of ivabradine and LPS on the human pacemaker current, the separate action of these clinically relevant substances was tested. In the first step the acute S-LPS action on the pacemaker current was investigated, followed by a comparison of the chronic effect of S-LPS and R595 on I_f and I_{inst}. The acute effect of R595 on I_f had already been reported by Klöckner et al., 2011 [11] and was therefore not repeated.
In the second step the action of ivabradine on the pacemaker current was tested, followed by the analysis of the combined effect of endotoxin and ivabradine.

The pacemaker current of all examined cardiomyocytes comprised two components, namely a time- and voltage-independent component referred to as I_{inst} and a voltage- and time-dependent component referred to as I_f. The insert in Figure 24B shows how I_{inst} was measured (detailed description in the methods section). The term "pacemaker current" means a common description of both components together.
Whereas I_f activates between -60 and -70 mV, I_{inst} is already present at -40 mV and represents the major pacemaker current component up to -80 mV. At more negative membrane potentials I_{inst} contributes at least 41 % to total pacemaker current (Figure 23).
The mean cell capacitance of human atrial myocytes used in this study amounted to 91.9 ± 6.0 pF (n = 87). Only I_f but not I_{inst} showed a time dependent rundown amounting to 16 ± 2.6 %.

Representative recordings of pacemaker currents of human atrial myocytes

Figure 24 shows representative traces of pacemaker currents under control, ivabradine and endotoxic conditions, namely S-LPS or R595 incubation (10 µg/mL, 6. The pacemaker current was elicited by hyperpolarizing voltage steps from of -40 to -130 mV (detailed description of I_{inst} and I_f-measurement in the methods section).
When septic conditions were mimicked *in vitro* (incubation with endotoxins) I_f activated at more negative membrane potentials only in S-LPS but not in R595 incubated myocytes. The reason for observed differences in endotoxin-mediated effects is the absence/presence of the O-chain but not the source of endotoxin preparations: In this study S-LPS extracted from *Escherichia coli* but R595 extracted from *Salmonella enterica* serotype *Minnesota*

were used. In order to have the possibility to compare results from these two bacterial strains it was proved that cells incubated with S-LPS from *S. e. minnesota* showed a similar steady-state activation profile like cells incubated with S-LPS from *E. coli* (Figure 25).

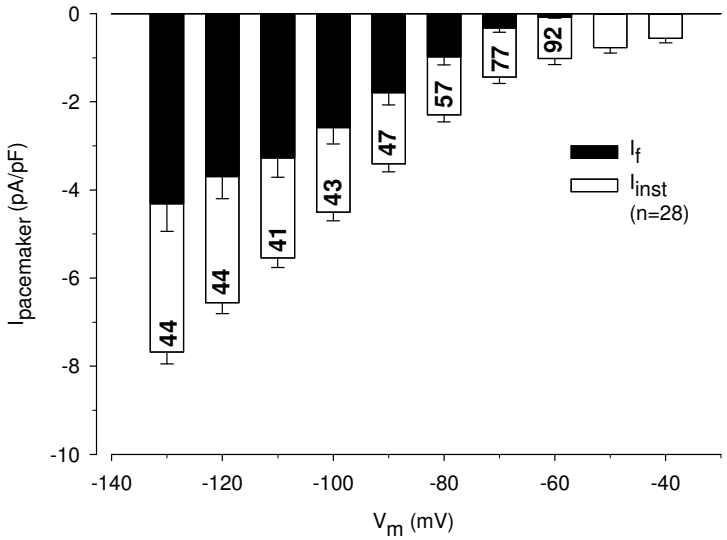

Figure 23. Contribution of I_f and I_{inst} to the total pacemaker current.
The numbers in the white bars indicate the percentage of the pacemaker current I_{inst} accounts for.

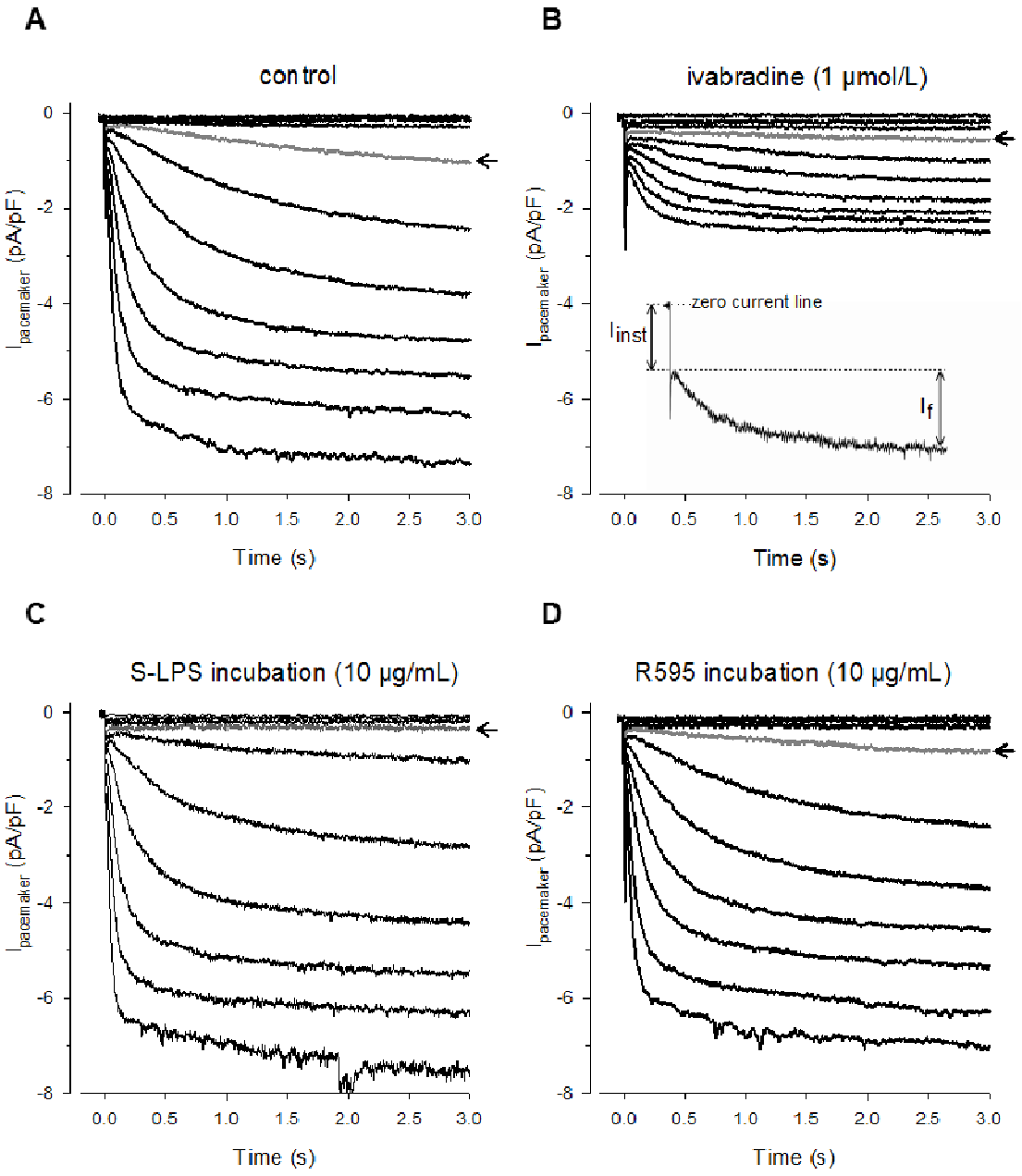

Figure 24. Representative recordings of pacemaker currents in human atrial myocytes.
The insert in panel (B) shows how I_f and I_{inst} were determined.

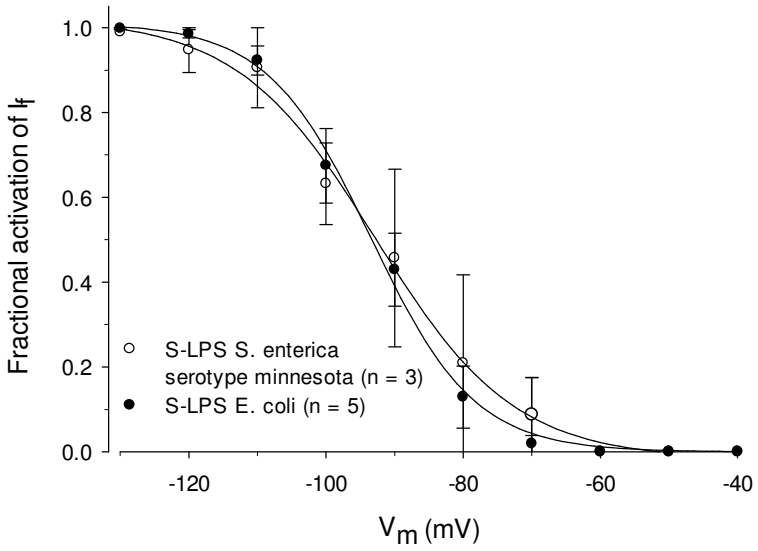

Figure 25. Voltage-dependence of I_f steady-state activation of human atrial myocytes incubated with different S-LPS preparations.
Cells were incubated with S-LPS extracted from *E. coli* or *S. enterica* serotype *Minnesota* (10 µg/mL) for 6 h. Normalized conductances were fitted by a Boltzmann function to obtain voltage-dependence of steady-state activation. *E.coli*: $V_{1/2}$=93.0±2.1 mV, k=6.4±0.5 mV; *S. enterica*: $V_{1/2}$=-90.6±7.9 mV, k=6.3±0.5 mV.

D.1 Effect of LPS on the Pacemaker Current

D.1.1 Acute Effect of LPS on the Pacemaker Current

Effect on I_f: Figure 26A shows superimposed original current traces before and after S-LPS perfusion at exemplary membrane potentials. *I-V* relations of I_f are shown in panel (B) (n = 9). S-LPS significantly reduced I_f current densities at membrane potentials between -60 and -130 mV. S-LPS dependent I_f reduction was significantly larger than the time dependent I_f rundown, panel (E). Mean current-densities to voltage relations were measured before and after S-LPS perfusion and percentage of reduction was calculated.

Furthermore, S-LPS significantly shifted the voltage-dependence of steady-state activation by -12.6 ± 4.8 mV to a more negative membrane potential compared to control values, panel (C): Control $V_{1/2}$ and slope factor yielded to -85.4 ± 3.0 mV and 8.9 ± 0.8 mV. S-LPS significantly changed $V_{1/2}$ and slope factor to -98.0 ± 3.1 mV and 6.3 ± 0.4 mV.

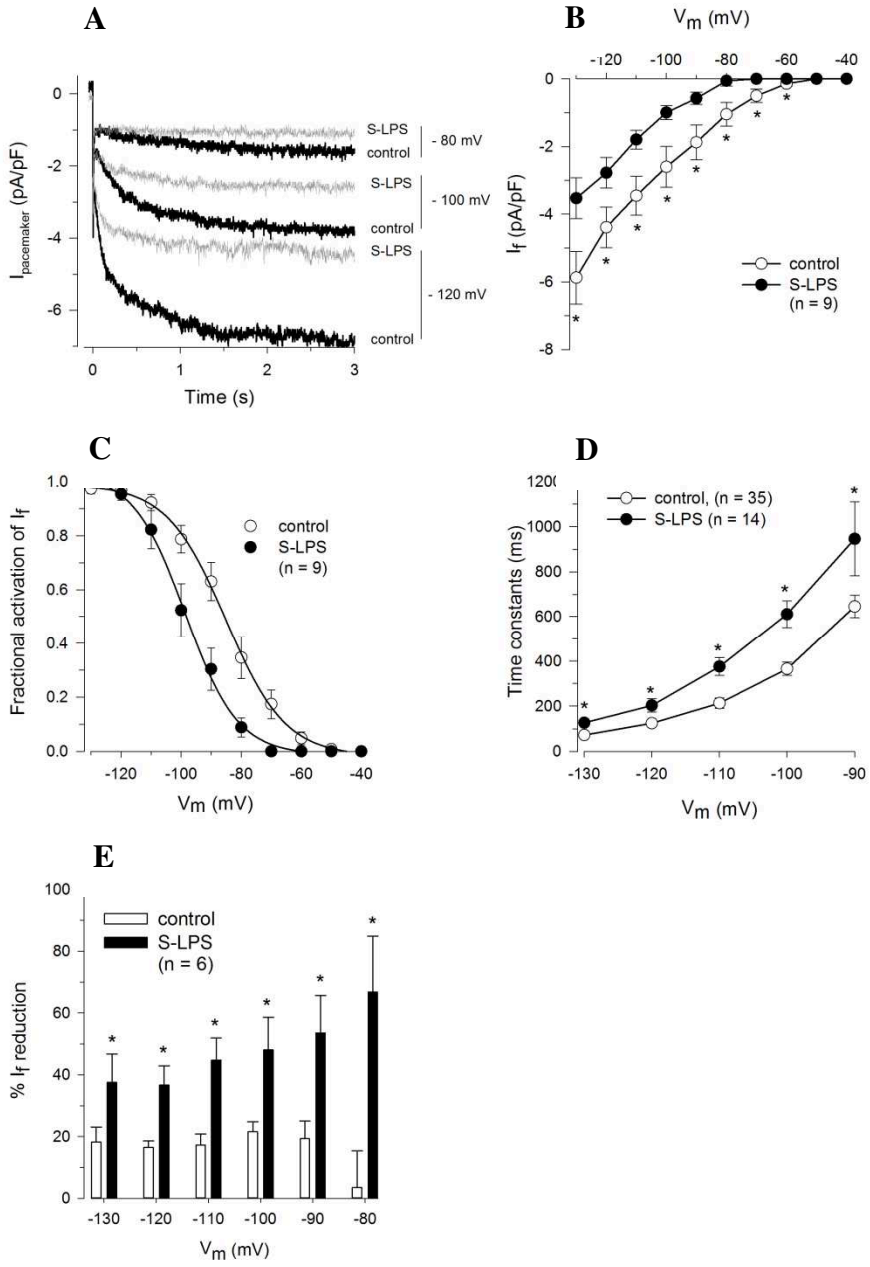

Figure 26. Acute effect of S-LPS on I_f characteristics.
I_f was measured before and after superfusion with I_f-Tyrode containing (10 µg/mL, 6 min) LPS. **(A)** Superimposed current traces before and after S-LPS treatment. **(B)** Reduction of mean current densities. **(C)** Voltage-dependence of I_f steady-state activation before and after S-LPS superfusion. Normalized conductances were fitted by a Boltzmann function to obtain voltage-dependence of steady-state activation. Control: $V_{1/2}$=-85.4 ± 3.0 mV, k = 8.8 ±0 .8 mV; S-LPS: $V_{1/2}$ = -98.0 ± 3.1 mV, k = 6.3 ± 0.4 mV. **(D)** Mean time constants of I_f steady-state activation before and after S-LPS superfusion. Values were obtained by fitting a monoexponential function to current traces. **(E)** LPS induced I_f reduction compared to time dependent current rundown. *p≤0.05 vs. control.

Values were obtained by fitting a Boltzmann function to normalized conductances. Maximal conductance values were also significantly reduced by S-LPS: g_{fmax} yielded to 50.2 ± 6.7 pS/pF before versus 31.5 ± 5.7 pS/pF after S-LPS perfusion.
To estimate the time course of I_f activation monoexponential fits to the current traces were performed. Panel (D) depicts the significant slower mean time constants of current activation (τ) due to S-LPS administration compared to control cells. E.g. at -90 mV τ was only 645.3 ± 50.6 ms in control versus 1037.2 ± 167.1 ms in S-LPS treated cells. At -130 mV time constants in control cells amounted to 71.6 ± 6.9 ms and in S-LPS treated cells to 115.0 ± 12.7 ms.

Effect on I_{inst}: The mean current density was not affected by acute S-LPS application, as can be seen in Figure 27. Furthermore, I_{inst} was not subjected to a time dependent rundown, panel (B).

To study the time dependence of the LPS effect on I_f and I_{inst} voltage steps to -80 mV of 2 Hz were applied. (Figure 28). At timepoint zero LPS was equally distributed around cells. I_{inst} remained unchanged whereas after 4 min the reducing S-LPS effect on I_f levelled off at around 90 %. From min 1 onwards I_f reduction by S-LPS was significantly different from control cells which underwent the same protocol without S-LPS perfusion.

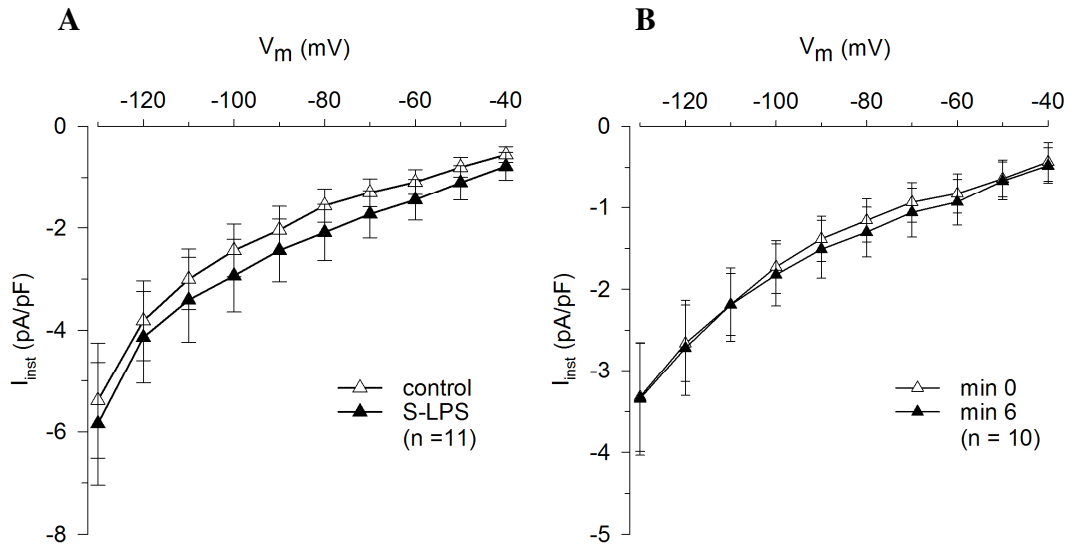

Figure 27. Effect of S-LPS on I_{inst}.
(A) I_{inst} is neither reduced by S-LPS perfusion nor subjected to time-dependent rundown **(B).**

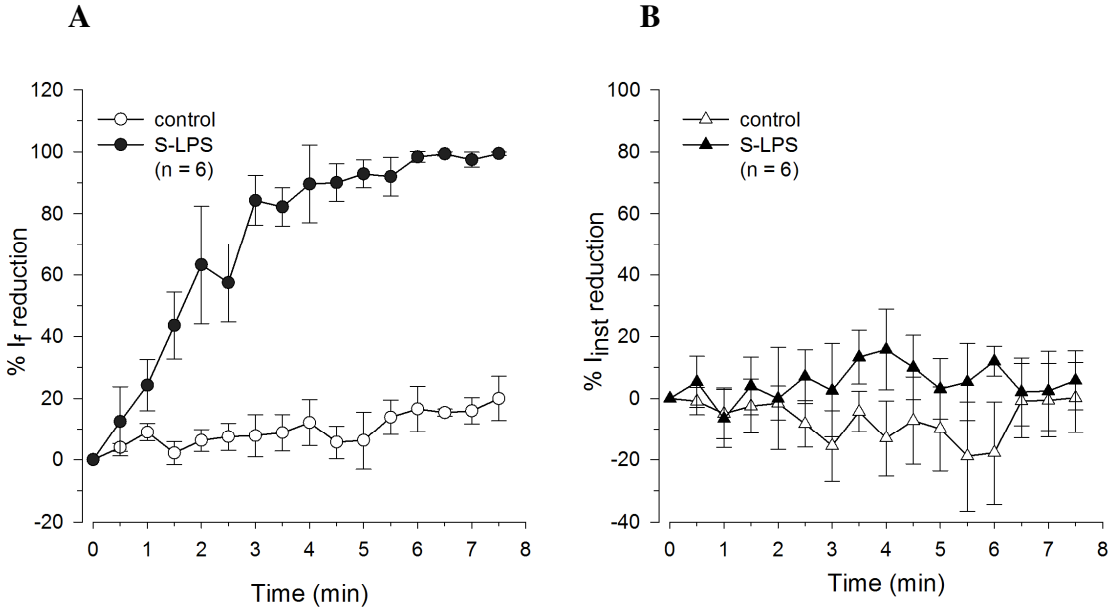

Figure 28. Time-dependence of the S-LPS effect on the pacemaker current.
The pacemaker current was elicited by voltage steps to -80 mV at 2 Hz. **(A)** I_f was substantially impaired by S-LPS perfusion and statistically different from control from min 1 onwards ($p \leq 0.05$). **(B)** I_{inst} was not influenced by S-LPS.

The presented data clearly show that acute S-LPS application does not affect I_{inst}, but significantly reduces I_f mean current density, voltage-dependence of I_f steady-state activation and time constants of I_f activation.

D.1.2 Effect of Incubation with R595-mutant LPS on Properties of I_f and I_{inst} and Comparison with the Chronic S-LPS Effect

It has been previously shown that the O-chain of the LPS molecule is responsible for the impairment of the pacemaker current I_f. R595, a LPS mutant lacking the O-chain, does not impair I_f under acute application. [11] For investigating the chronic effect of R595 and S-LPS on I_f and I_{inst} cardiomyocytes were incubated with either R595 or S-LPS (10 µg/mL, 6 h).

Effect on I_f: Incubation with R595 did neither significantly alter voltage-dependence nor time constants of I_f activation compared to control cells, as shown in Figure 29. Steady-state activation curves (panel A) of control cells and R595 incubated cells showed $V_{1/2}$ values (mV) of -83.3 ± 1.2 and -81.1 ± 1.1, respectively. The slope factor (mV) of control

cells was 7.8 ± 0.4 and of R595 treated cells 7.2 ± 0.3. τ at -90 mV tau (ms) amounted to 645.3 ± 50.6 in control versus 607.2 ± 41.2 in R595 incubated cells. At -130 mV time constants reached values of 71.9 ± 6.9 in control versus 66.4 ± 5.9 in R595 incubated cells.

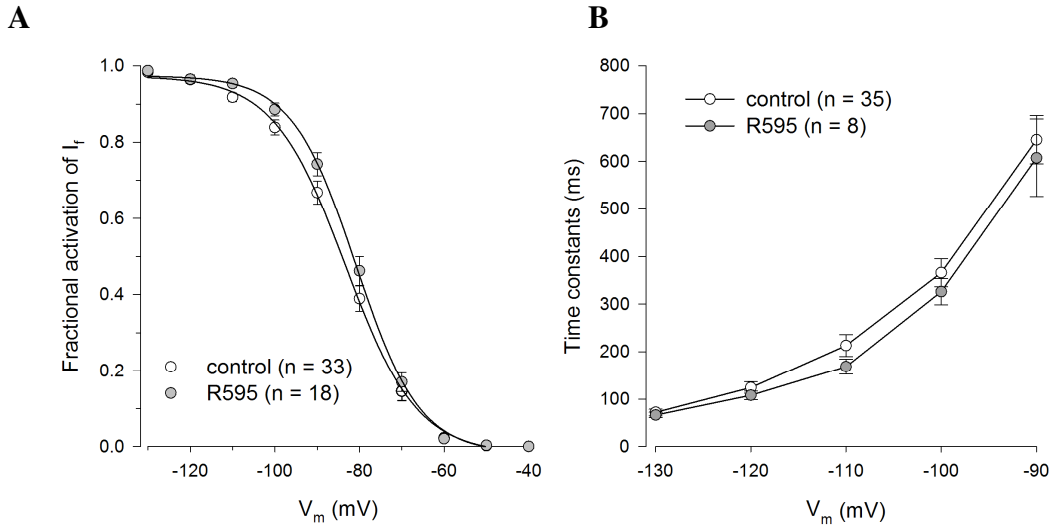

Figure 29. Chronic effect of R595 on I_f properties of human atrial myocytes.
Cells were incubated with R595 (10 µg/mL) for 6-10 h. **(A)** Voltage-dependence of I_f steady-state activation for control and R595-treated cells. Normalized conductances were fitted by a Boltzmann function to obtain voltage-dependence of steady-state activation. Control: $V_{1/2}$=-83.3±1.2 mV, *k*=7.8±0.4 mV; R595: $V_{1/2}$=-80.3±1.3 mV, *k*=7.0±0.5 mV. **(B)** Mean time constants of I_f activation for control and R595-treated cells. Values were obtained by fitting a monoexponential function to current traces.

Figure 30A illustrates the absolute mean I_f current densities of control cells, S-LPS and R595 incubated cells. At -60 and -70 mV I_f was not detectable in S-LPS incubated myocytes (as previously reported [12]) but in control and R595 incubated cells. At -80 mV I_f was significantly larger in control and R595 incubated cells than in S-LPS incubated cells: control: -1.3 ± 0.3, R595: -1.5 ± 0.3 and S-LPS: -0.3 ± 0.2 pA/pF. At -90 mV I_f was significantly higher only in R595 incubated cells compared to S-LPS incubated cells: -2.6 ± 0.5 pA/pF in R595 cells versus -0.9 ± 0.28 pA/pF in S-LPS cells (control I_f was -1.6 ± 0.3 pA/pF).

Effect on I_{inst}: At all tested membrane potentials, incubated cardiomyocytes with either S-LPS or R595 showed significantly less I_{inst} current density compared to control cells, as illustrated in Figure 30B. For example, at -40 mV current density in control cells amounted

to -0.6 ± 0.1 pA/pF, in S-LPS incubated cells to -0.1 ± 0.1 pA/pF and in R595 incubated cells to -0.2 ± 0.1 pA/pF. At -130 mV values reached to -3.4 ± 0.3 pA/pF in control, to -1.8 ± 0.3 pA/pF in S-LPS and to -2.2 ± 0.4 pA/pF in R595 incubated cells.

Current densities of S-LPS incubated cells compared to R595 incubated cells were not statistically different.

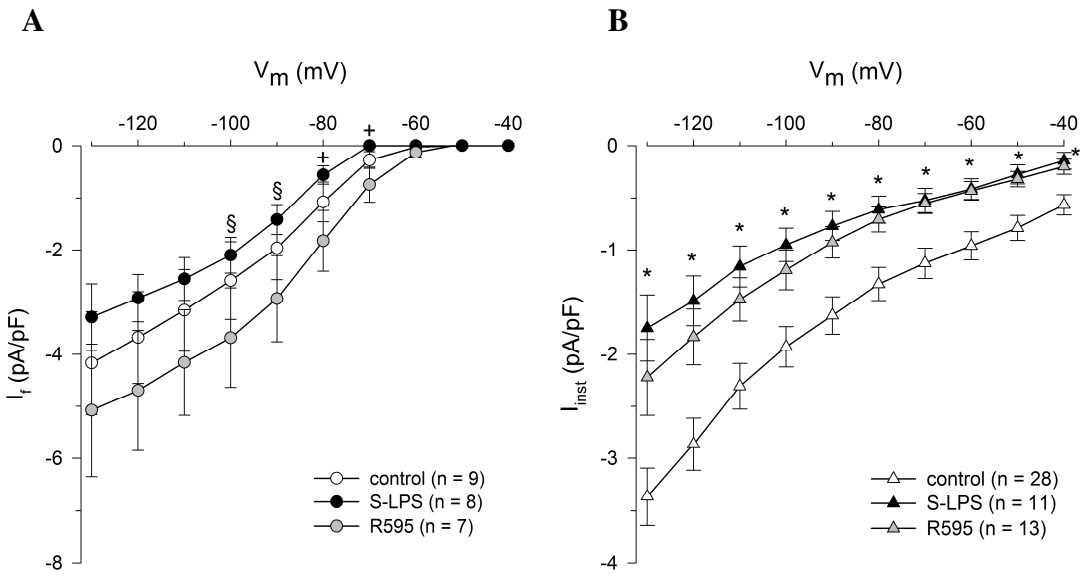

Figure 30. Chronic effects of S-LPS and R595 on the pacemaker current of human atrial myocytes.
Cells were incubated with S-LPS or R595 (10 µg/mL) for 6-10 h. **(A)** Mean *I-V* relations of I_f in control and endotoxin-treated cells. **(B)** Corresponding *I-V* relations of I_{inst}. $^{+}p \leq 0.05$ vs. control and R595; $^{\S}p \leq 0.05$ vs. R595; $^{*}p \leq 0.05$ of S-LPS and R595 vs. control.

The presented data clearly show that under chronic conditions S-LPS substantially impairs I_f and I_{inst} whereas R595 only impairs I_{inst}. The I_f reducing effect of the LPS molecule is mediated via the O-chain moiety of the LPS molecule.

D.2 Interactions of Endotoxins with HCN Channels

Experiments in this section were performed with the help of MSc. Chintan Koyani from the Institute of Molecular Biology and Biochemistry, Medical University of Graz.

Acute S-LPS perfusion rapidly decreased I_f in human myocytes (Figure 28). S-LPS perfusion of HEK293 cells expressing human HCN2 reduced I_f by 30% in about 8 s. [11] These findings imply a direct interaction of S-LPS with HCN channels. El Chemaly and coworkers [21] have reported that HCN2 is the major isoform expressed in human atrial myocytes. In order to test a possible interaction, LPS preparations were cross-linked to membranes followed by incubation with HCN2, which was isolated by immunoprecipitation from mouse heart, Figure 31.

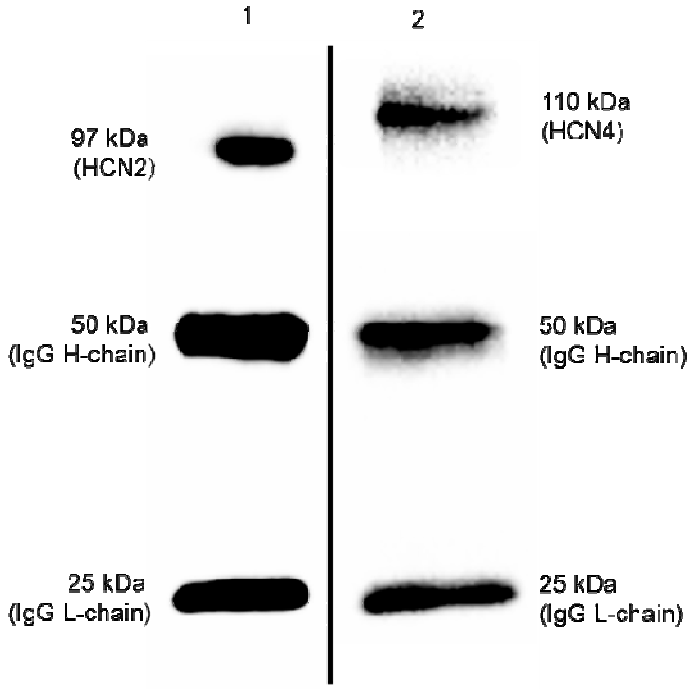

Figure 31. Immunoprecipitation and western blots of HCN2 and HCN4 proteins. Immunoprecipitation of HCN2 and HCN4 proteins was performed by incubating mouse heart homogenates with anti-HCN2 or anti-HCN4 antibody. Immunoprecipitates (IP) were separated by SDS-PAGE and HCN2 (1) as well as HCN4 (2) were visualized by western blot experiments.

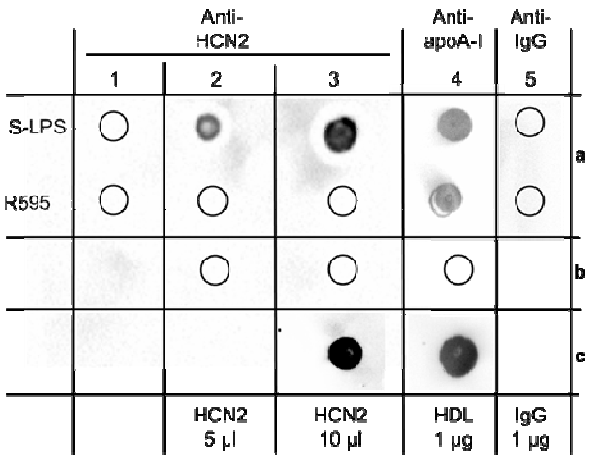

Figure 32. Dot-blot analysis for LPS-HCN2 binding.
S-LPS but not R595 binds to the HCN protein. **(a)** S-LPS and R595 (10 µg) were cross-linked with methanol prewetted PVDF membranes. Membranes were dried and dots were incubated with PBS (1a), indicated volumes of immunoprecipitated HCN2 protein (2a/3a), HDL (4a) or purified total mouse IgG (5a). **(b)** Prewetted PVDF membranes were dried followed by dotting with immunoprecipitated HCN2 protein (2b/3b) or HDL (4b). **(c)** Immunoprecipitated HCN2 protein (3c) or HDL (4c) was dotted onto prewetted membranes. After all incubation steps lane 1-5 were incubated with indicated primary antibody and immunoreactive dots were visualized; empty circles represent no immunoreactivity.

These data are the first to prove binding of S-LPS to HCN2 to but not to R595. Figure 32/4a shows binding of high-density lipoprotein, a known ligand for endotoxins, [114] to S-LPS and R595. To further validate our findings, endotoxin-cross-linked membranes were incubated with IgG, still present in immunoprecipitated HCN2 preparations, Figure 32/5a; Results confirm the observed S-LPS-HCN interaction to be specific and independent of IgG. Figure 32 further represents negative (1a and 2b-4b) and positive controls (3c/4c) for membrane cross-linking conditions. Since HCN4 is the major isoform in SANC and therefore of great interest regarding pacemaking, dot-blot analysis were also performed with immunoprecipitated HCN4 protein also demonstrating binding of S-LPS to HCN4 but not to R595, Figure 33.

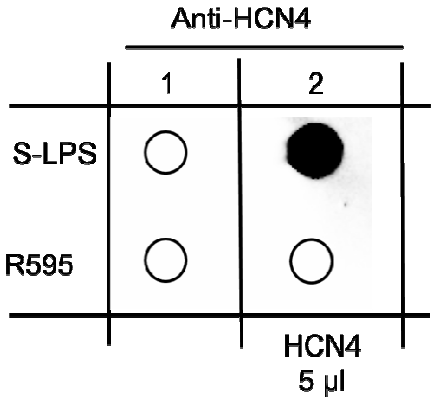

Figure 33. Dot-blot analysis for LPS-HCN4 binding.

As I_f is impaired under acute (Figure 26) and chronic S-LPS conditions (
Figure 30) in a similar manner and S-LPS interacts with HCN2/HCN4 (Figure 32, Figure 33) it was additionally tested whether endotoxins could also modulate HCN channel expression. For these experiments HL-1 cells (previously reported to be responsive to S-LPS regarding I_f reduction [93]) were used. Results demonstrate that neither S-LPS nor R595 treatment altered HCN (1, 2 and 4) mRNA expression (up to 24 h) or HCN2 protein expression (6 and 24 h); only the 6 h time point is shown in Figure 34.

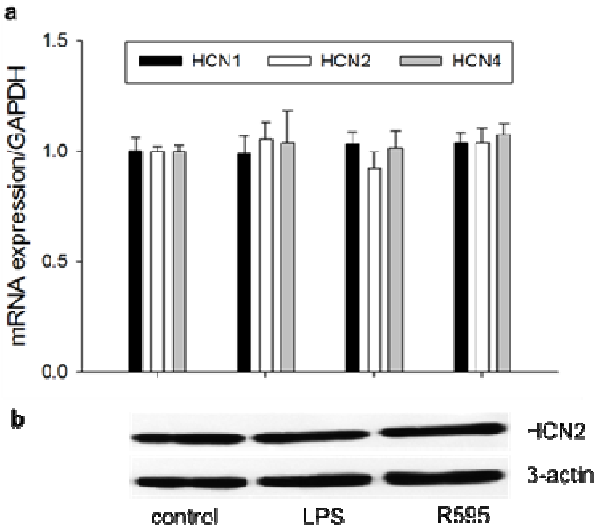

Figure 34. mRNA and protein expression of HCN isoforms after endotoxin treatment
Incubation with S-LPS or R595 (10 µg/mL, 6 h) did neither alter mRNA **(a)** nor protein expression **(b)** of HCN isoforms in HL-1 cells, determined by qPCR and western blot, respectively.

Results show that S-LPS binds to the HCN channel protein whereas R595-mutant LPS does not. This data fit well with the observation that only LPS containing an O-chain does affect I_f properties. Therefore, the primary mechanism of LPS action on I_f seems to be binding of the LPS molecule to the channel protein.

D.3 Effect of Ivabradine on the Human Pacemaker Current

To test the ivabradine effect a combination of 2 protocols was used. Protocol *p1*: Trains (total duration 9 min) of activating/deactivating voltage steps (-100 mV for 3 s; 0 mV for 0.4 s) from a holding potential of -40 mV. Voltage steps were applied every 6 s since ivabradine acts as a use-dependent inhibitor. Protocol *p2*: Hyperpolarizing voltage steps (3 s duration) from -40 mV to -130 mV (10 mV increment, holding potential -40 mV) before and after ivabradine perfusion (i.e. before and after *p1*). The insert in Figure 35A shows the voltage-clamp protocol. More detailed information is given in the *MATERIAL AND METHODS* section.

Effect on I_f: Figure 35 shows the effect of 1 µmol/L ivabradine on I_f characteristics. Panel (A) shows the *I-V* relation before and after ivabradine treatment. At membrane potentials more negative than -70 mV ivabradine significantly reduced I_f compared to control values. For example, control I_f densities amounted to -1.1 ± 0.4 pA/pF and -4.2 pA/pF ± 1.0 pA/pF in the absence versus 0.3 ± 0.1 pA/pF and -1.4 ± 0.2 pA/pF in the presence of ivabradine at -80 mV and -130 mV, respectively. Ivabradine did neither shift voltage-dependence nor mean time constants of I_f activation as shown in panels 35B and C, respectively.

Effect on I_{inst}: Ivabradine did not reduce I_{inst} but rather seemed to augment this current component (n = 7). Anyhow, a significant increase in the *I-V* relation could be detected only at -70 and -80 mV, Figure 35D.

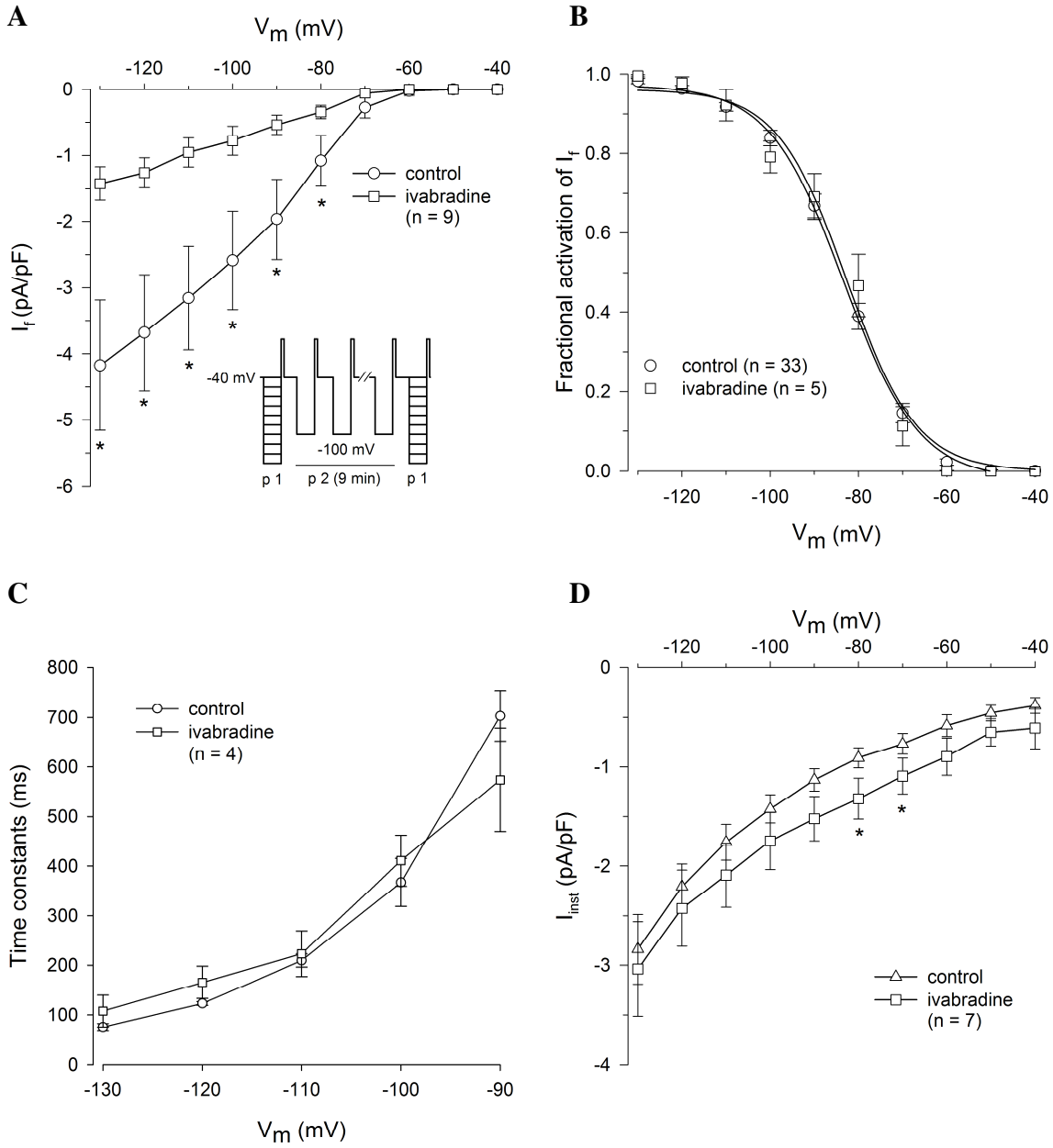

Figure 35. Effect of ivabradine on the pacemaker current of human atrial myocytes. **(A)** Mean *I-V* relations of I_f before and after ivabradine superfusion (1 µmol/L, 7 min). The insert shows the voltage clamp protocol. **(B)** Voltage-dependence of I_f steady-state activation in control and ivabradine superfused cells. Normalized conductances were fitted by a Boltzmann function to obtain voltage-dependence of steady-state activation. Control: $V_{1/2}$= -83.3 ± 1.2 mV, *k* = 7.8 ± 0.4 mV; ivabradine: $V_{1/2}$= -84.1 ± 4.0 mV, *k* = 7.9 ± 2.5 mV. **(C)** Mean time constants of I_f activation before and after ivabradine superfusion. Values were obtained by fitting a monoexponential function to current traces. **(D)** Influence of ivabradine on *I-V* relations of I_{inst}. *p≤0.05 vs. control.

D.4 Effect of Ivabradine on the Human Pacemaker Current under Septic Conditions

Effect on I_f: Figure 36A, shows the impact of ivabradine on *I-V* relations in S-LPS incubated cells. Ivabradine was still able to significantly block I_f but only at membrane potentials more negative than -80 mV. E.g., at -90 mV and -130 mV current densities before ivabradine treatment amounted to -1.4 ± 0.3 pA/pF and -3.3 ± 0.6 pA/pF versus -1.0 ± 0.2 pA/pF and -2.1 ± 0.4 pA/pF after ivabradine treatment.

The more negative voltage activation profile of I_f due to S-LPS incubation was not affected by ivabradine application, resulting in steady-state curves typical for S-LPS treated cardiomyocytes.

However, the efficacy of ivabradine to block I_f seemed to be reduced in S-LPS incubated myocytes compared to control cells. Keeping in mind that I_f is not affected by R595 treatment we wondered whether ivabradine's potency to block I_f would be the same in R595 incubated cells like in control cells. Actually, the *I-V* relations indicate that ivabradine's blocking potency is also attenuated in R595 incubated cells, Figure 36B.

In order to statistically discriminate S-LPS/R595 dependent differences in the efficacy of ivabradine, I_f reduction by ivabradine was compared in control, S-LPS and R595 incubated cells. Additionally, values were compared to the time dependent current rundown, which was not different between control, S-LPS and R595 incubated cells. Results are shown in Figure 36C. In detail, the ivabradine block of I_f was significantly larger in S-LPS/R595 incubated cells compared to rundown at membrane potentials more negative than -80 mV. As already supposed before, ivabradine in fact inhibited I_f significantly stronger in control cells than in cells incubated with either S-LPS or R595 at all tested membrane potentials except for -120 mV. Anyhow, the ivabradine effect was by trend higher in R595 than in S-LPS incubated cells but reached statistical difference only at -120 mV. I_f reduction by ivabradine calculated across tested membrane potentials averaged to 66.3 ± 1.6 % in control, to 46.2 ± 2.5 % in R595 incubated and to 32.1 ± 4.8 % in S-LPS incubated cells, time dependent rundown amounted to 18.0 ± 2.4 %.

Figure 36D shows the time dependence of the ivabradine induced I_f block in control, S-LPS and R595 incubated cells. In control cells (n = 8) I_f block by ivabradine was higher than in pretreated cells and amounted to 55.1 ± 1.7 % compared to 42.4 ± 2.9 % and 44.7 ± 4.1 % in S-LPS (n = 8) and R595 (n = 6) incubated cells, respectively.

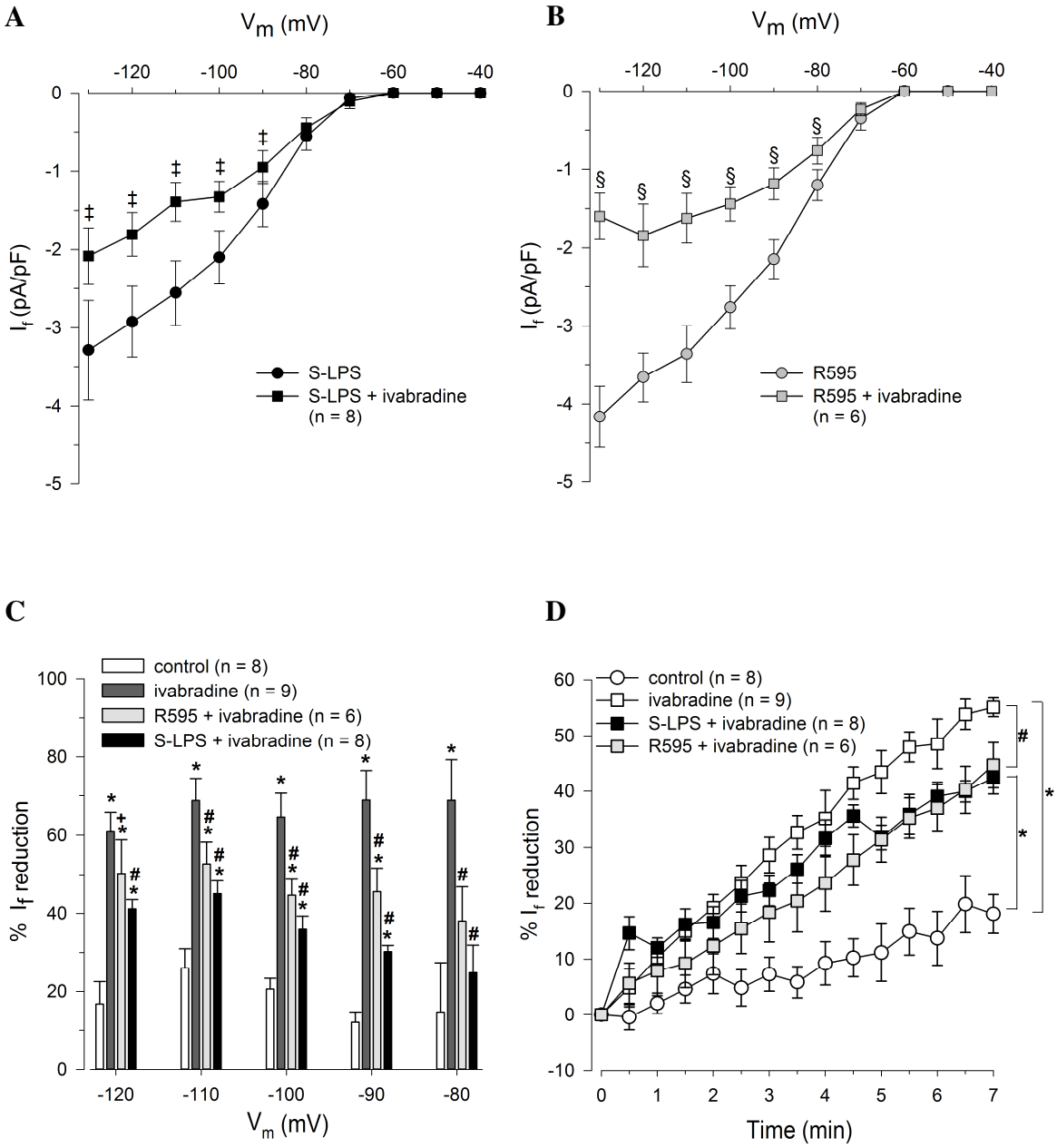

Figure 36. Effect of ivabradine on I_f characteristics in human atrial myocytes under septic conditions.

Cells were incubated with endotoxins (10 µg/mL, 6-10 h) and superfused with ivabradine (1 µmol/L, 7 min). Mean *I-V* relations of **(A)** S-LPS or **(B)** R595 incubated cells before and after ivabradine superfusion. **(C)** Percent I_f reduction by ivabradine was calculated from the underlying *I-V* relations before and after ivabradine superfusion. **(D)** Time dependence of ivabradine blockage on I_f. Currents were elicited by hyperpolarizing voltage steps to -100 mV (3 s duration) at 1/6 Hz. $^{‡}p\leq0.05$ vs. S-LPS; $^{§}p\leq0.05$ vs. R595; $^{*}p\leq0.05$ vs. control; $^{\#}p\leq0.05$ vs. ivabradine; $^{+}p\leq0.05$ vs. S-LPS + ivabradine.

Furthermore, I_f reduction by ivabradine was significantly different from min 4.5 onwards between control and incubated cells (S-LPS and R595). In all ivabradine treated cardiomyocytes (ivabradine alone and endotoxin plus ivabradine) I_f reduction was significantly different from control (i.e. rundown) already from min 2.5 on.

Effect on I_{inst}: Ivabradine did not reduce I_{inst} in endotoxin incubated cells but rather seemed to augment this current component, as can be seen for S-LPS in Figure 37. The same observation was made in untreated cells (see Figure 35D).

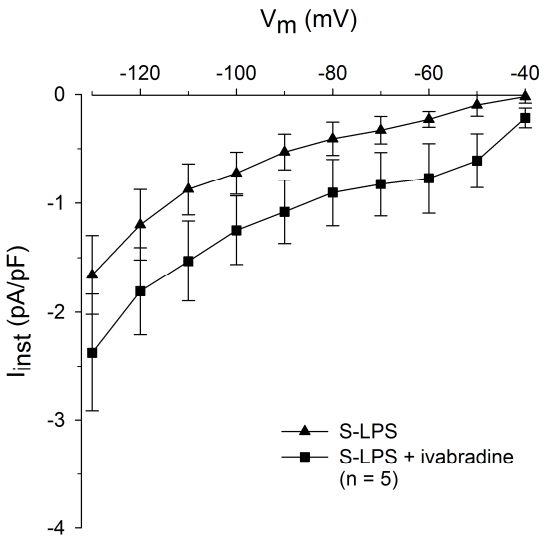

Figure 37. Effect of ivabradine on I_{inst} under elevated S-LPS levels.

D.5 Effect of Endotoxins on the Intracellular Ivabradine Concentration in Guinea Pig Ventricular Myocytes

This set of experiments was perforemd with the help of Assoz. Prof. Priv.-Doz. Dipl.-Ing. Dr. techn. Seth Hallström from the Institute of Physiological Chemistry, Medical University of Graz.

As reduction of I_f current density by ivabradine is more pronounced under control conditions than in cells incubated with either kind of LPS used in this study (see Figure 36), binding of S-LPS to the channel protein cannot be the (sole) reason for the reduced efficacy of ivabradine, as R595 does not bind to HCN2/HCN4 but still attenuates the

ivabradine induced I_f block. Therefore, we hypothesized that S-LPS/R595 incubation could correlate with a lower availability of ivabradine to block pacemaker channels in cardiomyocytes. As ivabradine obviously passes through the cell membrane [97] and acts from inside the cell, [17] and S-LPS is known to change cell membrane integrity, [115] we figured that endotoxin incubation would possibly constrain the passage of ivabradine through the cell membrane and consequently the intracelluar concentration of ivabradine would be lesser. To further investigate this hypothesis intracellular concentrations of ivabradine were measured in control cells and S-LPS/R595 incubated cells. These experiments were conducted in isolated guinea pig ventricular myocytes due to the needed amount of cells and the limited yield of human atrial myocytes. The HPLC-chromatograms illustrated in Figure 38A are representative fluorimetric measurements of intracellular ivabradine concentrations in myocyte samples with comparable protein values. Intracellular ivabradine concentrations ranged from 1.6 to 3.3 pmoL/mg protein in control cells of different preparations (control, S-LPS, R595).

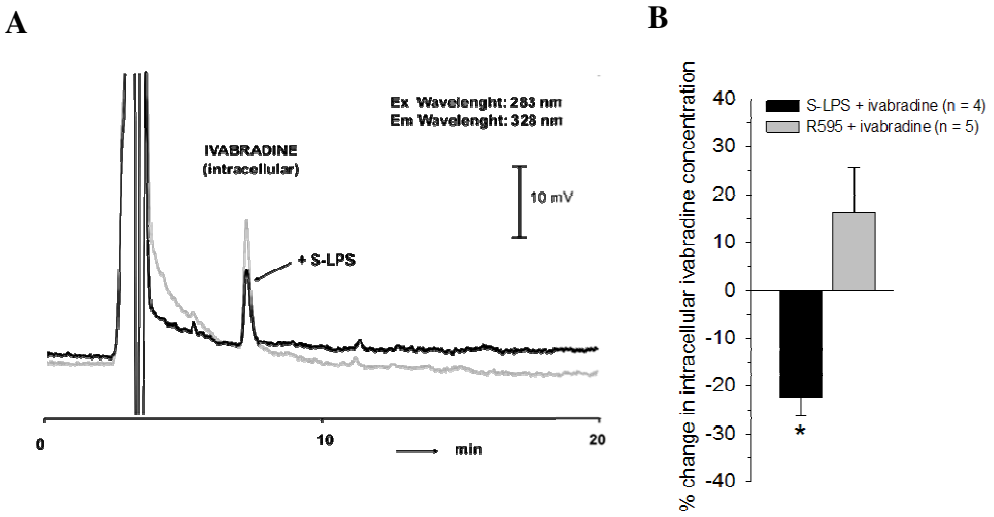

Figure 38. Intracellular ivabradine concentrations in guinea pig ventricular myocytes under control and septic conditions.
Untreated (controls) and endotoxin-treated (S-LPS or R595, 10 µg/mL, 6 h) cells were incubated with ivabradine (1 µmol/L, 15 min). **(A)** Representative HPLC-chromatograms for intracellular ivabradine content in control and S-LPS treated cells. **(B)** Percentage change of intracellular ivabradine concentrations in S-LPS and R595 incubated cells compared to the respective controls. *p≤0.05 vs. control.

Results show that intracellular ivabradine is significantly reduced under concomitant incubation with S-LPS (6 h of which the last 15 min together with ivabradine) compared to incubation with ivabradine only (15 min). In R595 incubated cells the ivabradine concentration was not reduced but rather augmented compared to control. Figure 38B shows that S-LPS but not R595 incubation significantly reduced the intracellular ivabradine concentration compared to respective controls.

D.6 Combined Effect of LPS and Ivabradine on Pacemaking – Computer Simulation Experiment

Simulation experiments were performed with the help of Sen.-Scientist Mag. Dr. rer. nat. Zorn-Pauly and Ass. Prof. Dipl.-Ing. Dr. techn. Dieter Platzer, both from the Institute of Biophysics, Medical University of Graz.

To explore the functional significance of S-LPS and ivabradine induced I_f changes on pacemaker activity, an *in silico* approach was chosen. Due to the unavailability of an appropriate human computational model a recently published rabbit sinoatrial pacemaker cell model was used, [23] which reproduces the effect of I_f inhibition on beating rate in good agreement to experimental findings.

Based on experimental data in human myocytes, the effect of S-LPS was implemented in the model as an I_f $V_{1/2}$ shift of -14 mV [12] representing a shift of I_f $V_{1/2}$ from -52.5 to -66.5 mV in the sinoatrial cell model. The action of ivabradine was simulated by reduction of I_f conductance (66 % and 35 % in control and S-LPS incubated cells, respectively - Figure 35A and Figure 36A). In the simulation experiment ivabradine reduced I_f at all membrane potentials, while S-LPS had a reducing effect on I_f between -50 and -100 mV, Figure 39A. At membrane potentials positive to ~ -65 mV I_f reduction by S-LPS was more pronounced than by ivabradine. Combining the effects of ivabradine and S-LPS resulted in the most prominent decrease of I_f between -40 and -70 mV. The gradual decrease of I_f at physiologically relevant membrane potentials (Figure 39A) resulted in a gradual increase in cycle length (CL) from 355 ms (control) to 455 ms (ivabradine), 569 ms (S-LPS) and 604 ms (S-LPS and ivabradine), Figure 39B. A systematic variation of the two I_f model parameters (Figure 39C) predicts that CL is stronger influenced by a I_f $V_{1/2}$ shift (to more negative membrane potentials) than by reduction of I_f conductance. For example, CL alteration by a $V_{1/2}$ shift of only -2 mV is equivalent to a 20 % decrease in I_f conductance.

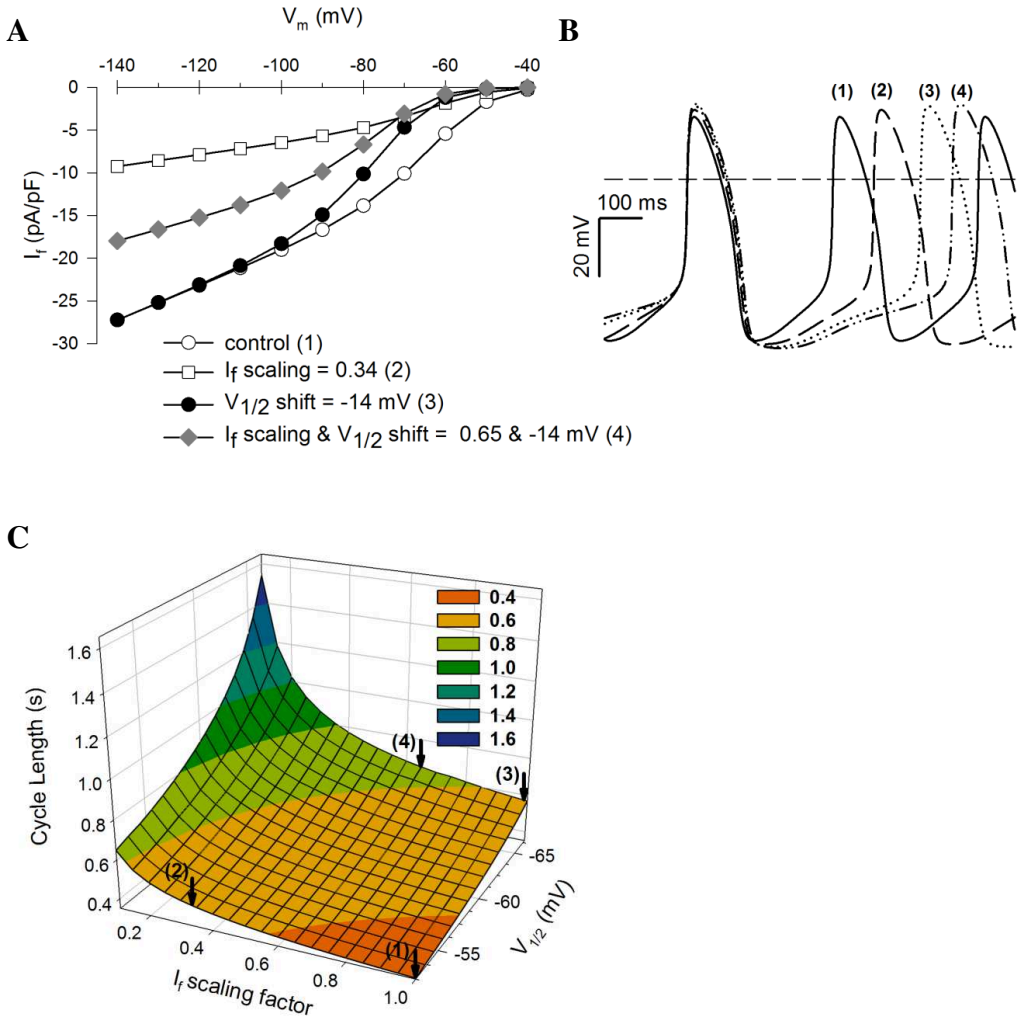

Figure 39. Effects of S-LPS and ivabradine on the pacemaker activity of a computational sinoatrial cell model.

A rabbit sinoatrial pacemaker cell model was used to investigate S-LPS-induced $V_{1/2}$ shift of -14 mV and ivabradine-induced I_f reduction (66 % and 35 % in control and S-LPS-treated cells, respectively). **(A)** *I-V* relations of I_f using the computational model: I_f was voltage clamped from -40 to -140 mV in 10 mV steps of 3 s duration for indicated conditions (1) to (4). **(B)** Time course of spontaneous APs computed for indicated conditions (1) to (4). **(C)** Changes in cycle length are represented as a function of reduction in I_f conductance (I_f scaling factor) and the shift of $V_{1/2}$ to more negative membrane potentials. The arrows indicate the specific parameter setting (1) to (4) as shown in (A) and (B).

Moreover, at all given $V_{1/2}$ values (shifted by S-LPS) a reduction of I_f conductance (by ivabradine) is still able to further decrease CL of the cell model. To summarize, the potency of ivabradine to reduce sinoatrial beating rate is preserved under septic conditions.

E. DISCUSSION

The present study provides the first description of ivabradine action on the native human pacemaker current under elevated endotoxin levels mimicking septic conditions. The results reveal that despite of I_f impairment due to S-LPS, ivabradine is still able to further inhibit I_f.

However, this inhibition is significantly reduced compared to control conditions. Using an *in silico* approach it can be demonstrated that under septic conditions ivabradine still decreases the beating frequency of a sinoatrial cell model.

A further novel finding of this study is, that I_f impairment by endotoxin is mediated via its binding to the HCN channel protein and depends on the polysaccharide part of the LPS molecule, the so called O-chain.

Another novelty is the first detailed description of the influence of LPS and ivabradine on I_{inst}.

LPS action on the pacemaker current components I_f and I_{inst}

The first description of I_f impairment by S-LPS was previously published by Zorn-Pauly et al., 2007, showing that chronic S-LPS incubation (6-10 h) reduces I_f current density in the physiologically relevant membrane potential range and shifts the steady-state activation to more negative membrane potentials (-14 mV). [12] Meanwhile it was shown that S-LPS also acutely impairs I_f, namely in HL-1 cardiomyocytes, in HEK293 cells overexpressing human HCN2 and HCN4 as well as in murine sinoatrial cells. [11,93] I_f impairment was demonstrated to be mediated by the O-chain of the molecule. [11]

So far, research has mainly focused on the time- and voltage-dependent current component I_f and its modulation. Only scarce data are available on the second pacemaker current component, the voltage- and time-independent I_{inst}. Up to date it is not known whether I_{inst} is produced by a distinct population of HCN channels [14] or I_{inst} is flowing through a "leaky" closed state of HCN channels. [54] The physiological role of I_{inst} is still a matter of research. I_{inst} may underlie the inward sodium background current ($I_{b,Na}$) described for cardiomyocytes including sinoatrial cells, which contributes to the diastolic depolarization and to the stabilization of nodal pacemaker frequency along with I_f. [54-56] Another evidence for the contribution of I_{inst} to maintain a stable pacing rhythm was proved in

newborn rat ventricular cells. [16] Taking into account that at least for HCN2 channels I_{inst} can account for ~ 10 % of the totally available current [116,117] its physiological role in cardiac automaticity becomes reasonable.

Results of this study show that in human atrial myocytes I_{inst} represents the sole pacemaker current component at membrane potentials more positive than -60 mV and remains the major component up to -80 mV. At more negative membrane potentials contribution of I_{inst} to total pacemaker current amounts at least to ~ 40 %. However, it remains to be elucidated whether the measured I_{inst} current is partly made up by a background current or can be totally attributed to the pacemaker current as its second component. Nevertheless, the fact that I_{inst} contributes to a relevant extent to depolarizing HCN currents makes this pacemaker current component an interesting candidate in generation and maintenance of pathological induced abnormal activities – in particular when considering that the second pacemaker current component I_f is suggested to contribute to abnormal automaticity under pathological conditions in non-pacemaker regions of the heart. [118-121]

Our data show that S-LPS also exerts an acute effect on I_f besides the described chronic one. Acute S-LPS administration significantly reduces I_f current density at all tested membrane potentials as well as the maximal I_f conductance. Furthermore, S-LPS shifts the steady-state activation profile to more negative membrane potentials and slows mean time constants of I_f activation. These results are in line with previously reported acute effects of S-LPS in HEK293 cells overexpressing human HCN2. [11] Furthermore, altered activation kinetics by enhancing I_f deactivation and to a lesser extend inhibiting I_f activation were shown as well as a reduction of I_f at negative membrane potentials in HL-1 cells. [93] I_f reduction by S-LPS occurs within a few minutes in human atrial myocytes. Klöckner and coworkers reported a 30% reduction even within a few seconds in HCN2 overexpressing HEK293 cells. [11] The rapid development of I_f reduction suggests a direct interaction of S-LPS with the HCN channel protein. The data presented in this thesis explain for the first time that binding of S-LPS to HCN channel protein most likely is the underlying mechanism of I_f impairment. Interestingly, R595 did not bind to the HCN channel protein. Additionally, R595 did not impair I_f in human myocytes due to the lack of the O-chain as previously reported. [11] Furthermore, in the present thesis it is shown that mRNA expression levels of HCN1, 2 and 4 as well as HCN2 protein expression were not changed after 6 h LPS incubation in HL-1 cells. Therefore, it can be concluded that I_f impairment by endotoxin requires O-chain dependent binding to HCN channel protein. This conclusion

is supported by a recently published work by Klöckner et al., 2014, that states that lipid A of the LPS molecule is required for the intercalation of the LPS molecule into the cell membrane and that the O-chain is most likely interacting with the HCN channel protein. [11]

In contrast to I_f, I_{inst} impairment only occurs in chronic endotoxin treated myocytes but is not dependent on the O-chain and hence cannot be explained by endotoxin binding to the HCN channel. Therefore, I_{inst} impairment is probably caused by the lipid anchor of LPS, termed lipid A or the "endotoxic principle", which is well known to harbour important biological activities of the molecule. [122] As already mentioned, it is not known if I_{inst} is flowing through a distinct population of HCN channels or through a leaky closed state of the same channels. Since I_f and I_{inst} are affected differently by LPS under acute and chronic conditions and additionally show different sensitivity towards the structure of the LPS molecule, these current components have to be affected independently from each other in the case of a leaky closed state model. It is tempting to speculate about the physiological relevance of LPS induced I_{inst} reduction. Under septic conditions nodal pacemaking processes may not only be affected by I_f impairment but additionally by I_{inst} inhibition under the assumption that I_{inst} is also involved in stabilization of pacing rhythm. Further studies are needed to get a more complete insight in endotoxin induced alterations of the pacemaking process.

Ivabradine

Ivabradine exerts its heart rate lowering action via a selective inhibition of I_f which is well documented for native cardiomyocytes (including human atrial cells, [21]) as well as for HCN expressing cell lines. [18,97] In accordance with these findings our results show a significant I_f reduction by ivabradine (1 µmol/L) in a membrane potential range from -80 mV to -120 mV amounting to ~ 66 %. At this concentration no effects on other membrane currents have been reported. [19,20,99] In our experiments, ivabradine did not inhibit I_{inst}, the second component of the pacemaker current. Therefore, ivabradine´s heart rate lowering effect is likely to be mediated only via the I_f component. Interestingly, the I_f-block of ivabradine was significantly reduced in S-LPS/R595 treated cells compared to control conditions showing ivabradine´s smallest blocking potency under S-LPS treatment. This finding correlates well with the significantly reduced intracellular ivabradine concentration, which might account for the reduced ivabradine effect. However, this

mechanism cannot be supposed for R595 treatment since intracellular ivabradine concentration was not affected by R595. Thus, the precise mechanism by which elevated S-LPS/R595 levels cause a reduced action of ivabradine stays open and further investigations are required. The susceptibility of Gram-negative bacteria towards hydrophobic agents also depends on the LPS form expressed on their surface. [123] In case of R-LPS mutants hydrophobic antibiotics easily access the cell surface and diffuse into the cell interior through the cell membrane in contrast to bacterial strains expressing S-LPS, in which no accumulation of antibiotics was observed. [124] Therefore, it can be assumed that the passage of ivabradine, a hydrophobic agent, through the lipid bilayer is hindered by S-LPS molecules on the cell surface.

To assess wether ivabradine is still able to slow down the cellular sinoatrial pacemaking process under septic conditions computational analyses were done with a rabbit sinoatrial cell model. Simulations predict that sinoatrial beating frequency can still be reduced by ivabradine under septic conditions. These results might provide valuable additional information to the clinical MODI_fY trial. [22] This clinical study evaluated potential benefits of heart rate reduction in patients suffering from MODS, which in most cases is caused by sepsis. In sepsis-related MODS heart rate is usually elevated due to increased oxygen demand and elevated cytokine levels, [125] and heart rate acts as an independent risk factor for mortality. [126,127] Since ivabradine at therapeutical dosis does not show compromising cardiovascular side effects it is preferable to beta-blockers which are anyhow contraindicated in most cases due to high amounts of needed catecholamines for stabilizing the blood pressure in sepsis. Therefore, pure heart reduction with ivabradine could improve the outcome of patients in sepsis by lowering myocardial oxygen demand, improving coronary perfusion and acting on the negative force-frequency relationship of failing heart. [125]

In conclusion, the analysis presented here indicates that the administration of ivabradine to septic patients could reduce heart rate, improve the cardiovascular status and consequently increase the chance for survival of sepsis.

BIBLIOGRAPHY

[1] Cohen J. The immunopathogenesis of sepsis. Nature 2002;420(6917):885-891.

[2] Fernandes Jr CJ, de Assuncao MSC. Myocardial dysfunction in sepsis: a large, unsolved puzzle. Crit Care Res Pract 2012;2012: Article ID 896430.

[3] Werdan K, Müller U, Reithmann C, Pfeifer A, Hallström S, Koidl B, et al. Mechanisms in acute septic cardiomyopathy: evidence from isolated myocytes. Basic Res Cardiol 1991;86(5):411-421.

[4] Huber M, Kalis C, Keck S, Jiang Z, Georgel P, Du X, et al. R-form LPS, the master key to the activation ofTLR4/MD-2-positive cells. Eur J Immunol 2006;36(3):701-711.

[5] Blunck R, Scheel O, Müller M, Brandenburg K, Seitzer U, Seydel U. New insights into endotoxin-induced activation of macrophages: involvement of a K^+ channel in transmembrane signaling. J Immunol 2001;166(2):1009-1015.

[6] Hoang LM, Chen C, Mathers DA. Lipopolysaccharide rapidly activates K^+ channels at the intracellular membrane face of rat cerebral artery smooth muscle cells. Neurosci Lett 1997;231(1):25-28.

[7] Wilkinson M, Earle M, Triggle C, Barnes S. Interleukin-1beta, tumor necrosis factor-alpha, and LPS enhance calcium channel current in isolated vascular smooth muscle cells of rat tail artery. The FASEB journal 1996;10(7):785-791.

[8] Mayr A, Knotzer H, Pajk W, Luckner G, Ritsch N, Dünser M, et al. Risk factors associated with new onset tachyarrhythmias after cardiac surgery –a retrospective analysis. Acta Anaesthesiol Scand 2001;45(5):543-549.

[9] Goodman S, Shirov T, Weissman C. Supraventricular arrhythmias in intensive care unit patients: short and long-term consequences. Anesth Analg 2007;104(4):880-886.

[10] Aoki Y, Hatakeyama N, Yamamoto S, Kinoshita H, Matsuda N, Hattori Y, et al. Role of ion channels in sepsis-induced atrial tachyarrhythmias in guinea pigs. Br J Pharmacol 2012;166(1):390-400.

[11] Klöckner U, Rueckschloss U, Grossmann C, Ebelt H, Müller-Werdan U, Loppnow H, et al. Differential reduction of HCN channel activity by various types of lipopolysaccharide. J Mol Cell Cardiol 2011;51(2):226-235.

[12] Zorn-Pauly K, Pelzmann B, Lang P, Mächler H, Schmidt H, Ebelt H, et al. Endotoxin impairs the human pacemaker current I_f. Shock 2007;28(6):655-661.

[13] Accili EA, Proenza C, Baruscotti M, DiFrancesco D. From funny current to HCN channels: 20 years of excitation. News Physiol Sci 2002 Feb;17:32-37.

[14] Proenza C, Yellen G. Distinct populations of HCN pacemaker channels produce voltage-dependent and voltage-independent currents. J Gen Physiol 2006;127(2):183-190.

[15] Macri V, Proenza C, Agranovich E, Angoli D, Accili EA. Separable gating mechanisms in a mammalian pacemaker channel. J Biol Chem 2002;277(39):35939-35946.

[16] Zhao X, Bucchi A, Oren RV, Kryukova Y, Dun W, Clancy CE, et al. In vitro characterization of HCN channel kinetics and frequency dependence in myocytes predicts biological pacemaker functionality. J Physiol (Lond) 2009;587(7):1513-1525.

[17] Postea O, Biel M. Exploring HCN channels as novel drug targets. Nat Rev Drug Discov 2011 Nov 18;10(12):903-14.

[18] Thollon C, Bedut S, Villeneuve N, Coge F, Piffard L, Guillaumin JP, et al. Use-dependent inhibition of hHCN4 by ivabradine and relationship with reduction in pacemaker activity. Br J Pharmacol 2007 Jan;150(1):37-46.

[19] Bois P, Bescond J, Renaudon B, Lenfant J. Mode of action of bradycardic agent, S 16257, on ionic currents of rabbit sinoatrial node cells. Br J Pharmacol 1996 Jun;118(4):1051-1057.

[20] Koncz I, Szél T, Bitay M, Cerbai E, Jaeger K, Fülöp F, et al. Electrophysiological effects of ivabradine in dog and human cardiac preparations: Potential antiarrhythmic actions. Eur J Pharmacol 2011;668(3):419-426.

[21] El Chemaly A, Magaud C, Patri S, Jayle C, Guinamard R, Bois P. The heart rate-lowering agent ivabradine inhibits the pacemaker current I_f in human atrial myocytes. J Cardiovasc Electrophysiol 2007 Nov;18(11):1190-1196.

[22] Nuding S, Ebelt H, Hoke RS, Krummenerl A, Wienke A, Müller-Werdan U, et al. Reducing elevated heart rate in patients with multiple organ dysfunction syndrome by the I_f (funny channel current) inhibitor ivabradine. Clin Res Cardiol 2011;100(10):915-923.

[23] Severi S, Fantini M, Charawi LA, DiFrancesco D. An updated computational model of rabbit sinoatrial action potential to investigate the mechanisms of heart rate modulation. J Physiol 2012 Sep 15;590(18):4483-4499.

[24] Madhero88. Electrical conduction system of the heart. Available from: http://commons.wikimedia.org/wiki/File%3AConductionsystemoftheheart.png. Accessed 2013/04/03.

[25] Hille B. Ion channels of excitable membranes. 3rd ed. Sunderland (MA): Sinauer Association, Inc.; 2001.

[26] Katz AM. Physiology of the Heart. 3rd ed. Philadelphia (PA): Lippincott Williams & Wilkins; 2006.

[27] Jalife J, Delmar M, Davidenko JM, Anumonwo JMB. Basic cardiac electrophysiology for the clinician. Armonk (NY): Futura Publishing Company, Inc.; 1999.

[28] Klabunde R. Cardiovascular physiology concepts. 2nd ed. Philadelphia (PA): Lippincott Williams & Wilkins; 2011.

[29] Stühmer W, Conti F, Suzuki H, Wang XD, Noda M, Yahagi N, et al. Structural parts involved in activation and inactivation of the sodium channel. Nature 1989 Jun 22;339(6226):597-603.

[30] Iftinca M. Neuronal T–type calcium channels regulation. J Med life 2011;4(2):126.

[31] IUPHAR. Ion Channels. Available from: http://www.iuphar-db.org/DATABASE/ReceptorFamiliesForward?type=IC. Accessed 27/04/2014.

[32] Sandoz G, Levitz J. Optogenetic techniques for the study of native potassium channels. Front Mol Neurosci 2013 Apr 11;6:6.

[33] Shieh CC, Coghlan M, Sullivan JP, Gopalakrishnan M. Potassium channels: molecular defects, diseases, and therapeutic opportunities. Pharmacol Rev 2000 Dec;52(4):557-594.

[34] Lady of Hats, Mariana, Ruiz. Cell membrane, detailed diagramm. Available from: http://commons.wikimedia.org/wiki/File%3ACell_membrane_detailed_diagram_en.svg. Accessed 2013/04/04.

[35] Fozzard HA, Haber E, Jennings RB, Katz AM. The heart and cardiovascular system. New York: Raven Press; 1986.

[36] Nattel S, Maguy A, Le Bouter S, Yeh Y. Arrhythmogenic ion-channel remodeling in the heart: heart failure, myocardial infarction, and atrial fibrillation. Physiol Rev 2007;87(2):425-456.

[37] Grant AO. Cardiac ion channels. Circ Arrhythm Electrophysiol 2009;2(2):185-194.

[38] Silbernagl S, Despopoulos A. Taschenatlas der Physiologie. 5th ed. Stuttgart: Georg Thieme Verlag; 2001.

[39] Irisawa H, Brown H, Giles W. Cardiac pacemaking in the sinoatrial node. Physiol Rev 1993;73(1):197-227.

[40] Joung B, Chen PS, Lin SF. The role of the calcium and the voltage clocks in sinoatrial node dysfunction. Yonsei Med J 2011 Mar 1;52(2):211-219.

[41] Maltsev VA, Lakatta EG. Dynamic interactions of an intracellular Ca^{2+} clock and membrane ion channel clock underlie robust initiation and regulation of cardiac pacemaker function. Cardiovasc Res 2008;77(2):274-284.

[42] Zipes DP, Jalife J. Cardiac electrophysiology: From cell to bedside. Philadelphia (PA): Saunders Elsevier; 1990.

[43] Park S, Park H, Hwang HJ, Shim J, Sung J, Kim J, et al. Heart rate acceleration of a subsidiary pacemaker by β-adrenergic stimulation. Korean circ j 2011;41(11):658-665.

[44] Bucchi A, Baruscotti M, Robinson RB, DiFrancesco D. Modulation of rate by autonomic agonists in SAN cells involves changes in diastolic depolarization and the pacemaker current. J Mol Cell Cardiol 2007;43(1):39-48.

[45] Vinogradova TM, Zhou Y, Maltsev V, Lyashkov A, Stern M, Lakatta EG. Rhythmic ryanodine receptor Ca^{2+} releases during diastolic depolarization of sinoatrial pacemaker cells do not require membrane depolarization. Circ Res 2004;94(6):802-809.

[46] Bers DM. Calcium cycling and signaling in cardiac myocytes. Annu Rev Physiol 2008;70:23-49.

[47] Bers DM. Calcium and cardiac rhythms physiological and pathophysiological. Circ Res 2002;90(1):14-17.

[48] Vinogradova TM, Zhou Y, Bogdanov KY, Yang D, Kuschel M, Cheng H, et al. Sinoatrial node pacemaker activity requires Ca^{2+}/calmodulin-dependent protein kinase II activation. Circ Res 2000;87(9):760-767.

[49] Lakatta EG, Maltsev VA, Bogdanov KY, Stern MD, Vinogradova TM. Cyclic variation of intracellular calcium a critical factor for cardiac pacemaker cell dominance. Circ Res 2003;92(3):e45-e50.

[50] Schindler RF, Poon KL, Simrick S, Brand T. The Popeye domain containing genes: essential elements in heart rate control. Cardiovasc Diagn and Ther 2012;2(4):308-319.

[51] Lakatta EG, Maltsev VA. Reprogramming paces the heart. Nat Biotechnol 2013 Jan;31(1):31-32.

[52] Lakatta EG, Maltsev VA, Vinogradova TM. A coupled System of intracellular Ca^{2+} clocks and surface membrane voltage clocks controls the timekeeping mechanism of the heart's pacemaker. Circ Res 2010;106(4):659-673.

[53] Pelzmann B. Die Wirkung von Bariumionen auf Spontanaktivität und Ionenströme isolierter embryonaler Hühnerherzventrikelzellen. PhD dissertation. Graz: Medical University of Graz 1996.

[54] Macri V, Accili EA. Structural elements of instantaneous and slow gating in hyperpolarization-activated cyclic nucleotide-gated channels. J Biol Chem 2004;279(16):16832-16846.

[55] Noble D, Denyer J, Brown H, DiFrancesco D. Reciprocal role of the inward currents $I_{b,Na}$ and I_f in controlling and stabilizing pacemaker frequency of rabbit sino-atrial node cells. Proc Biol Sci 1992:199-207.

[56] Hagiwara N, Irisawa H, Kasanuki H, Hosoda S. Background current in sino-atrial node cells of the rabbit heart. J Physiol (Lond) 1992;448(1):53-72.

[57] Michels G, Brandt MC, Zagidullin N, Khan IF, Larbig R, van Aaken S, et al. Direct evidence for calcium conductance of hyperpolarization-activated cyclic nucleotide-gated channels and human native I_f at physiological calcium concentrations. Cardiovasc Res 2008;78(3):466-475.

[58] Biel M, Wahl-Schott C, Michalakis S, Zong X. Hyperpolarization-activated cation channels: from genes to function. Physiol Rev 2009;89(3):847-885.

[59] Baruscotti M, Bucchi A, Viscomi C, Mandelli G, Consalez G, Gnecchi-Rusconi T, et al. Deep bradycardia and heart block caused by inducible cardiac-specific knockout of the pacemaker channel gene HCN4. Proc Natl Acad Sci U S A 2011 Jan 25;108(4):1705-10.

[60] Michels G, Er F, Khan I, Sudkamp M, Herzig S, Hoppe UC. Single-channel properties support a potential contribution of hyperpolarization-activated cyclic nucleotide-gated channels and I_f to cardiac arrhythmias. Circulation 2005 Feb 1;111(4):399-404.

[61] Szabo G, Farkas V, Grunnet M, Mohacsi A, Nanasi PP. Enhanced repolarization capacity: new potential antiarrhythmic strategy based on HERG channel activation. Curr Med Chem 2011;18(24):3607-3621.

[62] Zwermann L. Kardiale" Delayed Rectifier" Kaliumkanäle. PhD dissertation. München: Ludwig-Maximilians-Universität 2005.

[63] Sanguinetti MC, Jurkiewicz NK. Delayed rectifier outward K^+ current is composed of two currents in guinea pig atrial cells. Am J Physiol 1991;260(2):H393-H399.

[64] Kurata Y, Hisatome I, Imanishi S, Shibamoto T. Dynamical description of sinoatrial node pacemaking: improved mathematical model for primary pacemaker cell. Am J Physiol Heart Circ Physiol 2002;283(5):H2074-H2101.

[65] Zorn-Pauly K. Elektrische Erregbarkeit von ventrikulären Herzmuskelzellen: Untersuchung mittels Patch-Clamp Experimenten und mathematischer Modellbildung/Simulation. PhD dissertation. Graz: Medical University of Graz 2002.

[66] Lacinová L, Hofmann F. Voltage-dependent calcium channels. In: Sperelakis N, Kurachi Y, Terzic A, V. Cohen M. Heart Physiology and Pathophysiology. 4th ed. San Diego (CA): Academic Press 2001; pp. 247-57.

[67] Kodama I, Nikmaram M, Boyett M, Suzuki R, Honjo H, Owen J. Regional differences in the role of the Ca^{2+} and Na^{+} currents in pacemaker activity in the sinoatrial node. Am J Physiol Heart Circ Physiol 1997;272(6):H2793-H2806.

[68] Baruscotti M, DiFrancesco D, Robinson RB. Na^{+} current contribution to the diastolic depolarization in newborn rabbit SA node cells. Am J Physiol Heart Circ Physiol 2000;279(5):H2303-H2309.

[69] Zhang H, Holden AV, Boyett MR. Sustained inward current and pacemaker activity of mammalian sinoatrial node. J Cardiovasc Electrophysiol 2002;13(8):809-812.

[70] Mitsuiye T, Shinagawa Y, Noma A. Sustained inward current during pacemaker depolarization in mammalian sinoatrial node cells. Circ Res 2000;87(2):88-91.

[71] Attwell D, Cohen I, Eisner D, Ohba M, Ojeda C. The steady state TTX-sensitive ("window") sodium current in cardiac Purkinje fibres. Pflügers Arch 1979;379(2):137-142.

[72] YuI Z, Starmer C, Starobin J, Grant A. Late Na channels in cardiac cells: the physiological role of background Na^{+} channels. Biophys J 1994;67(1):153-160.

[73] Cohen I, DiFrancesco D, Mulrine N, Pennefather P. Internal and external K^{+} help gate the inward rectifier. Biophys J 1989;55(1):197-202.

[74] Gadsby DC, Nakao M. Steady-state current-voltage relationship of the Na^{+}/K^{+} pump in guinea pig ventricular myocytes. J Gen Physiol 1989;94(3):511-537.

[75] Bers DM, Weber CR. $Na^{+}/Ca2^{+}$ exchange function in intact ventricular myocytes. Ann N Y Acad Sci 2002;976(1):500-512.

[76] Galley HF, Webster NR. The immuno-inflammatory cascade. Br J Anaesth 1996 Jul;77(1):11-16.

[77] Davies M, Hagen PO. Systemic inflammatory response syndrome. Br J Surg 2005;84(7):920-935.

[78] Robertson CM, Coopersmith CM. The systemic inflammatory response syndrome. Microbes and infection/Institut Pasteur 2006;8(5):1382.

[79] Gyorfy Z, Duda E, Vizler C. Interactions between LPS moieties and macrophage pattern recognition receptors. Vet Immunol Immunopathol 2013 Mar 15;152(1-2):28-36

[80] Rietschel ET, Brade H, Holst O, Brade L, Muller-Loennies S, Mamat U, et al. Bacterial endotoxin: Chemical constitution, biological recognition, host response, and immunological detoxification. Curr Top Microbiol Immunol 1996;216:39-81.

[81] Holst O, Ulmer AJ, Brade H, Flad HD, Rietschel ET. Biochemistry and cell biology of bacterial endotoxins. FEMS Immunol Med Microbiol 1996 Dec 1;16(2):83-104.

[82] Brandenburg K, Wiese A. Endotoxins: relationships between structure, function, and activity. Curr Top Med Chem 2004;4(11):1127-1146.

[83] Tipmj. Lipopolysaccharide. Available from: http://commons.wikimedia.org/wiki/File%3ALipopolysaccharide.jpg. Accessed 2013/04/03.

[84] Ulevitch RJ, Mathison JC, da Silva Correia J. Innate immune responses during infection. Vaccine 2004 Dec 6;22 Suppl 1:S25-30.

[85] Rietschel ET, Galanos C, Tanaka A, Ruschmann E, Luderitz O, Westphal O. Biological activities of chemically modified endotoxins. Eur J Biochem 1971 Sep 24;22(2):218-224.

[86] Loppnow H, Brade H, Durrbaum I, Dinarello CA, Kusumoto S, Rietschel ET, et al. IL-1 induction-capacity of defined lipopolysaccharide partial structures. J Immunol 1989;142(9):3229-3238.

[87] Nielsen JS, Larsson A, Ledet T, Turina M, Tonnesen E, Krog J. Rough-form-lipopolysaccharide increase apoptosis in human $CD4^+$ and $CD8^+$ T-lymphocytes. Scand J Immunol 2011;75(2):193-202.

[88] Perl M, Chung CS, Swan R, Ayala A. Role of programmed cell death in the immunopathogenesis of sepsis. Drug Discov Today Dis Mech 2008;4(4):223-230.

[89] Hotchkiss RS, Swanson PE, Freeman BD, Tinsley KW, Cobb JP, Matuschak GM, et al. Apoptotic cell death in patients with sepsis, shock, and multiple organ dysfunction. Crit Care Med 1999;27(7):1230-1251.

[90] Coopersmith CM, Stromberg PE, Dunne WM, Davis CG, Amiot II DM, Buchman TG, et al. Inhibition of intestinal epithelial apoptosis and survival in a murine model of pneumonia-induced sepsis. JAMA 2002;287(13):1716-1721.

[91] Kaisho T, Akira S. Toll-like receptors as adjuvant receptors. Biochim Biophys Acta 2002;1589(1):1.

[92] Molenaar R, Antoni C. Van Ginneken, Antoni. Acute effect of bacterial lipopolysaccharide on cardiac sodium current. Biophys J 2013;104(2):294a.

[93] Wondergem R, Graves BM, Ozment-Skelton TR, Li C, Williams DL. Lipopolysaccharides directly decrease Ca^{2+} oscillations and the hyperpolarization-activated nonselective cation current I_f in immortalized HL-1 cardiomyocytes. Am J Physiol Cell Physiol 2010 Sep;299(3):C665-71.

[94] Klöckner U, Rueckschloss U, Grossmann C, Matzat S, Schumann K, Ebelt H, et al. Inhibition of cardiac pacemaker channel hHCN2 depends on intercalation of lipopolysaccharide into channel-containing membrane microdomains. J Physiol 2014 Mar 15;592(Pt 6):1199-1211.

[95] Wondergem R, Graves BM, Li C, Williams DL. Lipopolysaccharide prolongs action potential duration in HL-1 mouse cardiomyocytes. Am J Physiol Cell Physiol 2012;303(8):C825-C833.

[96] Werdan K, Schmidt H, Ebelt H, Zorn-Pauly K, Koidl B, Hoke RS, et al. Impaired regulation of cardiac function in sepsis, SIRS, and MODS. Can J Physiol Pharmacol 2009 Apr;87(4):266-274.

[97] Bucchi A, Tognati A, Milanesi R, Baruscotti M, DiFrancesco D. Properties of ivabradine-induced block of HCN1 and HCN4 pacemaker channels. J Physiol 2006 Apr 15;572(Pt 2):335-346.

[98] Böhm M, Borer J, Ford I, Gonzalez-Juanatey JR, Komajda M, Lopez-Sendon J, et al. Heart rate at baseline influences the effect of ivabradine on cardiovascular outcomes in chronic heart failure: analysis from the SHIFT study. Clin Res Cardiol 2013 Jan;102(1):11-22.

[99] Thollon C, Vilaine JP. I_f inhibition in cardiovascular diseases. Adv Pharmacol 2010;59:53-92.

[100] Sulfi S, Timmis A. Ivabradine – the first selective sinus node I_f channel inhibitor in the treatment of stable angina. Int J Clin Pract 2006;60(2):222-228.

[101] Ferrari R, Ceconi C. Selective and specific I_f inhibition with ivabradine: new perspectives for the treatment of cardiovascular disease. Expert Rev Cardiovasc Ther 2011 Aug;9(8):959-973.

[102] Suenari K, Cheng C, Chen Y, Lin Y, Nakano Y, Kihara Y, et al. Effects of ivabradine on the pulmonary vein electrical activity and modulation of pacemaker currents and calcium homeostasis. J Cardiovasc Electrophysiol 2011;23(2):200-206.

[103] Suffredini S, Stillitano F, Comini L, Bouly M, Brogioni S, Ceconi C, et al. Long-term treatment with ivabradine in post-myocardial infarcted rats counteracts f-channel overexpression. Br J Pharmacol 2012;165(5):1457-1466.

[104] Custodis F, Baumhäkel M, Schlimmer N, List F, Gensch C, Böhm M, et al. Heart rate reduction by ivabradine reduces oxidative stress, improves endothelial function, and prevents atherosclerosis in apolipoprotein E–deficient mice. Circulation 2008;117(18):2377-2387.

[105] Custodis F, Fries P, Müller A, Stamm C, Grube M, Kroemer HK, et al. Heart rate reduction by ivabradine improves aortic compliance in apolipoprotein E-Deficient mice. J Vasc Res 2012;49(5):432-440.

[106] Bilz0r. Patchmodes. Available from: http://upload.wikimedia.org/wikipedia/commons/1/1f/Patchmodes.svg. Accessed 2013/05/14

[107] World Medical Association General Assembly. World Medical Association Declaration of Helsinki: ethical principles for medical research involving human subjects. J Int Bioethique 2004 Mar;15(1):124-129.

[108] Piper HM, Probst I, Schwartz P, Hutter FJ, Spieckermann PG. Culturing of calcium stable adult cardiac myocytes. J Mol Cell Cardiol 1982 Jul;14(7):397-412.

[109] Claycomb WC, Lanson NA, Stallworth BS, Egeland DB, Delcarpio JB, Bahinski A, et al. HL-1 cells: a cardiac muscle cell line that contracts and retains phenotypic characteristics of the adult cardiomyocyte. Proc Natl Acad Sci USA 1998;95(6):2979-2984.

[110] Porciatti F, Pelzmann B, Cerbai E, Schaffer P, Pino R, Bernhart E, et al. The pacemaker current I_f in single human atrial myocytes and the effect of beta-adrenoceptor and A1-adenosine receptor stimulation. Br J Pharmacol 1997 Nov;122(5):963-969.

[111] Barry PH. JPCalc, a software package for calculating liquid junction potential corrections in patch-clamp, intracellular, epithelial and bilayer measurements and for correcting junction potential measurements. J Neurosci Methods 1994;51(1):107-116.

[112] Rossmann C, Rauh A, Hammer A, Windischhofer W, Zirkl S, Sattler W, et al. Hypochlorite-modified high-density lipoprotein promotes induction of HO-1 in endothelial cells via activation of p42/44 MAPK and zinc finger transcription factor Egr-1. Arch Biochem Biophys 2011 May 1;509(1):16-25.

[113] Klippert P, Jeanniot JP, Polvé S, Lefèvre C, Merdjan H. Determination of ivabradine and its N-demethylated metabolite in human plasma and urine, and in rat and dog plasma by a validated high-performance liquid chromatographic method with fluorescence detection. J Chromatogr B Biomed Sci Appl 1998;719(1):125-133.

[114] Ulevitch R, Johnston A, Weinstein D. New function for high density lipoproteins. Isolation and characterization of a bacterial lipopolysaccharide-high density lipoprotein complex formed in rabbit plasma. J Clin Invest 1981;67(3):827.

[115] Cardoso FL, Kittel Á, Veszelka S, Palmela I, Tóth A, Brites D, et al. Exposure to lipopolysaccharide and/or unconjugated bilirubin impair the integrity and function of brain microvascular endothelial cells. PloS one 2012;7(5):e35919.

[116] Chen J, Mitcheson JS, Tristani-Firouzi M, Lin M, Sanguinetti MC. The S4–S5 linker couples voltage sensing and activation of pacemaker channels. Proc Natl Acad Sci USA 2001;98(20):11277-11282.

[117] Decher N, Chen J, Sanguinetti MC. Voltage-dependent gating of hyperpolarization-activated, cyclic nucleotide-gated pacemaker channels: molecular coupling between the S4–S5 and C-linkers. J Biol Chem 2004;279(14):13859-13865.

[118] Cerbai E, Sartiani L, DePaoli P, Pino R, Maccherini M, Bizzarri F, et al. The properties of the pacemaker current I_f in human ventricular myocytes are modulated by cardiac disease. J Mol Cell Cardiol 2001;33(3):441-448.

[119] Fernández-Velasco M, Goren N, Benito G, Blanco-Rivero J, Boscá L, Delgado C. Regional distribution of hyperpolarization-activated current (I_f) and hyperpolarization-activated cyclic nucleotide-gated channel mRNA expression in ventricular cells from control and hypertrophied rat hearts. J Physiol (Lond) 2003;553(2):395-405.

[120] Zorn-Pauly K, Schaffer P, Pelzmann B, Lang P, Mächler H, Rigler B, et al. I_f in left human atrium: a potential contributor to atrial ectopy. Cardiovasc Res 2004;64(2):250-259.

[121] Li J, Wang H, Xu B, Wang X, Fu Y, Chen M, et al. Hyperpolarization activated cation current (I_f) in cardiac myocytes from pulmonary vein sleeves in the canine with atrial fibrillation. J Geriatr Cardiol: JGC 2012;9(4):366.

[122] Seydel U, Hawkins L, Schromm AB, Heine H, Scheel O, Koch MH, et al. The generalized endotoxic principle. Eur J Immunol 2003;33(6):1586-1592.

[123] Delcour AH. Outer membrane permeability and antibiotic resistance. Biochim Biophys Acta 2009;1794(5):808-816.

[124] Tsujimoto H, Gotoh N, Nishino T. Diffusion of macrolide antibiotics through the outer membrane of Moraxella catarrhalis. J Infect Chemother 1999;5(4):196-200.

[125] De Santis V, Vitale D, Santoro A, Magliocca A, Porto AG, Nencini C, et al. Ivabradine: potential clinical applications in critically ill patients. Clin Res Cardiol 2013 Mar;102(3):171-178.

[126] Hoke RS, Muller-Werdan U, Lautenschlager C, Werdan K, Ebelt H. Heart rate as an independent risk factor in patients with multiple organ dysfunction: a prospective, observational study. Clin Res Cardiol 2012 Feb;101(2):139-147.

[127] Parker MM, Shelhamer JH, Natanson C, Alling DW, Parrillo JE. Serial cardiovascular variables in survivors and nonsurvivors of human septic shock: heart rate as an early predictor of prognosis. Crit Care Med 1987 Oct;15(10):923-929.